

Electronic Thesis and Dissertation Repository

---

10-4-2023 3:00 PM

## Acceptorless Dehydrogenation of Amines using Metal Ligand Cooperative Catalysts

Amrit Singh, *Western University*

Supervisor: Blacquiere, Johanna M., *The University of Western Ontario*

A thesis submitted in partial fulfillment of the requirements for the Master of Science degree in Chemistry

© Amrit Singh 2023

Follow this and additional works at: <https://ir.lib.uwo.ca/etd>

 Part of the [Inorganic Chemistry Commons](#), [Medicinal-Pharmaceutical Chemistry Commons](#), and the [Other Chemistry Commons](#)

---

### Recommended Citation

Singh, Amrit, "Acceptorless Dehydrogenation of Amines using Metal Ligand Cooperative Catalysts" (2023). *Electronic Thesis and Dissertation Repository*. 9845.  
<https://ir.lib.uwo.ca/etd/9845>

This Dissertation/Thesis is brought to you for free and open access by Scholarship@Western. It has been accepted for inclusion in Electronic Thesis and Dissertation Repository by an authorized administrator of Scholarship@Western. For more information, please contact [wlsadmin@uwo.ca](mailto:wlsadmin@uwo.ca).

## Abstract

Catalytic acceptorless dehydrogenation (AD) is an atom economic route for synthesizing imines and enamines, which are common final or intermediary functionalities in various pharmaceutically relevant molecules and materials. Imines, for example, are present in a wide range of syntheses due to their versatility. Meanwhile, indole is the 9<sup>th</sup> most common nitrogen heterocycle in FDA approved drugs. For imine synthesis via AD, selectivity challenges remain. Reactions often afford a product mixture of imine, nitrile, and a secondary amine. Previously, we showed that the metal-ligand cooperative (MLC) catalyst  $[\text{Ru}(\text{Cp})(\text{P}^{\text{Ph}}_2\text{N}^{\text{Bn}}_2)(\text{MeCN})]\text{PF}_6$  showed improved selectivity over a non-MLC catalyst. Herein, a broader scope of activity and selectivity assessment for the AD of amines, for a range of  $[\text{M}(\text{Cp})(\text{P}^{\text{R}}_2\text{N}^{\text{R}'_2})(\text{MeCN})]\text{PF}_6$  catalysts will be discussed.  $[\text{Ru}(\text{Cp})(\text{P}^{\text{R}}_2\text{N}^{\text{R}'_2})(\text{MeCN})]\text{PF}_6$  catalysts were explored for the AD of indoline to indole, which revealed that the activity depended on both the R and R' groups of the  $\text{P}^{\text{R}}_2\text{N}^{\text{R}'_2}$  ligand. In addition, both ruthenium and iron catalyst derivatives were explored for the AD of benzylamine, which showed that the iron-centered catalyst was highly selective towards the imine product. Investigations into the mechanism will be discussed that reveal connections between catalyst structure and performance.

## Keywords

Acceptorless dehydrogenation, primary amines, *N*-heterocycles, homogeneous catalysis, metal-ligand cooperative catalyst, selectivity, earth-abundant metal, iron, Iron(II), ruthenium, Ruthenium(II),  $\text{P}_2\text{N}_2$ , dihydrogen, imine, nitrile

## Summary for Lay Audience

This thesis investigates the use of various catalysts for a chemical transformation crucial to the synthesis of significant molecules, with applications spanning the pharmaceutical, agrochemical, and fine chemical industries. Catalysts are substances that speed up chemical reactions without getting used up in the process. The best catalyst works for a long time without breaking down and exhibits selectivity for one specific product. However, during the chemical transformation of interest, the reaction can often yield more than one product, even with the catalyst's intervention. In chemistry, molecules like imine, nitriles, and *N*-heterocycles stand out as significant players. Imines and nitriles, with their versatile nature, often act as middlemen in various chemical reactions to create more diverse compounds. Indoles, a nitrogen containing compound is the 9<sup>th</sup> most common structure found in FDA approved medications. Nonetheless, the process of synthesizing imines with the chemical transformation of interest has issues with selectivity to produce the desired product. In this work, A catalyst featuring an iron metal center emerged as uniquely selective, generating a single imine product. To better understand this phenomenon, an array of structurally distinct catalysts were tested, revealing clear correlations between structural attributes and catalytic performance. Adjustments to the catalysts' structures can enhance or change their efficacy. The iron catalyst's role in the chemical transformation was confirmed via control reactions, which showed that without the catalyst, the reaction did not achieve the desired outcomes. The iron-based catalytic system presents a cost-effective alternative to traditional methods utilizing precious and costly metals such as ruthenium. Traditionally, ruthenium has been favored for these transformations due to its inherent ability to facilitate the chemical transformation of interest compared to other metals like iron. The implications of employing this iron-based catalyst are far-reaching marking a significant stride towards creating a more sustainable future.

## Co-Authorship Statement

The work described in this thesis contains contributions from the author as well as co-workers James M. Stubbs, Claire E. Cannon, Matthew D. Hoffman, Kiran Nandi, and supervisor Dr. Johanna M. Blacquiere. The contributions of each are described below.

Chapter 1 was written by the author and edited by Dr. Johanna M. Blacquiere.

Chapter 2 illustrates using *N*-heterocycles as AD substrates with ruthenium/iron catalysts. All experiments were completed by the author and parts of this chapter have been published (Stubbs, J.; Nanuwa, A. S.; Hoffman, M. D.; Blacquiere, J. M. *Synlett* **2023**. 445-450.). To conduct a comparative analysis of the substrate scope using **Ru1f**, work previously investigated by James M. Stubbs using **Ru1b** was also described for the indoline derivatives (Figure 2.3). Also, the AD of oxazole using **Ru1f** was completed by Claire E. Cannon. The complexes  $[\text{Ru}(\text{Cp})(\text{P}^{\text{Ph}}_2\text{N}^{\text{Ph}}_2)(\text{MeCN})]\text{PF}_6$  (**Ru1b**) and  $[\text{Ru}(\text{Cp})(\text{P}^{\text{tBu}}_2\text{N}^{\text{Ph}}_2)(\text{MeCN})]\text{PF}_6$  (**Ru1f**) were synthesized in collaboration with Megan A. Hoffer following a previously established procedure. The chapter was written by the author and edited by Dr. Johanna M. Blacquiere.

Chapter 3 dives into the synthesis of novel iron complexes. All experiments were completed by the author. The chapter was written by the author and edited by Dr. Johanna M. Blacquiere.

Chapter 4 investigates selectivity for the synthesis of imines via AD. All experiments were completed by the author, except within the catalyst screen, Matthew D. Hoffman completed the following entries (1, 3-5, 8 & 9) in Table 4.1. Also, the control reactions (Table 4.2, Entries 14, 15, and 16) were described by Kiran Nandi. The chapter was written by the author and edited by Dr. Johanna M. Blacquiere.

Chapter 5 was written by the author and edited by Dr. Johanna M. Blacquiere.

## Acknowledgments

First and foremost, I would like to express my deepest gratitude to my supervisor, Dr. Johanna M. Blacquiere. Joining the Blacquiere group without prior research experience was a leap of faith, made easier by Johanna's exceptional guidance, patience, and unyielding belief in me. Her mentorship has been transformative, pushing me to confront challenges head-on something I often avoided before joining the group. It's been an invaluable two years under your supervision, and for that, I am forever thankful.

I owe a heartfelt thank you to my parents, whose unwavering support has been the bedrock of my academic journey. The trips you made to London to deliver home-cooked meals meant so much to me, they were a taste of home and a reminder of your constant love and support.

To my grandmother, who has been a source of warmth, thank you for the nightly calls and for insisting that I be excused from washing dishes at home, ahaha! Your support and love have kept me grounded.

My sisters deserve a special mention for their infinite encouragement. Your excitement for my new ventures has always been a source of inspiration. I'm fortunate to have such empowering role models as older siblings.

I would also like to extend my gratitude to my Hinata, Manfrotto, Macros, Mantis, and Macromango. Your companionship and support have been invaluable to me. Though our regular visits to The Keg are now memories, they will always be cherished ones.

Thanks to the friends I've made within the Chemistry Department (you know who you are), I will never forget our late-night proctoring sessions.

Lastly, a big shoutout to both past and current members of the Blacquiere group. Working alongside such talented individuals has been a pleasure and remember "Don't burn down the lab!" while I'm gone!

# Table of Contents

Abstract.....	ii
Summary for Lay Audience.....	iii
Co-Authorship Statement.....	iv
Acknowledgments.....	v
Table of Contents.....	vi
List of Tables.....	ix
List of Figures.....	x
List of Schemes.....	xii
List of Appendices.....	xv
List of Abbreviations.....	xvi
Chapter 1 Introduction.....	1
1.1 An Introduction to Catalysts and their Role in Sustainable Chemistry.....	1
1.2 Traditional Methods for Synthesizing Imines, Nitriles, and <i>N</i> -Heterocycles: Their Global Impact and Alternative Synthesis Pathways.....	3
1.3 Acceptorless Dehydrogenation of Amines using Transition Metal Catalysts.....	11
1.4 Metal-Ligand Cooperative Catalysis using $P^{R_2}N^{R'_2}$ Ligands as Proton Shuttles..	19
1.5 Scope of Thesis.....	22
1.6 References.....	23
Chapter 2.....	29
2 Comparing Catalyst Performance for Acceptorless Dehydrogenation of <i>N</i> -Heterocycles using $[M(Cp)(MeCN)(P^{R_2}N^{R'_2})]PF_6$ .....	29
2.1 Catalyst Comparison for Acceptorless Dehydrogenation of <i>N</i> -Heterocycles using $[M(Cp)(MeCN)(P^{R_2}N^{R'_2})]PF_6$ Complexes.....	30
2.2 Comparing Catalyst Performance using $[M(Cp)(MeCN)(P^{R_2}N^{R'_2})]PF_6$ Complexes: Time Trace Analysis and Scope Study.....	31
2.3 Conclusions.....	35

2.4	References.....	36
Chapter 3.....		37
3	Challenges in the Synthesis of Novel Iron Complex: Exploration of Diverse Methodologies and Outcomes.....	37
3.1	Attempts to Modify and Improve the Synthesis of $\text{FeCl}(\text{Cp})(\text{P}^{\text{Ph}}_2\text{N}^{\text{Ph}}_2)$ .....	37
3.2	Attempts to Modify and Improve the Synthesis of $\text{FeCl}(\text{Cp})(\text{P}^{\text{Ph}}_2\text{N}^{\text{Bn}}_2)$ .....	42
3.3	Conclusion .....	44
3.4	References.....	45
Chapter 4.....		46
4	Comparing Catalyst Performance for Acceptorless Dehydrogenation of Benzylamine using $[\text{M}(\text{Cp})(\text{MeCN})(\text{P}^{\text{R}}_2\text{N}^{\text{R}'_2})]\text{PF}_6$ complexes .....	46
4.1	Catalyst Screen for Acceptorless Dehydrogenation of Benzylamine .....	46
4.2	Acceptorless Dehydrogenation of Benzylamine using Fe1b – Optimization.....	49
4.3	Understanding Selectivity Through Control Reactions and Evaluating Fe1b Robustness .....	52
4.4	Scope Study: Targeting Homocoupled and Heterocoupled Imines.....	53
4.5	Fe1b Decomposition Analysis and Mechanistic Elucidation of a Novel Fe-H Complex.....	56
4.5.1	Evaluation of Catalyst Stability: Thermal Decomposition Analysis over Time, Competitive Coordination, and Air Exposure Influence .....	56
4.5.2	Attempted Synthesis of a Novel Fe-H Complex: Insights and Challenges in Mechanistic Elucidation .....	60
4.6	Conclusion .....	63
4.7	References.....	64
Chapter 5.....		65
5	General Conclusions and Future Work .....	65
5.1	General Conclusions .....	65
5.2	Future Work .....	66
6	Experimental .....	68

6.1	General Experimental Procedure .....	68
6.2	General Procedure for [Ru(Cp)(P2N2)(MeCN)]PF <sub>6</sub> .....	69
6.3	Modified FeCl(Cp)(CO) <sub>2</sub> Synthesis.....	69
6.4	General Procedure for FeCl(Cp)(P <sup>Ph</sup> <sub>2</sub> N <sup>Ph</sup> <sub>2</sub> ) Synthesis .....	70
6.5	General Procedure for the Catalytic AD of Indoline and Benzylamine Substrates using [Ru] Complexes, with Quantification by GC-FID .....	70
6.6	General Procedure for the Catalytic AD of Benzylamine Substrates using Fe1b, with Quantification by GC-FID .....	71
6.7	General Procedure for the Catalytic AD of Benzylamine/Nitrile/Dibenzylamine in an 'Open' System or Under a H <sub>2</sub> Headspace Using Fe1b, with Quantification by GC-FID .....	72
6.8	References.....	72
	Curriculum Vitae.....	82



## List of Tables

<b>Table 2.1</b> The performance of catalysts Ru1b, Ru1f, and Fe1b towards the AD of indoline. <sup>[a]</sup> .....	31
<b>Table 3.1</b> Solubility testing of [CpFe(CO) <sub>2</sub> Cl] and FeCl(Cp)(P <sup>Ph</sup> <sub>2</sub> N <sup>Ph</sup> <sub>2</sub> ) in solvents. ....	42
<b>Table 3.2</b> Summary of Optimization Parameters and Their Impact on Fe-Cl Yield. ....	44
<b>Table 4.1</b> Acceptorless dehydrogenation of BnNH <sub>2</sub> by M(Cp/Cp*)(P <sup>R</sup> <sub>2</sub> N <sup>R'</sup> <sub>2</sub> )(MeCN)JPF <sub>6</sub> catalysts.....	48
<b>Table 4.2</b> Optimization of the reaction conditions for the AD of BnNH <sub>2</sub> using Fe1b. <sup>[a]</sup> .....	50

## List of Figures

<b>Figure 1.1</b> The AD of primary amine to DAD by representative catalysts with their respective reaction conditions. <sup>42,49,53,54</sup> .....	17
<b>Figure 1.2</b> AD of indoline to indole by various catalysts with their respective reaction conditions. <sup>61-64</sup> .....	18
<b>Figure 1.3</b> The $P^R_2N^{R'}_2$ ligand structure and it coordinating to a metal via the phosphine groups.....	19
<b>Figure 1.4</b> Iron complexes that are $H_2$ production electrocatalysts (M) and models (K and L) for $H_2$ oxidation electrocatalysts.....	22
<b>Figure 2.1</b> The catalyst structures of $[Fe(Cp)(MeCN)(P^{Ph}_2N^{Ph}_2)]PF_6$ (Fe1b), $[Ru(Cp)(MeCN)(P^{Ph}_2N^{Ph}_2)]PF_6$ (Ru1b), $[Fe(Cp)(MeCN)(P^{t-Bu}_2N^{Ph}_2)]PF_6$ (Ru1f).....	29
<b>Figure 2.2</b> Reaction profile for acceptorless dehydrogenation of indoline at 110 °C in anisole with 0.5 mol% $P^R_2N^{Ph}_2$ catalysts Ru1b (R = Ph; blue) or Ru1f (R = <i>t</i> Bu; green) The conversion was monitored by calibrated GC-FID. ....	32
<b>Figure 2.3</b> Scope AD of substituted indolines using MLC catalysts Ru1b and Ru1f. <i>Reaction conditions:</i> Substrate (250 mM), catalyst (1 mol%), anisole, 110 °C, 24 h, sealed vial. Tetralin (100 mM) was used as an internal standard. <sup>2</sup> All data are averages of at least two trials; errors were all within ±5%. Product yields were determined by GC-FID. <sup>a</sup> 125 °C, 3 h. <sup>b</sup> 125 °C, 12 h. <sup>c</sup> 125 °C, 24 h. ....	34
<b>Figure 3.1</b> <sup>1</sup> H NMR spectrum stack plot of a) Fp in $CDCl_3$ (*) purified using column chromatography. The green dot (●) indicates the unknown signals in the upfield region. The orange dot (●) corresponds to the broad Cp ligand of Fp <sub>2</sub> . The purple dot (●) corresponds to Fp. b) Fp in $CD_2Cl_2$ (*) purified with column chromatography and liquid-liquid extraction. The (●) corresponds to the product, Fp. The orange dot (●) corresponds to Fp <sub>2</sub> . The black dot (●) corresponds to water. ....	39

<b>Figure 3.2</b> $^1\text{H}$ NMR spectrum of crude material from the photolysis of $\text{Fp}_2$ and the $\text{P}^{\text{Ph}}_2\text{N}^{\text{Ph}}_2$ ligand in $\text{CD}_2\text{Cl}_2$ . The red dot (●) indicates the product $\text{FeCl}(\text{Cp})(\text{P}^{\text{Ph}}_2\text{N}^{\text{Ph}}_2)$ , and the blue dot (●) indicates the free $\text{P}^{\text{Ph}}_2\text{N}^{\text{Ph}}_2$ ligand. ....	41
<b>Figure 4.1</b> Ruthenium and iron $\text{P}^{\text{R}}_2\text{N}^{\text{R}'}_2$ catalysts employed in this study. ....	47
<b>Figure 4.2</b> a) Scope AD of substituted benzylamines targeting homocoupled imines using MLC catalyst Fe1b. b) Scope AD of benzylamine with amine additives targeting heterocoupled imines using MLC catalyst Fe1b. ....	55
<b>Figure 4.3</b> Thermal Decomposition Analysis of Fe1b Catalyst Stability Over Time. Catalyst Fe1b (orange) at $110^\circ\text{C}$ in anisole from 0 – 48 hours. Formation of a new unknown species (25 ppm) (Grey). The conversion of catalyst and unknown species was monitored by $^{31}\text{P}\{^1\text{H}\}$ NMR spectroscopy with $\text{PPh}_3$ as the internal standard. ....	57
<b>Figure 4.4</b> $^{31}\text{P}\{^1\text{H}\}$ NMR spectrum stack plot of a) Fe1b and $\text{PPh}_3$ in $\text{CD}_2\text{Cl}_2$ . b) Fe1b, tert-butylaniline, and $\text{PPh}_3$ in $\text{CD}_2\text{Cl}_2$ heated at $110^\circ\text{C}$ for 24 hours. c) Fe1b, tert-butylaniline, and $\text{PPh}_3$ in $\text{CD}_2\text{Cl}_2$ heated at $110^\circ\text{C}$ for 48 hours. The red dot (●) corresponds to Fe1b. The orange dot (●) corresponds to $\text{PPh}_3$ . The green dot (●) corresponds to $[\text{PF}_6]^-$ .....	58
<b>Figure 4.5</b> $^{31}\text{P}\{^1\text{H}\}$ NMR spectrum stack plot of a) Fe1b in $\text{CD}_2\text{Cl}_2$ . b) Fe1b exposed to $\text{O}_2$ in $\text{CD}_2\text{Cl}_2$ . c) Fe1b sample exposed to $\text{O}_2$ and heated for 5 hours at $70^\circ\text{C}$ . The red dot (●) corresponds to Fe1b. The orange dot (●) corresponds to unknown signal. The green dot (●) corresponds to $[\text{PF}_6]^-$ . ....	60
<b>Figure 4.6</b> $^{31}\text{P}\{^1\text{H}\}$ NMR spectrum of attempted synthesis Fe-H. The red dot (●) corresponds to Fe-Cl. The orange dot (●) corresponds to a signal for an unknown product. The green dot (●) corresponds to the free $\text{P}^{\text{Ph}}_2\text{N}^{\text{Ph}}_2$ ligand. ....	63

## List of Schemes

<b>Scheme 1.1</b> a) Dehydrogenation of formic acid for the release of H <sub>2</sub> with A. b) Hydrogenation of carbon dioxide for hydrogen storage cycles with A and B. <sup>6</sup> DBU (1,8-diazabicyclo[5.4.0]undec-7-ene). <sup>6</sup> .....	3
<b>Scheme 1.2</b> a) Dual role of imines: Pivotal intermediates in synthetic pathways and as integral structural moieties in pharmaceutically active molecules. <sup>7,9</sup> b) Acid-catalyzed condensation reaction of a carbonyl with a primary amine to synthesize an imine. <sup>11,12</sup> .....	4
<b>Scheme 1.3</b> a) Nitriles as integral structural moieties in pharmaceutically active compounds. <sup>15</sup> b) Sandmeyer reaction, aryl nitrile synthesis from aryl amines using a copper salt. <sup>16</sup> .....	5
<b>Scheme 1.4</b> a) <i>N</i> -heterocycles as integral structural moieties in pharmaceutically active compounds. <sup>17,18</sup> b) Fischer Indole Synthesis, Acid-catalyzed Reaction to Convert Arylhydrazone and an Aldehyde or Ketone to an Indole. <sup>20</sup> .....	6
<b>Scheme 1.5</b> Synthesis of Imines from amines using Shvo's catalyst in the presence of an oxidant and a hydrogen acceptor. <sup>21</sup> .....	7
<b>Scheme 1.6</b> Copper(I)-chloride catalyzed oxidation of amines to form imines and the aldehyde by-product. <sup>25</sup> .....	7
<b>Scheme 1.7</b> General scheme of <i>in situ</i> transfer dehydrogenation from amines and alkynes to produce imines and alkenes. <sup>26</sup> .....	8
<b>Scheme 1.8</b> a) Synthesis of secondary aldimine and an alkane by catalytic transfer dehydrogenation using dibenzylamine and an alkene sacrificial hydrogen acceptor. <sup>27</sup> b) Catalytic transfer dehydrogenation of benzylamine to form a product mixture of secondary aldimine and secondary amine. <sup>28</sup> .....	9
<b>Scheme 1.9</b> Acceptorless dehydrogenative coupling (ADC) of an alcohol and primary amine to synthesize an imine. <sup>8</sup> .....	10

<b>Scheme 1.10</b> a) Ru(II)-PNP pincer complex facilitating the acceptorless dehydrogenative coupling of primary alcohols and amines to form an imine. <sup>29</sup> b) Ru(II)-PNN pincer complex catalytic mechanism that displays the metal-ligand cooperation in the catalytic cycle. <sup>29</sup> .....	11
<b>Scheme 1.11</b> a) General scheme to synthesize imines by use of a catalyst via AD reaction. b) AD of primary amine to form homocoupled or heterocoupled ADC, DAD, and HB products. ....	12
<b>Scheme 1.12</b> Acceptorless dehydrogenative coupling of primary benzylic amines using Ru(II)-NHC complexes. <sup>42</sup> .....	13
<b>Scheme 1.13</b> a) Acceptorless dehydrogenation of benzylamine facilitated by pincer complexes containing cooperative imine/alkene moieties to synthesize a secondary aldimine. <sup>43</sup> b) Acceptorless dehydrogenation of benzylamine using complex G yielding an imine. Mechanistic studies on complex H hypothesized the formation of complex H' as an intermediate. <sup>31</sup> .....	14
<b>Scheme 1.14</b> Catalytic dehydrogenation of primary amines with Iridium complexes to give a mixture of ADC and HB products. <sup>44</sup> .....	15
<b>Scheme 1.15</b> Synthesis of nitrile and secondary imine via acceptorless dehydrogenation of benzylamine and dibenzylamine, respectively. <sup>33</sup> .....	16
<b>Scheme 1.16</b> General catalytic cycle for [Ru(Cp/Cp*)(P <sup>R</sup> <sub>2</sub> N <sup>R'</sup> <sub>2</sub> )(MeCN)]PF <sub>6</sub> complexes. <sup>64</sup> .	21
<b>Scheme 1.17</b> AD of primary amine to form homocoupled or heterocoupled ADC, DAD, and HB products. ....	23
<b>Scheme 2.1</b> Synthesis of Oxazoles via AD using Ru1f and Fe1b.....	35
<b>Scheme 3.1</b> General synthetic route for the synthesis of Fe1b catalyst. Optimized yield in this work and literature yield. <sup>1-3</sup> .....	38
<b>Scheme 3.2</b> Coordination of P <sup>Ph</sup> <sub>2</sub> N <sup>Bn</sup> <sub>2</sub> ligand to Fp: Synthesis of FeCl(Cp)(P <sup>Ph</sup> <sub>2</sub> N <sup>Bn</sup> <sub>2</sub> ).....	43
<b>Scheme 3.3</b> Synthesis of FeCl(Cp)(P <sup>R</sup> <sub>2</sub> N <sup>R'</sup> <sub>2</sub> ): Coordination reaction of Fp with P <sub>2</sub> N <sub>2</sub> ligands under optimized conditions to synthesize novel iron complexes.....	45

<b>Scheme 4.1</b> a) AD of primary amine to form the homocoupled or hetercoupled ADC, DAD, and HB products. b) Control reactions to understand the origin of selectivity.....	53
<b>Scheme 4.2</b> General hypothesized catalytic cycle focusing on the formation of the II and III (Fe(H <sub>2</sub> )-adduct) complexes. ....	61
<b>Scheme 4.3</b> Attempted synthesis of a new Fe-H complex. ....	62
<b>Scheme 5.1</b> Acceptorless dehydrogenation of various heterocycles to afford oxazole and thiazole products using Ru1b and Ru1f. ....	66
<b>Scheme 5.2</b> Synthesis of Fe-P2N2 from Fp and P2N2 ligands.....	67
<b>Scheme 5.3</b> Treatment of Fe1b with hydrogen gas to synthesize the iron-dihydrogen (Fe(H <sub>2</sub> )-adduct) species at catalytic temperatures. ....	67

## List of Appendices

<b>Appendix A.1.</b> ATR-FTIR spectrum of $\text{FeCO}_5$ dissolved in 0.5 mL of DCM. ....	74
<b>Appendix A.2.</b> ATR-FTIR spectrum of $\text{Fe}(\text{Cp})_2(\text{CO})_4$ dissolved in 0.5 mL of DCM.....	75
<b>Appendix A.3.</b> ATR-FTIR spectrum of $\text{FeCl}(\text{Cp})(\text{CO})_2$ dissolved in 0.5 mL of DCM. ....	76
<b>Appendix A.4.</b> $^1\text{H}$ NMR spectrum of $\text{FeCl}(\text{Cp})(\text{P}^{\text{Ph}}_2\text{N}^{\text{Ph}}_2)$ (400 MHz, $\text{CD}_2\text{Cl}_2$ ).....	77
<b>Appendix A.5.</b> $^{31}\text{P}\{^1\text{H}\}$ NMR spectrum of $\text{FeCl}(\text{Cp})(\text{P}^{\text{Ph}}_2\text{N}^{\text{Ph}}_2)$ (162 MHz, $\text{CD}_2\text{Cl}_2$ ). The red dot (●) corresponds to $\text{FeCl}(\text{Cp})(\text{P}^{\text{Ph}}_2\text{N}^{\text{Ph}}_2)$ .....	78
<b>Appendix A.6.</b> $^1\text{H}$ NMR spectrum of Fe1b (400 MHz, $\text{CD}_2\text{Cl}_2$ ).....	78
<b>Appendix A.7.</b> $^{13}\text{C}\{^1\text{H}\}$ NMR spectrum of Fe1b (101 MHz, $\text{CD}_2\text{Cl}_2$ ).....	79
<b>Appendix A.8.</b> $^{31}\text{P}\{^1\text{H}\}$ NMR spectrum of Fe1b (162 MHz, $\text{CD}_2\text{Cl}_2$ ). The red dot (●) corresponds to Fe1b. The green dot (●) corresponds to the $[\text{PF}_6]^-$ . ....	80
<b>Appendix A.9.</b> $^{31}\text{P}\{^1\text{H}\}$ NMR stack plot of Fe1b with IS ( $\text{PPh}_3$ in capillary) heated in 1 hour time intervals from 0 – 48 h at 110 °C. The red dot (●) corresponds to Fe1b. The orange dot (●) corresponds to a signal for an unknown product. The blue dot (●) corresponds to the internal standard triphenylphosphine ( $\text{PPh}_3$ ). The green dot (●) corresponds to the $[\text{PF}_6]^-$ . ..	81

## List of Abbreviations

°C	degrees Celsius
Å	angstrom
AD	acceptorless dehydrogenation
ADC	acceptorless dehydrogenation coupling
ADC <sub>hetero</sub>	Heterocoupled acceptorless dehydrogenative coupled
ADC <sub>homo</sub>	Homocoupled acceptorless dehydrogenative coupled
Ar	aryl
ATR-FTIR	Attenuated Total Reflectance –Fourier Transform Infrared
Bn	benzyl
BnNH <sub>2</sub>	benzylamine
Conv.	conversion
Cp	cyclopentadienyl
Cp*	pentamethylcyclopentadienyl
Cy	cyclohexyl
C $\alpha$	alpha carbon
C $\beta$	beta carbon
DAD	double acceptorless dehydrogenation
DBU	1,8-diazabicyclo[5.4.0]undec-7-ene
DCM	dichloromethane



DH	dehydrogenation
DMA	Dimethylacetamide
DMBQ	2,6-dimethoxyquinone
DMF	dimethylformamide
DMSO	dimethyl sulfoxide
Equiv.	equivalent
FDA	Food and Drug Administration
FTIR	Fourier-transform infrared spectroscopy
GC-FID	Gas Chromatograph – Flame Ionization Detector
h	hour
HB	hydrogen borrowing
Ind	indole
Int	intermediate
IR	infrared
L	ligand
M	molarity
Me	methyl
MeOH	methanol
min	minutes
MLC	metal ligand cooperative

mM	millimolar
mmol	millimole
NHC	N-heterocyclic carbene
NMR	nuclear magnetic resonance
ODH	Oxidative dehydrogenation
PDE	Permitted Daily Exposure
Ph	phenyl
pKa	acid dissociation constant
PPh <sub>3</sub>	triphenylphosphine
ppm	parts per million
Prod	product
py	pyridine
RT	room temperature
Sub	substrate
T <sub>0</sub>	initial time point
<i>t</i> Bu	<i>tert</i> -butyl
Temp.	temperature
THF	tetrahydrofuran
TM	transition metal
TMS	tetramethylsilane

TOF turnover frequency

TON turnover number

UV-Vis ultraviolet-visible

## Chapter 1 Introduction

### 1.1 An Introduction to Catalysts and their Role in Sustainable Chemistry

Catalysts are molecules applicable in both biochemical and synthetic processes by lowering the energy barrier, or activation energy needed, for a transformation from a reactant(s) to a desired product. Importantly, a catalyst returns to the starting structure after each product molecule is formed, is not consumed in the reaction, and does not alter the thermodynamics of the reaction; it only affects the rate at which the reaction achieves equilibrium. Catalysts can be broadly categorized into two main types: homogeneous and heterogeneous, based on the phase they share with the reactants. Homogeneous catalysts are in the same phase as the starting material(s) and are uniformly distributed. Heterogeneous catalysts exist in a different phase than the starting material(s) and often are solids while the starting material is in the gas or liquid phase. The primary focus of this Thesis will concentrate on the exploration and application of homogeneous catalyst.

Evaluating and comparing the performance of different catalysts is of importance in both academic research and industrial applications. A few key metrics are often used in conjunction for these purposes: turnover number (TON), turnover frequency (TOF), and selectivity. The TON measures catalytic activity by quantifying the number of productive cycles a catalyst performs before deactivation. The TOF is a rate metric, that measures how fast a catalyst turns over per unit time. In other words, TOF represents how quickly a catalyst can drive the reaction. Finally, selectivity is an essential parameter which measures the ability of a catalyst to make only one product when multiple products are possible.

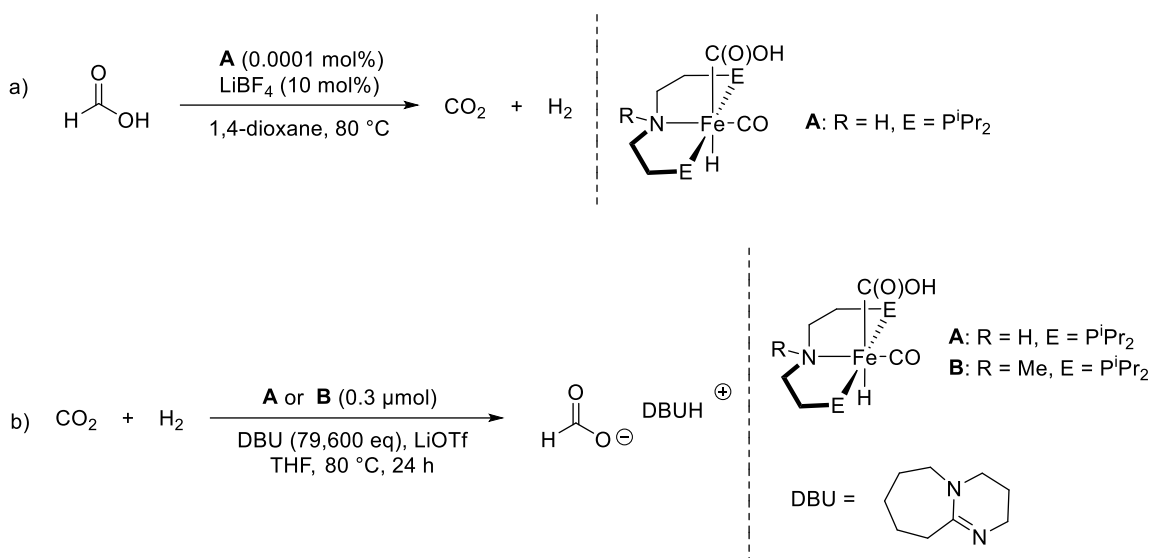
A variety of metal and metal-free systems have been explored for catalysis; however, within current literature, the choice between earth-abundant metals, such as iron (Fe), nickel (Ni), copper (Cu), and zinc (Zn) or platinum group metals, including palladium (Pd), ruthenium (Ru), rhodium (Rh), and iridium (Ir) for catalysts continues to be a subject of discussion. Earth-abundant metals offer several benefits, and iron serves as a prime example. Accounting for 6.3% of the Earth's crust, ensuring global availability.<sup>1</sup> Firstly, this availability protects countries from supply fluctuations and undesirable political price

manipulations often seen with metals with skewed global distributions.<sup>2</sup> Secondly, their economic viability is especially notable in the case of metal precursors used in the synthesis of hydrogenation catalysts. For example, for Fe-based catalysts, FeBr<sub>2</sub>, costs \$10.30 per gram.<sup>3</sup> On the other hand, for Ru-based catalysts, RuCl<sub>3</sub>, costs \$143.20 per gram.<sup>3</sup> Also, their affordability can often reduce or even eliminate the requisite of recycling steps that accompany the usage of platinum based-metal catalysts. Moreover, the environmental and pharmaceutical tolerance of these metals cannot be understated. In the industrial safety guidelines, the Q3D issued by the U.S. Food and Drug Administration (FDA) serves as the gold standard for the removal of impurities. According to the guideline, ruthenium (Ru) is categorized as a Class 2 element making it the second highest. The Q3D allows specific Permitted Daily Exposure (PDE) limits for elemental impurities like Ru, which are set at 10, 1, and 0.1 µg/g for oral, parenteral, and inhalation routes, respectively. In contrast, iron (Fe) is not subjected to any elemental impurity regulation concerning daily exposure highlighting the complications industry must acknowledge based on choice of metal.<sup>2</sup>

However, platinum group metals also come with their advantages. They tend to be more selective, possess tolerance to functional groups, and frequently demand less expensive ligands compared to their counterparts.<sup>4</sup> While the chemical industry consumes less than 50 tons of platinum group metals annually, the global reserves exceed 100,000 metric tons.<sup>5</sup> The narrative of resource scarcity may not be as urgent as often claimed. Additionally, in fine organic synthesis the common substrates and stoichiometric reagents deployed can be comparable expensive to catalytic amounts of noble metals.<sup>5</sup> A transition to implementing metals in row 3d as catalyst might not have significant economic benefits.<sup>5</sup> Both earth-abundant and platinum group metals offer distinct benefits and hurdles in chemical applications. Research should not be limited to one type, but instead should focus on innovative methods that capitalize on their strengths and address their challenges for a sustainable chemical future.

Methods for developing homogeneous iron-based catalysts have gained interest, due to sustainability and since iron displays "early" and "late" transition metal properties simultaneously, applying it to a wide range of chemistries.<sup>2</sup> A significant advancement is the iron-catalyzed dehydrogenation (DH) of formic acid for hydrogen evolution (Scheme

1.1).<sup>6</sup> Achieved using a PNP pincer-supported iron catalyst **A** in which a Lewis acid is used as a co-catalyst. The catalyst achieves a TON (24 h) of 38970 and a TOF of 18410 h<sup>-1</sup>. The reverse catalytic reaction for the hydrogenation of carbon dioxide was also achieved using a combination of an iron catalyst **A** or **B** and a Lewis acid with carbon dioxide as a cheap and abundant feedstock. This method, which also serves as a viable strategy for hydrogen storage cycles, is part of a broader movement towards meeting global energy demand through practical applications that utilize renewable feedstocks. By doing so, it contributes to a shift away from the environmentally harmful and depleting non-renewable fossil fuels.

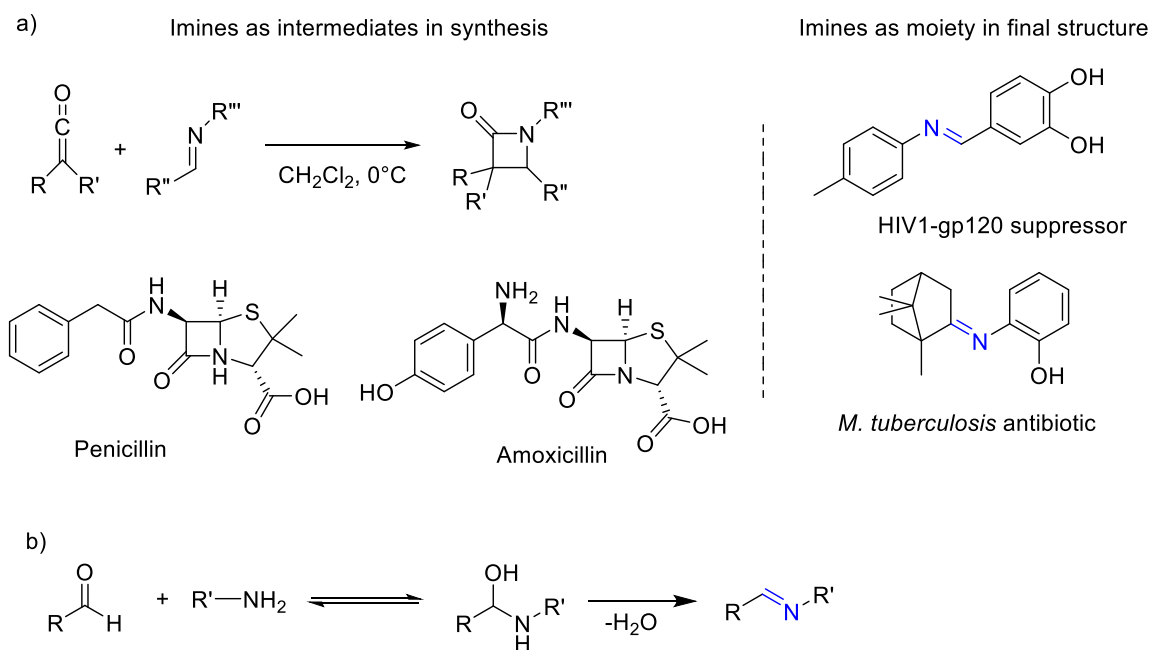


**Scheme 1.1** a) Dehydrogenation of formic acid for the release of H<sub>2</sub> with **A**. b) Hydrogenation of carbon dioxide for hydrogen storage cycles with **A** and **B**.<sup>6</sup> DBU (1,8-diazabicyclo[5.4.0]undec-7-ene).<sup>6</sup>

## 1.2 Traditional Methods for Synthesizing Imines, Nitriles, and *N*-Heterocycles: Their Global Impact and Alternative Synthesis Pathways

Imines are present in a wide range of syntheses; due to their versatility, they are used in larger, more complex structure creation or present as a moiety in the final structure.<sup>7,8</sup> An example of this is their roles in pharmaceuticals and medicinal chemistry where they are key components in medications. For instance, penicillin and amoxicillin, which are antibiotic and antibacterial drugs (Scheme 1.2a).<sup>9,10</sup> Also, imines can give rise to inhibitors,

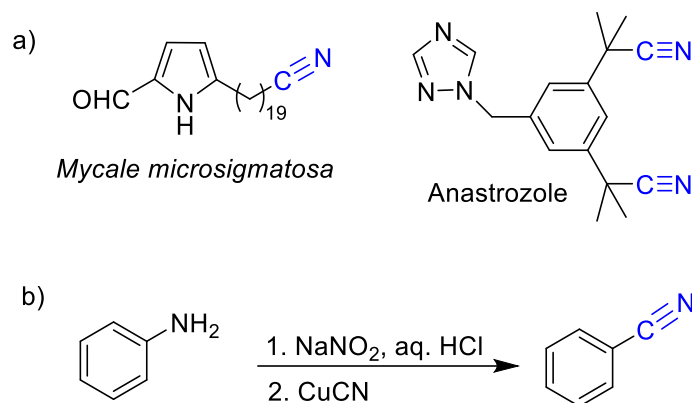
agents with antimalarial, and antifungal properties.<sup>7</sup> Traditional methods for the synthesis of imines involves the reaction of a ketone or aldehyde with a primary amine by acid-catalyzed condensation (Scheme 1.2b).<sup>11-13</sup> The method primarily requires electrophilic and nucleophilic aldehydes and amines, respectively, which limits the applicability to substituted substrates with similar electronics.



**Scheme 1.2** a) Dual role of imines: Pivotal intermediates in synthetic pathways and as integral structural moieties in pharmaceutically active molecules.<sup>7,9</sup> b) Acid-catalyzed condensation reaction of a carbonyl with a primary amine to synthesize an imine.<sup>11,12</sup>

Nitriles are essential moieties in organic chemistry, playing significant roles in a variety of applications due to their versatile chemical reactivity.<sup>14</sup> They are present in numerous compounds of industrial importance, with prominent use in pharmaceuticals, agrochemicals, dyes, and polymers. For example, *Mycale microigmatosa*, a natural product found in sponges from Venezuela.<sup>15</sup> In addition, anastrozole, a medication used in conjugation with other drugs for the treatment of breast cancer (Scheme 1.3a).<sup>15</sup> The traditional Sandmeyer reaction, discovered in 1884, is a widely used method to synthesize aryl nitriles from aryl amines (Scheme 1.3b).<sup>16</sup> This reaction involves the transformation of an aryl diazonium salt to an aryl nitrile using a copper salt. This reaction, despite being

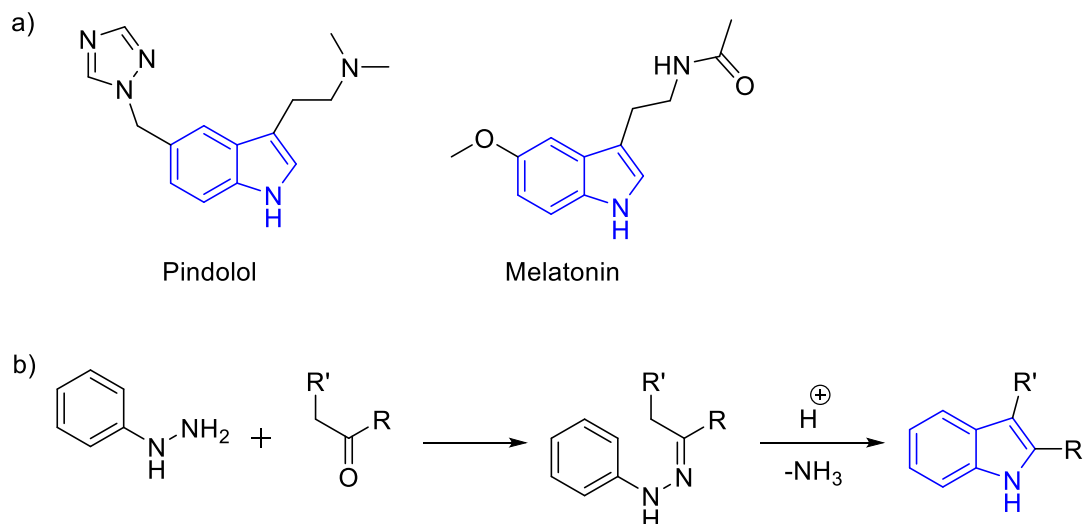
more than a century old, continues to be a reliable method for nitrile synthesis, highlighting the vital role of nitriles in various fields.



**Scheme 1.3** a) Nitriles as integral structural moieties in pharmaceutically active compounds.<sup>15</sup> b) Sandmeyer reaction, aryl nitrile synthesis from aryl amines with a nucleophilic substitution of a cyanide ion from  $\text{CuCN}$ <sup>16</sup>

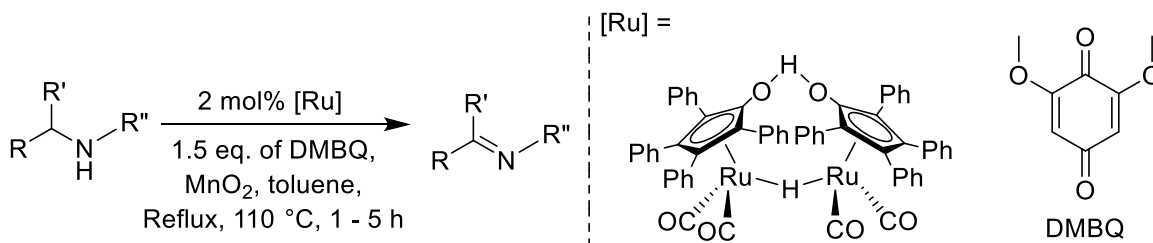
*N*-heterocycles are also recognized to play a prominent role in many active pharmaceutical ingredients due to the abundance of natural products containing an indole moiety.<sup>17,18</sup> For instance, pindolol, a medication used to regulate blood pressure and melatonin, a hormone regulating medication for sleep-wake cycles and possessing antioxidant properties (Scheme 1.4a).<sup>18</sup> Many syntheses for indoles exist and one traditional method, the Fischer indole synthesis, consists of the cyclization of an arylhydrazone with a carbonyl, using an acid catalyst (Scheme 1.4b).<sup>19</sup> However, the use of unsymmetric ketones results in poor regioselectivity making the classic method less applicable for the total synthesis of complex products.<sup>20</sup>





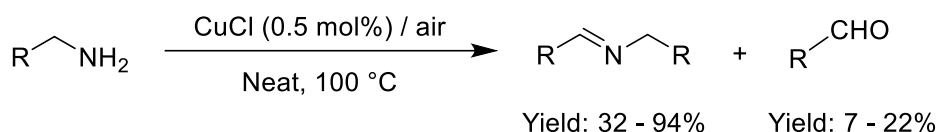
**Scheme 1.4** a) *N*-heterocycles as integral structural moieties in pharmaceutically active compounds.<sup>17,18</sup> b) Fischer Indole Synthesis, Acid-catalyzed reaction to convert arylhydrazone and an aldehyde or ketone to an indole.<sup>20</sup>

Transition-metal catalysts can be deployed for imine synthesis via oxidative dehydrogenation (ODH) of amines (Scheme 1.5).<sup>21</sup> A mixture of oxidized products is observed, such as imines, nitriles, and aldehydes, depending on the oxidant and reaction conditions. One example is Shvo's catalyst, a ruthenium-based catalyst, used in combination with MnO<sub>2</sub> as an oxidant to catalyze dehydrogenation to give imines selectively from amines. When deploying a variety of amines differing in electronic and steric properties the method achieved yields ranging from 30 – 90 %. From a sustainability standpoint, the utilization of MnO<sub>2</sub> as an oxidant and DMBQ (2,6-dimethoxyquinone) as a reversible H<sub>2</sub> acceptor at 1.5 equivalents presents drawbacks. Relying on excess of any reagent, like MnO<sub>2</sub> or DMBQ in this case makes the reaction less green and potentially more costly both environmentally and economically.



**Scheme 1.5.** Synthesis of Imines from amines using Shvo's catalyst in the presence of an oxidant and a hydrogen acceptor.<sup>21</sup>

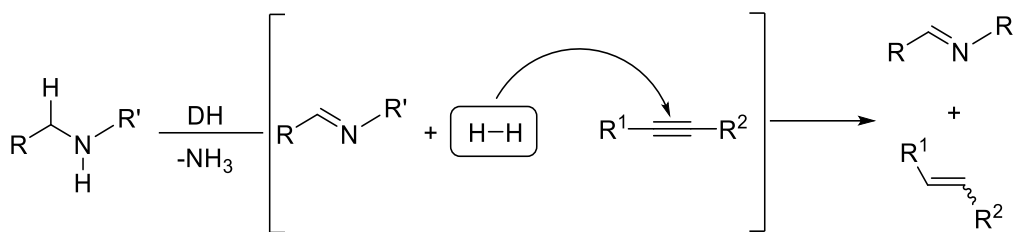
Aerobic oxidation of amines is a specific form of ODH. In this method, molecular oxygen ( $\text{O}_2$ ) from the air serves as the oxidizing agent. The process converts amines into their corresponding oxidized products, such as imines, nitriles, or amides. This method has mainly been studied by using metal catalysts that contain precious metals. Many copper-based catalysts have been reported for ODH of primary amines to give imines.<sup>22-24</sup> One example in 2012, Patil and co-workers deployed a copper(I) chloride catalyst for aerobic oxidation of amines to give the corresponding imines (Scheme 1.6).<sup>25</sup> The system proved to be applicable to a wide range of amines including benzylamines with electron-donating and withdrawing substituents, cyclic secondary amines, aliphatic amines, heteroaromatic amines and unsymmetrically coupled imines. However, for aryl-substituted primary amines, the corresponding aldehyde by-product yields were observed ranging from 7 – 22%, showcasing concerns with selectivity.



**Scheme 1.6** Copper(I)-chloride catalyzed oxidation of amines to form imines and the aldehyde by-product.<sup>25</sup>

Another approach to the synthesis of imines from amines is through the process of transfer dehydrogenation. This procedure involves a metal-catalyzed reaction wherein the substrate undergoes oxidation via hydrogen removal.<sup>26</sup> Essential to this reaction is the inclusion of an alkyne as a stoichiometric additive, acting in the crucial role of the hydrogen acceptor

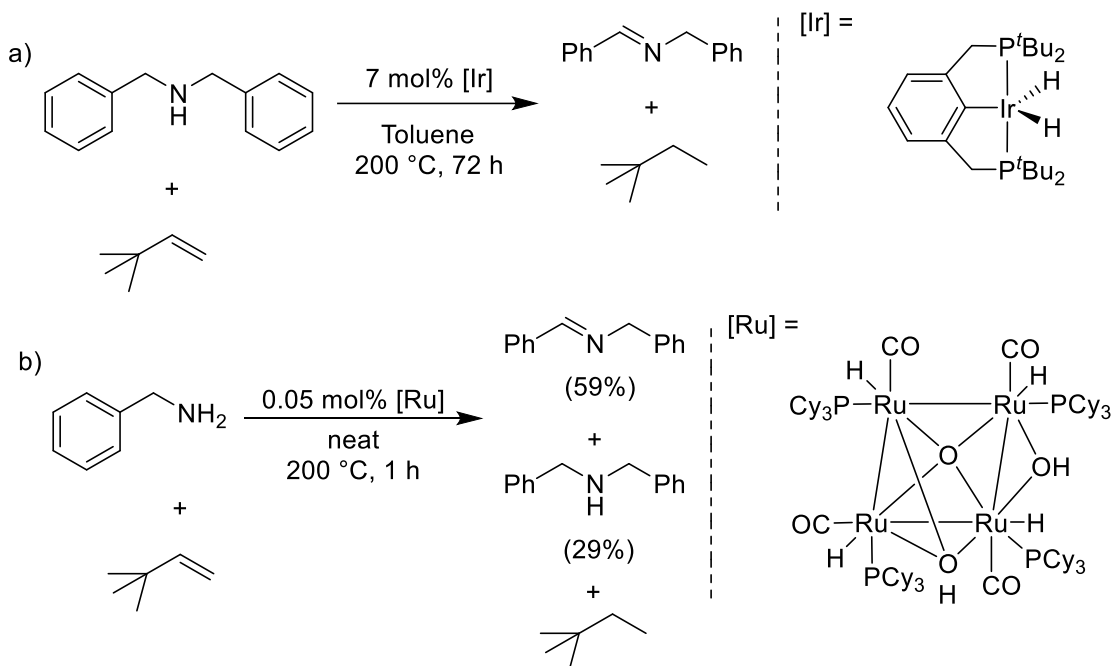
(H<sub>2</sub> acceptor) molecule to direct the reaction toward the product producing one equivalent of waste (Scheme 1. 7).<sup>26</sup>



**Scheme 1.7** General scheme of *in situ* transfer dehydrogenation from amines and alkynes to produce imines and alkenes.<sup>26</sup>

Transfer dehydrogenation to synthesize imines was demonstrated using an Ir(III)-PCP pincer complex in 2002 by Jensen and co-workers (Scheme 1.8a).<sup>27</sup> However, in this study the transformation required harsh reaction conditions. While this method offers an alternative way to synthesize the desired product, it requires a notably higher catalyst loading of 7 mol%, especially when compared to existing methods using platinum-based metals, which can operate with as low as 0.5 mol%. Also, executing reactions at elevated temperatures, such as 200 °C, presents significant challenges, often leading to increased costs and concerns about equipment durability. Furthermore, an extended reaction duration of 72 h is not ideal, as prolonged processes can reduce throughput and increase overall production timeline. Hence, finding reaction conditions that are more moderate and time-efficient would be more amenable. These demanding conditions highlight the need for optimization of this method. In 2008, Lee and Yi explored this area further, using a different catalyst, by developing a Ru-complex applicable for transfer dehydrogenation of amines (Scheme 1. 8b).<sup>28</sup> To test the catalyst efficacy a variety of amines and *N*-heterocycles were used, and found to be effective at achieving a TON ranging from a low of 35 to as high as 8000. However, in order to achieve good conversion high temperatures of 200 °C was needed and *tert*-butylethylene was used as the H<sub>2</sub> acceptor additive. A product mixture was observed that consisted of the symmetrical imine and a secondary amine, giving rise to complications with selectivity. Formation of the secondary amine indicates that hydrogenation of the imine occurred as a side reaction, instead of the complete hydrogenation of the sacrificial H<sub>2</sub> acceptor alkene. Overall, transfer

dehydrogenation is another alternative to synthesizing important moieties nonetheless disadvantages are present such as harsh reaction conditions (temperature, time, catalyst loading), use of a stoichiometric equivalent of a sacrificial H<sub>2</sub> acceptor molecule, and selectivity issues due to the formation of a product mixture.



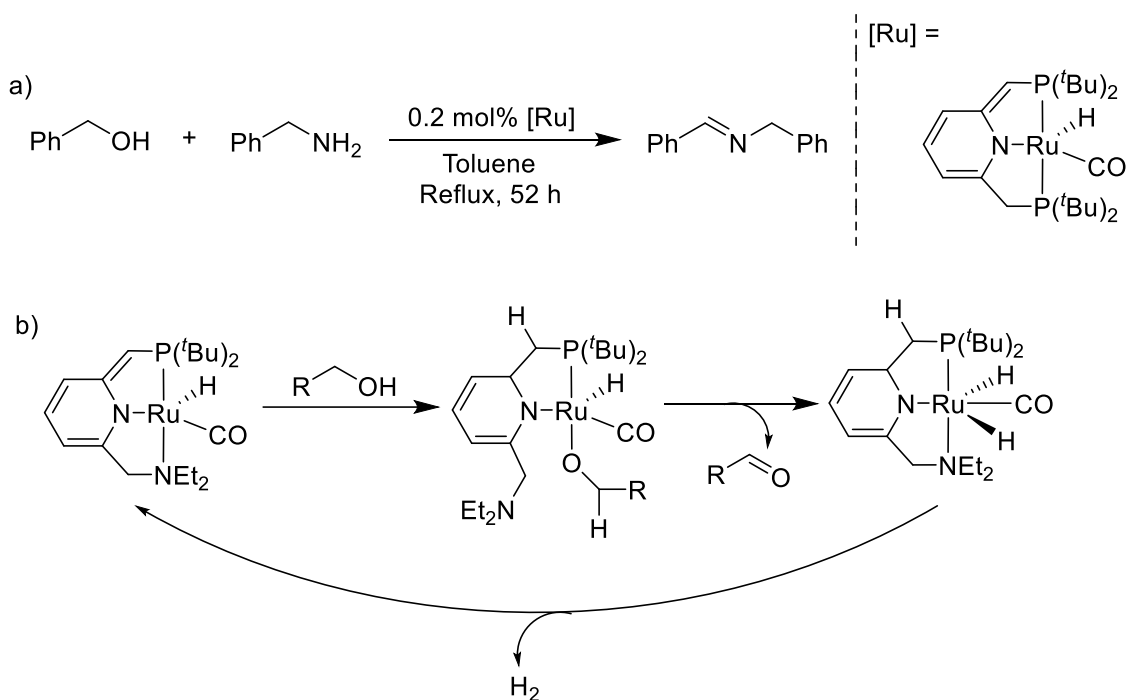
**Scheme 1.8** a) Synthesis of secondary aldimine and an alkane by catalytic transfer dehydrogenation using dibenzylamine and an alkene sacrificial hydrogen acceptor.<sup>27</sup> b) Catalytic transfer dehydrogenation of benzylamine to form a product mixture of secondary aldimine and secondary amine.<sup>28</sup>

Another catalytic method for accessing imines is through the coupling of alcohols and amines known as acceptorless dehydrogenative coupling (**ADC**) (Scheme 1.9).<sup>8</sup> Alcohols as starting materials pose many advantages such as being readily available, inexpensive, and should theoretically produce only water and hydrogen as by-products. This method improves sustainability since it does not require an H<sub>2</sub> sacrificial acceptor molecule reducing stoichiometric waste when compared to transfer dehydrogenation.



**Scheme 1.9** Acceptorless dehydrogenative coupling (ADC) of an alcohol and primary amine to synthesize an imine.<sup>8</sup>

In 2010, Milstein and co-workers reported a Ru(II)-PNP pincer complex that facilitated the acceptorless dehydrogenative coupling of primary alcohols and amines to form an imine. Impressively, the reaction yielded only the desired imine, avoiding the unwanted transformation of this imine into a secondary amine, a process that often complicates selectivity in similar reactions (Scheme 1.10a).<sup>29</sup> This innovative complex with pyridine part of the PNP ligand reveals a novel mode of metal-ligand cooperation. The ligand actively engages in the catalytic mechanism by deprotonating the primary alcohol and facilitating the alkoxide addition to the metal center making it a prime example of catalysis by a metal-ligand cooperative (MLC) pathway (Scheme 1.10b).<sup>29</sup> The aldehyde released can then couple with an amine. This class of catalysts holds a distinct edge over non-MLC catalysts because their ligand backbone houses an intramolecular base, eliminating the need for an exogenous base. The environmentally friendly attributes of this method are noteworthy and include, the use of readily available substrates, minimized waste, and produce water and hydrogen gas as the only by-products. Despite these advantages, acceptorless dehydrogenative coupling is not without room for improvement. Refinements in lowering reaction temperature and decreasing reaction time could enhance the process further.

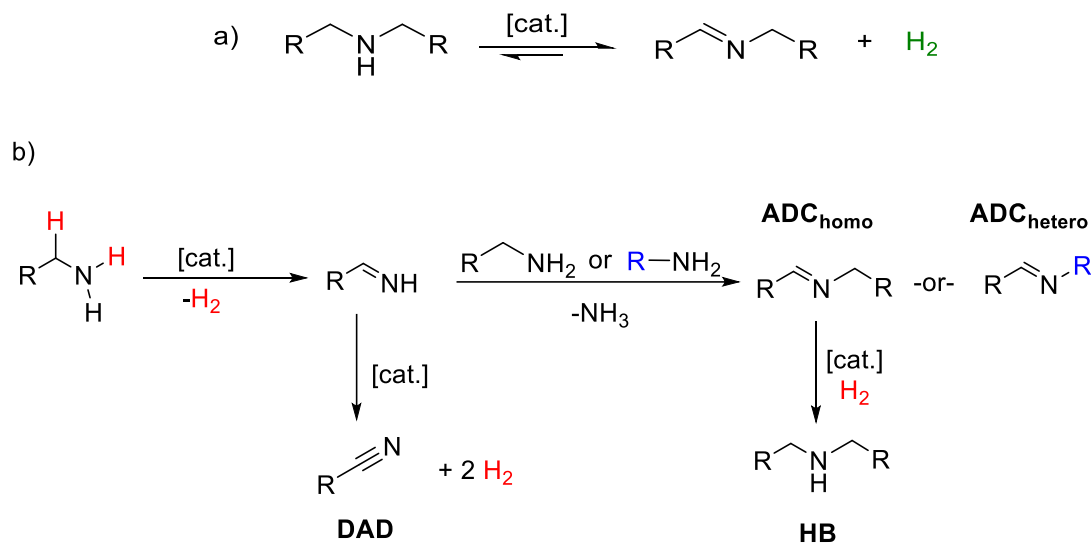


**Scheme 1.10** a) Ru(II)-PNP pincer complex facilitating the acceptorless dehydrogenative coupling of primary alcohols and amines to form an imine.<sup>29</sup> b) Ru(II)-PNN pincer complex catalytic mechanism that displays the metal-ligand cooperation in the catalytic cycle.<sup>29</sup>

### 1.3 Acceptorless Dehydrogenation of Amines using Transition Metal Catalysts

The synthesis of imines via condensation reactions must account for many factors: steric hinderance can prevent the approach of reactants; less reactive carbonyl compounds or amines, particularly secondary amines, may not participate in the reaction. Additionally, functional group sensitivity, unfavorable equilibrium conditions, and the need for dehydration agents which would further complicate or inhibit imine formation. These challenges in the condensation approach can limit the versatility of imine synthesis, prompting research into alternative methods to overcome such barriers. Acceptorless dehydrogenation (AD) is an effective method to synthesize imines from amines by use of a catalyst (Scheme 1.11a). AD reactions afford hydrogen gas as the only by-product, which is non-polluting and valuable, also the reaction avoids formation of toxic waste since AD reactions are oxidant free. However, AD reactions afford a product mixture when primary

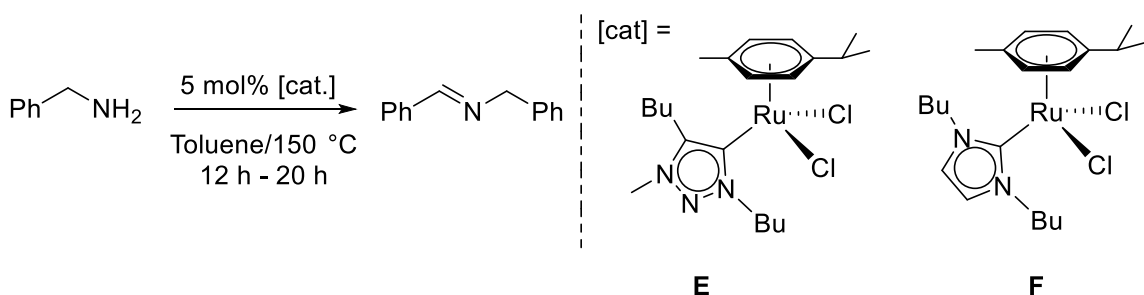
amines are deployed as the starting materials (Scheme 1.11b). A primary amine can undergo an AD reaction to afford a reactive primary imine, followed by a condensation reaction with another equivalent of substrate to give the homocoupled acceptorless dehydrogenative coupled (**ADC<sub>homo</sub>**) product. If a primary amine additive, devoid of alpha hydrogens, is present, the heterocoupled **ADC** (**ADC<sub>hetero</sub>**) product is formed. This is crucial, as the presence of alpha hydrogens would lead to the dehydrogenation of the coupling partner itself. Alternatively, the primary amine substrate could undergo two dehydrogenation steps to afford a nitrile, which is the double acceptorless dehydrogenation (**DAD**) product. In addition, the catalyst can also hydrogenate the **ADC** product to produce the hydrogen borrowing (**HB**) product. The **ADC** and **DAD** products contain 1 or 2 more units of unsaturation with respect to the substrate benzylamine, classifying them as the dehydrogenated products. The **HB** product is the same oxidation state as the substrate benzylamine, classifying it as the hydrogenation product. A ratio comparison of **AD:HB** (**ADC + DAD:HB**) for catalysts affords their selectivity for either **AD** or **HB** products.



**Scheme 1.11** a) General scheme to synthesize imines by use of a catalyst via AD reaction. b) AD of primary amine to form homocoupled or heterocoupled **ADC**, **DAD**, and **HB** products.

The majority of the AD field utilize platinum group metals in their catalyst systems.<sup>30-41</sup> Albrecht and co-workers in 2011, reported the first transformation of a base-free catalytic

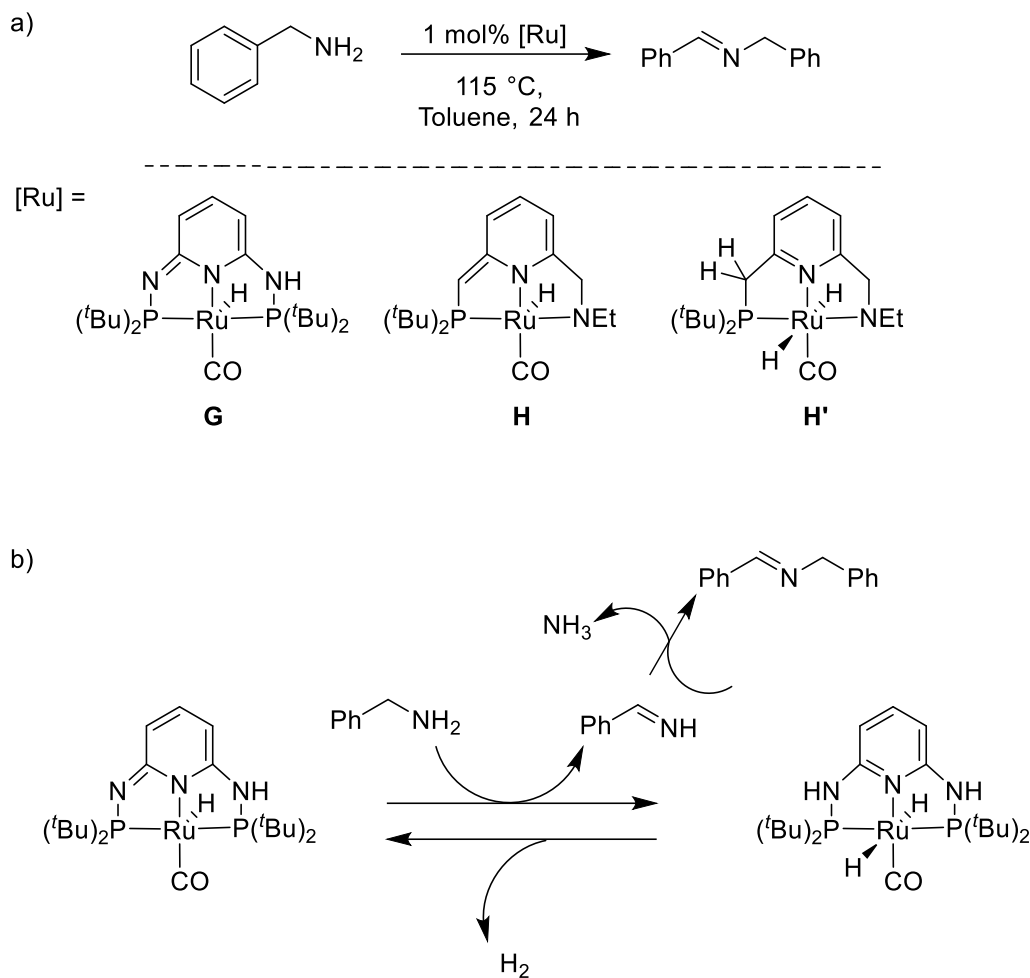
acceptorless dehydrogenation of primary amines.<sup>42</sup> A series of different Ru(II)-NHC complexes at 5 mol% catalyst loading were reacted with primary benzylic amines at 150 °C (Scheme 1.12).<sup>42</sup> The triazolylidene-based complex (**E**) was less active than the N-heterocyclic carbene (NHC) ligand complex (**F**), which reached complete conversion after 12 h. A consideration for this method is the reliance on relatively high temperatures and catalyst loading. Such conditions suggest that further refinement in catalyst structure might be warranted to potentially optimize the process.



**Scheme 1.12** Acceptorless dehydrogenative coupling of primary benzylic amines using Ru(II)-NHC complexes.<sup>42</sup>

In 2012, Huang and co-workers pioneered the use of a Ru(II) pyridine-based pincer transition-metal complex for dehydrogenative imine formation (Scheme 1. 13a).<sup>43</sup> They compared the performance of two complexes under identical conditions: complex **G**, a Ru-PNP complex featuring an imine in the ligand backbone; and complex **H**, a Ru-PNN complex with and alkene component. Complex **G** achieved 93% imine formation, outperforming **H**, which yielded 49% imine. This outcome suggests that the inclusion of an imine arm in the ligand enhances catalyst activity, by acting as an intramolecular base, leading to aromatization to form a pyridyl ring (Scheme 1. 13b).<sup>31</sup> The increased acidity of the N-H bonds in complex **G**'s hydrogenated imine intermediate, compared to the acidity of the C-H bonds in the alkene arm of complex **H** intermediate (**H'**), promotes a more rapid release of  $\text{H}_2$  and regeneration of the active catalyst. While the intermediate state of complex **G** has not been confirmed, it is hypothesized to follow the path of complex **H'**, which has been proven to exist.

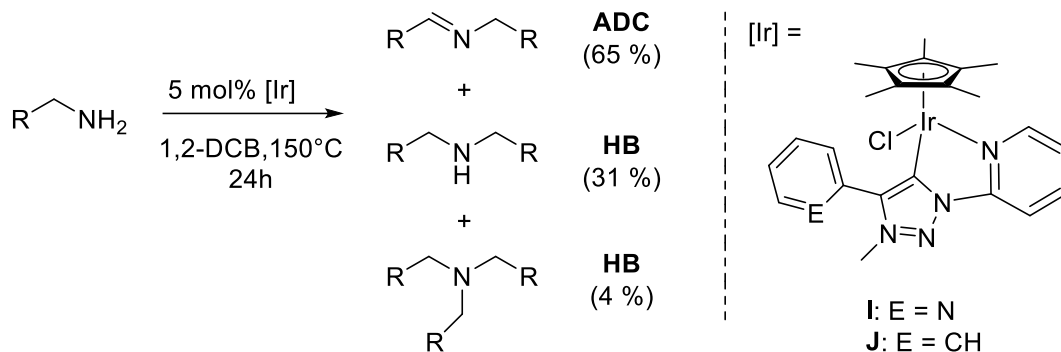




**Scheme 1.13** a) Acceptorless dehydrogenation of benzylamine facilitated by pincer complexes containing cooperative imine/alkene moieties to synthesize a secondary aldimine.<sup>43</sup> b) Acceptorless dehydrogenation of benzylamine using complex **G** yielding an imine. Mechanistic studies on complex **H** hypothesized the formation of complex **H'** as an intermediate.<sup>31</sup>

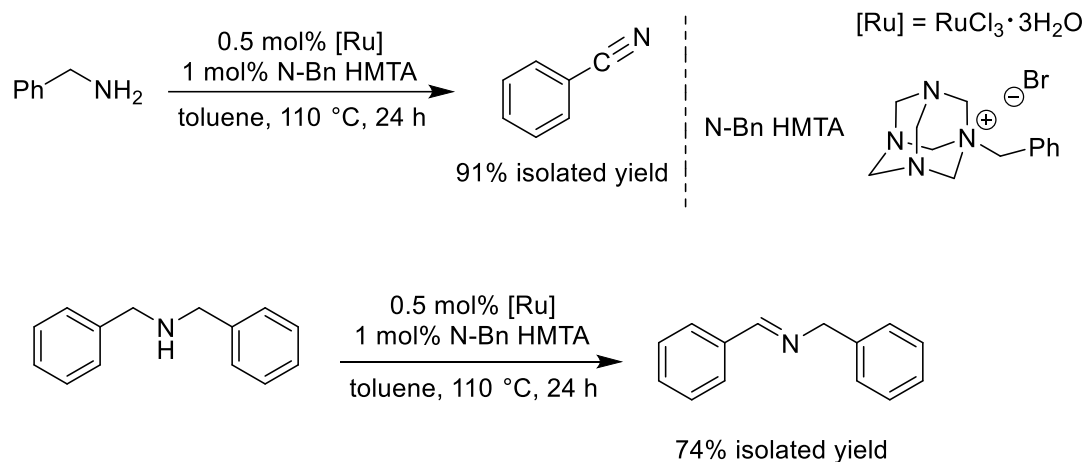
A study published by Albrecht and co-workers used two iridium(III) complexes containing a C,N-bidentate pyridyl-triazolydene ligand that differ in their pendant substituent (Scheme 1.14).<sup>44</sup> Complex **I** contained a non-coordinating pyridyl unit, and complex **J** contained a phenyl. Complex **I** revealed unique effects on the catalytic activity by showing higher rates and selectivity towards the imines. Both complexes resulted in high conversions after 24h giving a mixture of products comprised of **ADC** and **HB**. When **I** was used, the ratio of imine to secondary amine was 2:1. However, the phenyl-substituted triazolydene complex

**J** resulted in a ratio of 1:1. Suggesting that **I**, with the cooperative pyridyl moiety, resulted in higher selectivity towards the **ADC** product than the **HB** product when compared to the non-cooperative complex.



**Scheme 1.14** Catalytic dehydrogenation of primary amines with Iridium complexes to give a mixture of ADC and HB products.<sup>44</sup>

A noteworthy advancement in the field of AD of primary amines was made by Muthaiah and colleagues (Scheme 1.15).<sup>33</sup> They deployed ruthenium trichloride, supplemented with an additive, to facilitate AD of primary amines and secondary amines leading to the production of nitrile and imine products. The additive was hexamethylenetetramine (HMTA) or its derivatives, which serve multiple roles such as a hydride source, base, and reducing agent, essential for enabling  $\text{RuCl}_3$  to catalyze these substrates effectively. Under the influence of 0.5 mol%  $\text{RuCl}_3$  and 1 mol% N-Bn HMTA, an impressive 91% isolated yield of benzonitrile was achieved. Secondary amines like dibenzylamine were also explored, and a 74% isolated yield of the secondary imine was attained under similar conditions. Significantly, the utility of this catalyst/additive combination was further demonstrated with N-heterocycles, encompassing indolines, tetrahydroquinolines, and tetrahydroisoquinolines. This resulted in the synthesis of indoles, quinolines, and isoquinolines, correspondingly, all with high isolated yields.

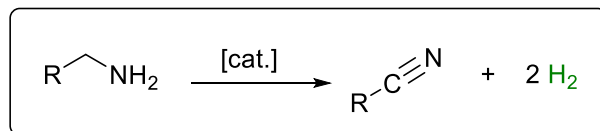


**Scheme 1.15** Synthesis of nitrile and secondary imine via acceptorless dehydrogenation of benzylamine and dibenzylamine, respectively.<sup>33</sup>

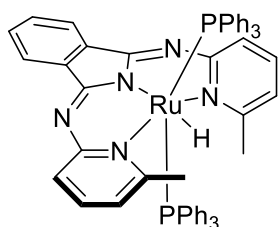
Many traditional methods exist to facilitate nitrile formation, such as the Sandmeyer reaction and oxidation of primary amines using metal catalysts mentioned above.<sup>16</sup> Acceptorless dehydrogenation (AD) of primary amines is an alternative to afford nitriles via a double acceptorless dehydrogenation, producing two equivalences of H<sub>2</sub> gas as the sole by-product (Figure 1.1). A number of transition metal catalyst have been reported for the AD of amines to nitriles.<sup>34,41,45,46</sup>

The first example by Szymczak in 2013, explored acceptorless dehydrogenation of primary amines to the corresponding nitriles (**DAD**).<sup>45</sup> The study centered on an amide-derived NNN-Ru(II) hydride complex, which operated through an oxidant-free, acceptorless, and chemoselective dehydrogenation system. Notably, this catalyst exhibited selectivity for the **DAD** product. Further mechanistic studies elucidated the catalysts preference for **DAD** over **ADC** product.

Mata and co-workers in 2016 reported that acceptorless dehydrogenation of primary amines to nitriles was possible with the ruthenium-based catalyst [(*p*-cym)Ru(NHC)Cl<sub>2</sub>]; however, an undesired **ADC** product was also formed.<sup>46</sup> Ruthenium catalysts with different electronic properties (Y = H, Me, or Cl) were evaluated, that all gave conversion >95%, and a mixture of **ADC** and **DAD**. The structural changes led to no significant difference in catalytic activity or product selectivity.

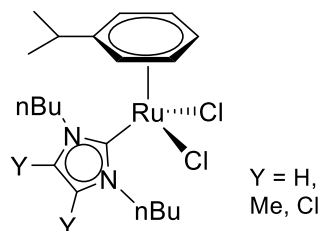


**Szymczack, 2013**



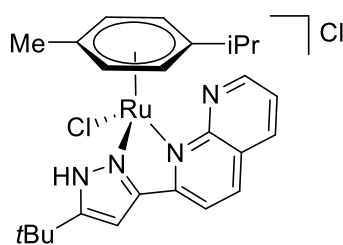
**1 mol%,**  
110 °C, 24 h

**Mata, 2016**



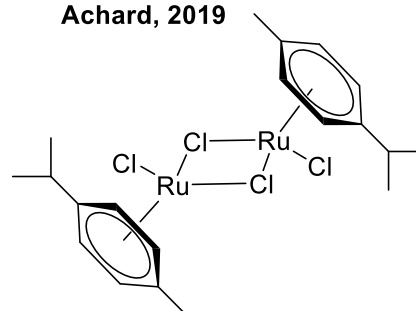
**2 mol%,**  
110 °C, ~8 h

**Holscher, Bera, 2018**



**2 mol%, KO<sup>t</sup>Bu**  
70 °C, 24 h

**Achard, 2019**



**2.5 mol%,**  
110 °C, 24 h

**Figure 1.1** The AD of primary amine to **DAD** by representative catalysts with their respective reaction conditions.<sup>34,41,45,46</sup>

In 2018, Bera and colleagues reported a ruthenium(I) complex equipped with a naphthyridine-functionalized pyrazole ligand, which catalyzed the oxidant-free and acceptorless selective double dehydrogenation of primary amines to nitriles under moderate conditions.<sup>41</sup> Notably, while the catalyst displayed selectivity across an extensive range of primary amines, the methodology included a substantial amount of additive base (KO<sup>t</sup>Bu) at 10 mol%. An additive poses challenges in atom economy, due to increasing the waste output of the reaction.

In 2019 Achard and co-workers explored a simple Ru(II) precursor, [Ru(*p*-cym)Cl<sub>2</sub>]<sub>2</sub>, exhibited selectivity in their optimization studies.<sup>34</sup> A scope study was conducted on alkyl

amines and benzylic amines under optimized conditions. Selective formation of the **DAD** product was observed for the alkyl amines, with product yields ranging from 50-85%. With benzylic amines, different steric and electronic effects were assessed with substituents on the phenyl ring; in all cases, selectivity decreased since the **ADC** by-product was observed. This method aids in the development of accessing nitriles from amines by use of a commercially available ruthenium precursor.

Numerous transition-metal catalysts have been reported for the AD of *N*-heterocycles.<sup>47-56</sup> Although the dehydrogenation of *N*-heterocycles is a thermodynamically uphill process, with the presence of a nitrogen atom the enthalpy of dehydrogenation is decreased compared to cycloalkanes. In 2014 Jones developed a Fe-pincer complex for the dehydrogenation of various *N*-heterocycles.<sup>54</sup> The products were isolated in good yields. Mechanistic studies supported the initial amine-dehydrogenation and highlight that the nitrogen atom as critical for lowering enthalpy to achieve successful dehydrogenation. A recent 2022 study by Gunanathan presented a readily accessible and selective ruthenium-catalyst, dinuclear monohydrido bridged complex  $[(\eta^6\text{-}p\text{-cymene})\text{RuCl}]_2(\mu\text{-H}-\mu\text{-Cl})$ .<sup>56</sup> The research delineated a two-step dehydrogenation process: an initial N-H activation by the metal center, followed by C-H activation and isomerization, leading to the release of molecular hydrogen and synthesis of imines.

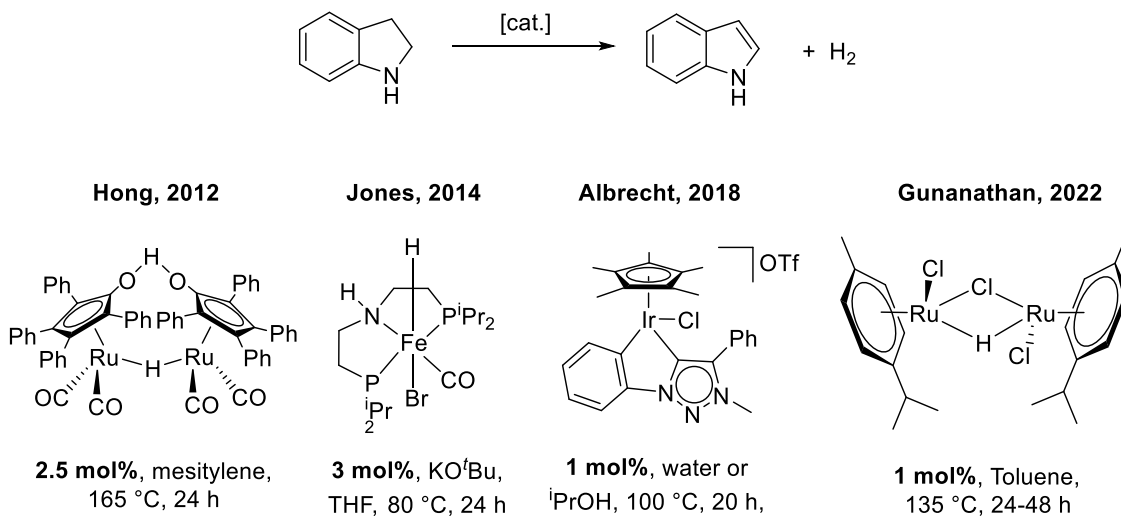


**Figure 1.2** AD of indoline to indole by various catalysts with their respective reaction conditions.<sup>53-56</sup>

## 1.4 Metal-Ligand Cooperative Catalysis using $P^{R_2}N^{R'_2}$ Ligands as Proton Shuttles

MLC catalysis refers to a catalytic transformation where both the metal center and the associated ligand directly participate in bond formation/cleavage steps. Within this framework, the 1,5-diaza-3,7-diphosphacyclooctane ( $P^{R_2}N^{R'_2}$ ) ligand showcases distinctive features such as cooperativity and adaptability.<sup>57-59</sup> Comprising an eight-membered ring structure, this ligand integrates two phosphine atoms located at the 1,5-positions, along with two nitrogen atoms situated at the 3,7-positions (Figure 1.3).<sup>60</sup> These atoms are interconnected by methylene groups. The ligand's adaptability originates from the R and R' groups, which can be modified to calibrate both steric and electronic characteristics.<sup>61,62</sup> When the phosphine atoms chelate to a metallic entity, the R group influences the metal center's electron density, as well as the steric conditions of the substrate binding region in the primary coordination sphere. Furthermore, the R'-groups play a crucial role in modulating the nitrogen atoms basicity and the spatial configuration of the amine, key factors that enable a pendant base to manage proton movement effectively within the secondary coordination sphere.

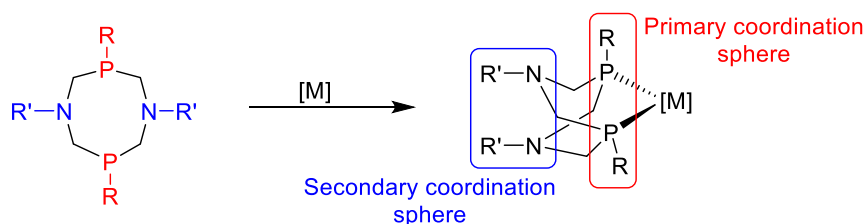
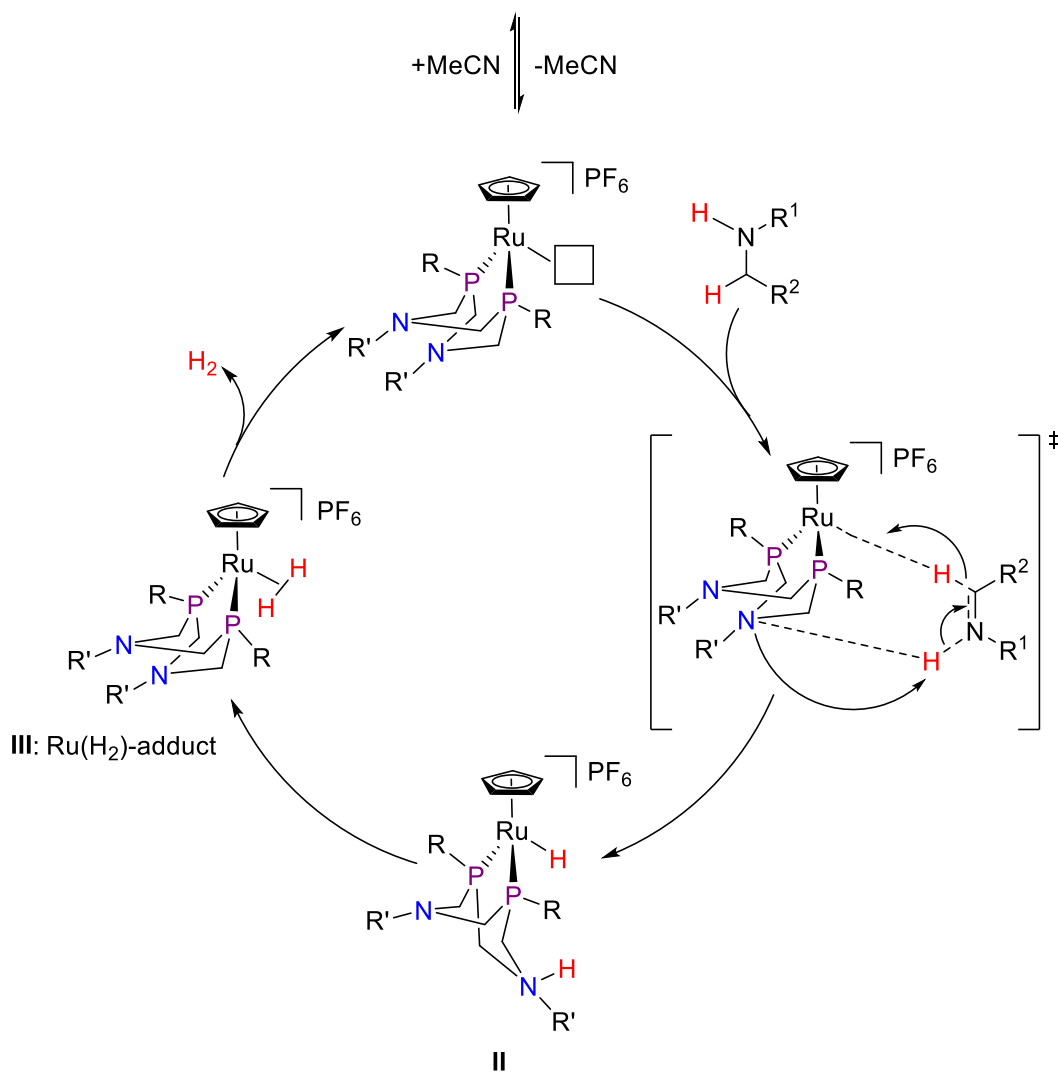


**Figure 1.3** The  $P^{R_2}N^{R'_2}$  ligand structure and its coordinating to a metal via the phosphine groups.

Metal-ligand cooperative catalysis is demonstrated in nature with hydrogenase enzymes, which catalyze the reversible heterolytic cleavage of  $H_2$ . The idea that a ligand can be involved in a chemical reaction at the metal center through proton-shuttling has influenced the design strategies for many catalysts. The designs prompt integration of acid/base groups into the supporting ligand structure. The versatility of  $P^{R_2}N^{R'_2}$  ligands in combination with ruthenium leads to an array of  $[Ru(Cp/Cp^*)(P^{R_2}N^{R'_2})(X/L)]PF_6$  complexes. These molecules are a piano stool-type anchored by a  $P^{R_2}N^{R'_2}$  ligand to the Ru core, coupled with

either a Cp or Cp\* unit. An open coordination site can readily become available for substrates since one coordination site is filled by a halide or solvent (X/L) during the catalytic cycle. The Blacquiere group has synthesized numerous analogous compounds, specifically  $[\text{Ru}(\text{Cp}/\text{Cp}^*)(\text{P}^{\text{R}}_2\text{N}^{\text{R}'_2})(\text{X}/\text{L})]\text{PF}_6$ , by substitution of ligands creating an effective strategy for generating Ru- $(\text{P}^{\text{R}}_2\text{N}^{\text{R}'_2})$  complexes for catalyst studies.<sup>63</sup> Mechanistic studies determined the catalytic mechanism with  $[\text{Ru}(\text{Cp})(\text{P}^{\text{Ph}}_2\text{N}^{\text{Ph}_2})(\text{MeCN})]\text{PF}_6$  (**Ru1b**) for the AD of amines (Scheme 1.16).<sup>64</sup> The mechanistic investigations have uncovered an outer-sphere cooperative mechanism for the catalytic cycle, where  $\text{H}_2$  is extracted from the substrate without any nitrogen binding. Evidence for this comes from the successful AD of N-methylindoline; where, the nitrogen atom lacks a proton, ruling out substrate binding at that site (inner sphere mechanism). Kinetic isotope effect studies reveal when using indole deuterated at the N/C2 positions, it decreases catalyst conversion. This suggests a concerted transfer of an equivalent of  $\text{H}_2$  to the active catalyst. The dehydrogenation process creates intermediate **II**. The role of the ligand in the heterolytic cleavage of  $\text{H}_2$  has been assessed in which  $\text{H}_2$  cleavage is reversible and facilitated by the  $\text{P}_2\text{N}_2$  ligand acting as a proton shuttle. These aspects make this class of catalyst unique compared to other known catalyst. The on cycle intermediate **III** (RuH<sub>2</sub>-adduct) can then release  $\text{H}_2$  to reform the catalyst to repeat the cycle. Furthermore, the Ru- $(\text{P}^{\text{R}}_2\text{N}^{\text{R}'_2})$  complexes have been engineered for  $\text{H}_2$  oxidation/production and alkyne hydrofunctionalization reactions.



**Scheme 1.16** General catalytic cycle for  $[\text{Ru}(\text{Cp/Cp}^*)(\text{P}^{\text{R}}_2\text{N}^{\text{R}'_2})(\text{MeCN})]\text{PF}_6$  complexes.<sup>64</sup>

Iron complexes analogous to the  $\text{Ru}(\text{P}^{\text{R}}_2\text{N}^{\text{R}'_2})$  complexes described above are hypothesized to operate through a similar catalytic mechanism. For instance, complex **M** containing  $\text{Cp}^*$  and  $\text{P}^{\text{Ph}}_2\text{N}^{\text{Ph}}_2$  ligands, functions as an active electrocatalyst for  $\text{H}_2$  production.<sup>65</sup> Conversely, a related complex bonded with an electron-deficient Cp derivative and  $\text{P}^{\text{tBu}}_2\text{N}^{\text{Bn}}_2$  is operative for the reverse  $\text{H}_2$  oxidation.<sup>66</sup> Fine tuning the ligand set allowed for isolation and characterization of likely  $\text{H}_2$  oxidation intermediates, including an iron dihydrogen adduct **L** and tautomer **M**, with hydride and protonated pendent amine.<sup>67,68</sup> The accessibility and catalytic activity of these compounds suggest that



an iron analogue of  $[\text{Ru}(\text{Cp})(\text{MeCN})(\text{P}^{\text{Ph}}_2\text{N}^{\text{Ph}}_2)]\text{PF}_6$  (**Ru1b**) would be a promising catalyst for the acceptorless dehydrogenation of amines.

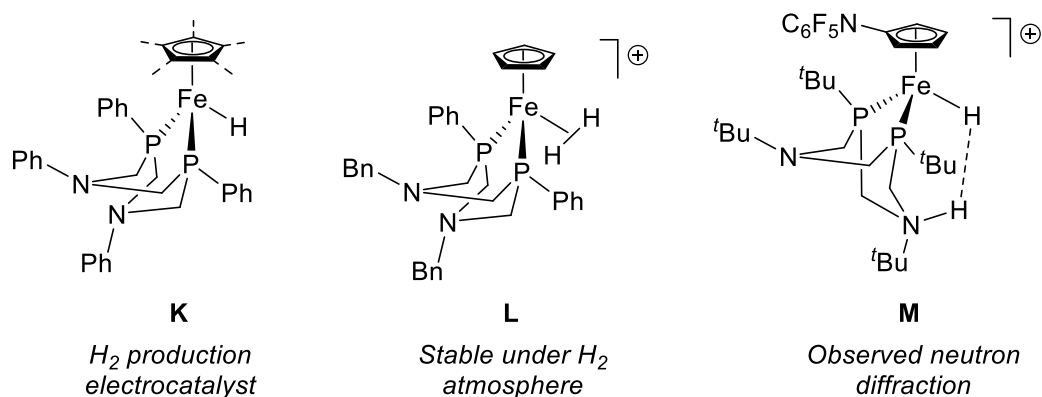


**Figure 1.4** Iron complexes that are H<sub>2</sub> production electrocatalysts (**M**) and models (**K** and **L**) for H<sub>2</sub> oxidation electrocatalysts.

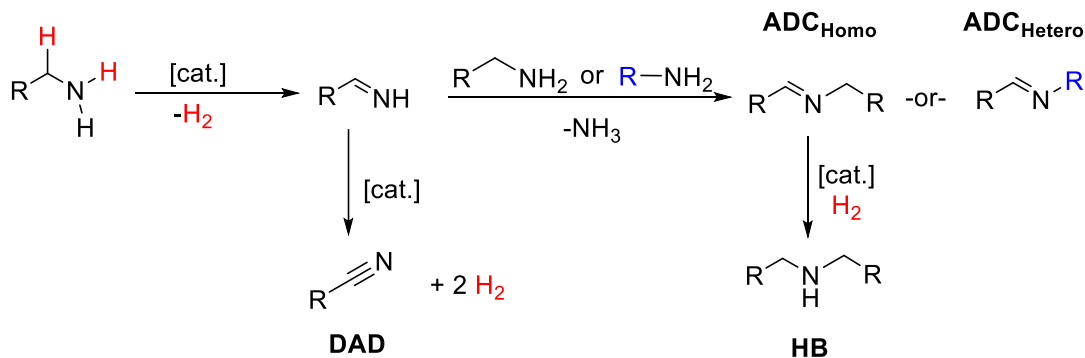
## 1.5 Scope of Thesis

This thesis outlines the assessment of MLC complexes of the type  $[\text{M}(\text{Cp}/\text{Cp}^*)(\text{MeCN})(\text{P}^{\text{R}}_2\text{N}^{\text{R}'}_2)]\text{PF}_6$  ( $\text{M} = \text{Ru}, \text{Fe}$ ) toward the AD of amines. Newly synthesized ruthenium and iron complexes (**Ru1f** & **Fe1b**) will be discussed. Acceptorless dehydrogenation of *N*-heterocycles was conducted with a selection of ruthenium complexes to assess catalyst performance. The primary and secondary coordination spheres were modified to identify optimal catalyst structure for best performance.

Efforts toward improving the synthesis of  $[\text{Fe}(\text{Cp})(\text{MeCN})(\text{P}^{\text{Ph}}_2\text{N}^{\text{Ph}}_2)]\text{PF}_6$  (**Fe1b**), a newly reported iron complex were conducted. By analyzing various reaction outcomes, the work aimed to refine the synthesis process and overcome the challenges associated with it. An analogous complex,  $[\text{Fe}(\text{Cp})(\text{MeCN})(\text{P}^{\text{Ph}}_2\text{N}^{\text{Bn}}_2)]\text{PF}_6$  (**Fe1a**), was targeted. However, the synthesis of this particular complex presented certain complications, which are explored and discussed. The focus is not to present only methodologies and outcomes but also an understanding underlying complexity in the synthesis of these iron complexes.

Acceptorless dehydrogenation of benzylamine was conducted with a selection of Ru and Fe complexes to assess catalyst selectivity by determining product distribution of

**ADC:DAD:HB.** In order to investigate the selectivity exhibited by the newly reported iron complex (**Fe1b**) mechanistic investigations were conducted to determine catalyst efficacy and selectivity (Scheme 1.17).



**Scheme 1.17** AD of primary amine to form homocoupled or heterocoupled **ADC**, **DAD**, and **HB** products.

## 1.6 References

1. Perry A. Frey and George H. Reed. *ACS Chem. Bio.* **2012**, 7 (9), 1477-481
2. Fürstner, A. *ACS Cent. Sci.* **2016**, 2 (11), 778-789.
3. Zell, T.; Langer, R. *ChemCatChem* **2018**, 10 (9), 1930-1940.
4. Roundtable, N. R. C. C. S. *Replacing Critical Materials with Abundant Materials*; National Academies Press, **2012**.
5. Komarova, A. A.; Perekalin, D. S. *Organometallics* **2023**, 42 (13), 1433-1438.
6. Balaraman, E.; Nandakumar, A.; Jaiswal, G.; K. Sahoo, M. *Catal. Sci. Technol.* **2017**, 7 (15), 3177-3195.
7. Gutiérrez, R. U.; Hernández-Montes, M.; Mendieta-Moctezuma, A.; Delgado, F.; Tamariz, J. *Molecules* **2021**, 26 (13), 4092.
8. Patil, R. D.; Adimurthy, S. *Asian J. Org. Chem.* **2013**, 2 (9), 726-744.

9. da Silva, C. M.; da Silva, D. L.; Modolo, L. V.; Alves, R. B.; de Resende, M. A.; Martins, C. V. B.; de Fátima, Â. *J. Adv. Res.* **2011**, *2* (1), 1–8.
10. Sheehan, J. C.; Henery-Logan, K. R. *J. Am. Chem. Soc.* **1959**, *81* (12), 3089–3094.
11. Huang, J.-M.; Zhang, J.-F.; Dong, Y.; Gong, W. *J. Org. Chem.* **2011**, *76* (9), 3511–3514.
12. BILLMAN, J. H.; TAI, K. M. *J. Org. Chem.* **1958**, *23* (4), 535–539.
13. Schiff, Hugo. *Eur. J. Org. Chem* **1864**, *131*(1), 118–119.
14. Patil, R. D.; Gupta, M. K. *ASC* **2020**, *362* (19), 3987–4009.
15. Scotti, C.; Barlow, J. W. *Nat. Prod. Commun.* **2022**, *17* (5), 325–329
16. Beletskaya, I. P.; Sigeev, A. S.; Peregudov, A. S.; Petrovskii, P. V. *Organometallics* **2004**, *689* (23), 3810–3812.
17. Altamimi, M. A.; Hussain, A.; Alshehri, S.; Imam, S. S.; Alnami, A.; Bari, *Processes* **2020**, *8* (11), 1476.
18. Vitaku, E.; Smith, D. T.; Njardarson, J. T. *J. Med. Chem.* **2014**, *57* (24), 10257–10274.
19. Kaushik, N. K.; Kaushik, N.; Attri, P.; Kumar, N.; Kim, C. H.; Verma, A. K.; Choi, E. H. *Molecules* **2013**, *18* (6), 6620–6662.
20. Çelebi-Ölçüm, N.; Boal, B. W.; Hutters, A. D.; Garg, N. K.; Houk, K. N. *J. Am. Chem. Soc.* **2011**, *133* (15), 5752–5755.
21. Ell, A. H.; Samec, J. S. M.; Backvall, J.-E. *Chem. Commun.* **2002**, *33* (35), 1144–1145.
22. Sayre, L. M.; Tang, W.; Reddy, K. V.; Nadkarni, D. *Bioinorganic Chemistry of Copper* **1993**, *25*, 236–248.

23. Zhu, J.; Mirkin, C. A.; Braun, R. M.; Winograd, N. *J. Am. Chem. Soc.* **1998**, *120* (20), 5126–5127.
24. Minakata, S.; Ohshima, Y.; Takemiya, A.; Ryu, I.; Komatsu, M.; Ohshiro, Y. *Catalytic Chem. Lett.* **1997**, *26* (4), 311–312.
25. Patil, Rajendra Damu and Subbarayappa Adimurthy. *RSC Adv.* **2012**, 5119–5122.
26. Reyes-Sánchez, A.; Cañavera-Buelvas, F.; Barrios-Francisco, R.; Cifuentes-Vaca, O. L.; Flores-Alamo, M.; García, J. J. *Organometallics* **2011**, *30* (12), 3340–3345.
27. Gu, X.-Q.; Chen, W.; Morales-Morales, D.; Jensen, C. M. *J. Mol. Catal. A. Chem.* **2002**, *189* (1), 119–124.
28. Yi, C. S.; Lee, D. W. *Organometallics* **2009**, *28* (4), 947–949.
29. Gnanaprakasam, B.; Zhang, J.; Milstein, D. *Angew. Chem., Int. Ed.* **2010**, *49* (8), 1468–1471.
30. Venkanna, G. T.; Tammineni, S.; Arman, H. D.; Tonzetich, Z. J. *Organometallics* **2013**, *32* (16), 4656–4663.
31. Li, H.; Gonçalves, T. P.; Lupp, D.; Huang, K.-W. *ACS Catal.* **2019**, *9* (3), 1619–1629.
32. Cui, X.; Li, Y.; Bachmann, S.; Scalone, M.; Surkus, A.-E.; Junge, K.; Topf, C.; Beller, M. *J. Am. Chem. Soc.* **2015**, *137* (33), 10652–10658.
33. Kannan, M.; Muthaiah, S. *Synlett* **2020**, *31* (11), 1073–1076.
34. Achard, T.; Egly, J.; Sigrist, M.; Maise-François, A.; Bellemin-Laponnaz, S. *Chem. Eur. J.* **2019**, *25* (58), 13271–13274.
35. Takallou, A.; Habibi, A.; Halimehjan, A. Z.; Balalaie, S. *Appl. Organomet. Chem.* **2020**, *34* (3), 5379.

36. Bottaro, F.; Takallou, A.; Chehaiber, A.; Madsen, R. *EurJOC.* **2019**, *2019* (42), 7164–7168.
37. Chakraborty, S.; Leitus, G.; Milstein, D. *Angew. Chem. Int. Ed.* **2017**, *56* (8), 2074–2078.
38. Kannan, M.; Muthaiah, S. *Organometallics* **2019**, *38* (19), 3560–3567.
39. Utsumi, T.; Noda, K.; Kawauchi, D.; Ueda, H.; Tokuyama, H. *ASC* **2020**, *362* (17), 3583–3588.
40. Pretorius, R.; Olguín, J.; Albrecht, M. *Inorg. Chem.* **2017**, *56* (20), 12410–12420.
41. Dutta, I.; Yadav, S.; Sarbajna, A.; De, S.; Hölscher, M.; Leitner, W.; Bera, J. K. *J. Am. Chem. Soc.* **2018**, *140* (28), 8662–8666.
42. Prades, A.; Peris, E.; Albrecht, M. *Organometallics* **2011**, *30* (5), 1162–1167.
43. Thomas W. Myers and Louise A. Berben. *J. Am. Chem. Soc.* **2013**, *135* (27), 9988-9990
44. Valencia, M.; Pereira, A.; Müller-Bunz, H.; Belderraín, T. R.; Pérez, P. J.; Albrecht, M. *Chemistry* **2017**, *23* (37), 8901–8911.
45. Tseng, K.-N. T.; Rizzi, A. M.; Szymczak, N. K. *J. Am. Chem. Soc.* **2013**, *135* (44), 16352–16355.
46. Ventura-Espinosa, D.; Marzá-Beltrán, A.; Mata, J. A. *Chem. Eur. J.* **2016**, *22* (49), 17758–17766.
47. Yamaguchi, R.; Ikeda, C.; Takahashi, Y.; Fujita, K. *J. Am. Chem. Soc.* **2009**, *131* (24), 8410–8412.
48. Fujita, K.-I.; Wada, T.; Shiraishi, T. *Angew. Chem., Int. Ed.* **2017**, *56* (36), 10886–10889.

49. Fujita, K.; Tanaka, Y.; Kobayashi, M.; Yamaguchi, R. *J. Am. Chem. Soc.* **2014**, *136* (13), 4829–4832.
50. Stubbs, J. M.; Hazlehurst, R. J.; Boyle, P. D.; Blacquiere, J. M. *Catalytic Organometallics* **2017**, *36* (9), 1692–1698.
51. Muthaiah, S.; Hong, S. H. *ASC* **2012**, *354* (16), 3045–3053.
52. Esteruelas, M.; Lezáun, V.; Martínez, A.; Oliván, M.; Oñate, E. *Organometallics* **2017**, *36*.
53. Muthaiah, Senthilkumar; Hong, Soon Hyeok. *Adv. Synth. Catal.* **2012**, *354* (16), 3045–3053.
54. Chakraborty, S.; Brennessel, W. W.; Jones, W. D. *J. Am. Chem. Soc.* **2014**, *136* (24), 8564–8567.
55. Vivancos, Á.; Beller, M.; Albrecht, M. *ACS Catal.* **2018**, *8* (1), 17–21.
56. Manikpuri, D.; Pradhan, D. R.; Chatterjee, B.; Gunanathan, C. *Ruthenium. J. Chem. Sci.* **2022**, *134* (4), 112.
57. Bullock, R. M.; Helm, M. L. *Acc. Chem. Res.* **2015**, *48* (7), 2017–2026.
58. Jenny Y. Yang, Stuart E. Smith, Tianbiao Liu, William G. Dougherty, Wesley A. Hoffert, W. Scott Kassel, M. Rakowski DuBois, Daniel L. DuBois, and R. Morris Bullock. *J. Am. Chem. Soc.* **2013**, *135* (26), 9700–9712
59. Wiedner, E. S.; Yang, J. Y.; Dougherty, W. G.; Kassel, W. S.; Bullock, R. M.; DuBois, M. R.; DuBois, D. L. *Organometallics* **2010**, *29* (21), 5390–5401.
60. Märkl G, V.; Jin G, Y.; Schoerner, C. *Tetrahedron* **1980**, *21* (15), 1409–1412.
61. Tseng, Kuei-Nin & Kampf, Jeff & Szymczak, Nathaniel. *ACS Catal.* **2015**, *5*, 411–415.

62. Galan, B. R.; Schöffel, J.; Linehan, J. C.; Seu, C.; Appel, A. M.; Roberts, J. A. S.; Helm, M. L.; Kilgore, U. J.; Yang, J. Y.; DuBois, D. L.; Kubiak, C. P. *J. Am. Chem. Soc.* **2011**, *133* (32), 12767–12779.
63. Bow, J. J.; Boyle, P. D.; Blacquiere, J. M. *Eur. J. Inorg. Chem.* **2015**, *2015* (25), 4162–4166.
64. Hoffman, Matthew D., "Metal Ligand Cooperative Complexes for Acceptorless Dehydrogenation of Amines" (2021). *Electronic Thesis and Dissertation Repository*. 8306.
65. Weber, K.; Weyhermüller, T.; Bill, E.; Erdem, Ö. F.; Lubitz, W. *Inorg. Chem.* **2015**, *54* (14), 6928–6937.
66. Liu, T.; Dubois, D. L.; Bullock, R. M. *Nat. Chem.* **2013**, *5* (3), 228–233.
67. Liu, T.; Chen, S.; O'Hagan, M. J.; Rakowski DuBois, M.; Bullock, R. M.; DuBois, D. L. *J. Am. Chem. Soc.* **2012**, *134* (14), 6257–6272.
68. Liu, T.; Wang, X.; Hoffmann, C.; DuBois, D. L.; Bullock, R. M. *Angew. Chem. Int. Ed.* **2014**, *53* (21), 5300–5304.

## Chapter 2

### 2 Comparing Catalyst Performance for Acceptorless Dehydrogenation of *N*-Heterocycles using $[M(\text{Cp})(\text{MeCN})(\text{P}^{\text{R}}_2\text{N}^{\text{R}'}_2)]\text{PF}_6$

Acceptorless dehydrogenation (AD) was performed on indoline and indoline derivatives using different catalysts,  $[M(\text{Cp})(\text{MeCN})(\text{P}^{\text{R}}_2\text{N}^{\text{R}'}_2)]\text{PF}_6$  (Figure 2.1). The reaction involved heating to 110 °C for 24 h in anisole with varying catalyst loading (mol%) For indoline, the AD product indole was quantified by calibrated GC-FID analysis. The following sections will describe how differences in a catalyst performance arise, by highlighting key aspects of the reaction and catalyst structure. In addition, an aim to expand the applicability of the cooperative catalyst system to diverse substrates is explored. The catalyst comparison screen conducted by a previous member of the group revealed the optimal structural features for the placeholder ligand (Cp vs Cp\*) and the  $\text{P}^{\text{R}}_2\text{N}^{\text{R}'}_2$  substituents (R and R').<sup>1</sup> Together, the information indicated that the best-performing catalyst should be  $[\text{Ru}(\text{Cp})(\text{MeCN})(\text{P}^{t\text{-Bu}}_2\text{N}^{\text{Ph}}_2)]\text{PF}_6$  (**Ru1f**), which we prepared to evaluate this hypothesis. Additionally, **Ru1b** was chosen as the previous best catalyst and as a comparator for **Ru1f** to provide further insight into the differences and similarities between the two catalysts.

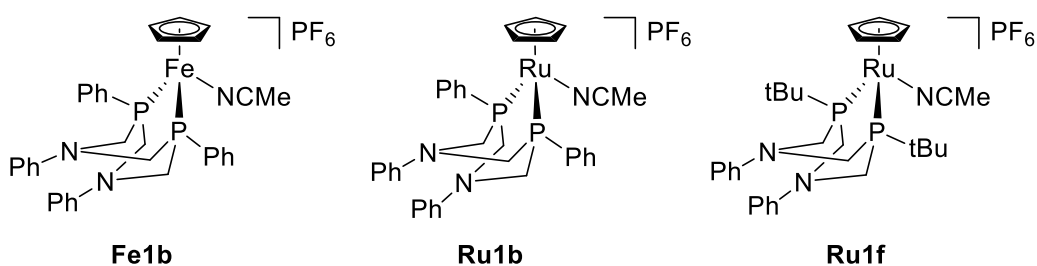


**Figure 2.1** The catalyst structures of  $[\text{Fe}(\text{Cp})(\text{MeCN})(\text{P}^{\text{Ph}}_2\text{N}^{\text{Ph}}_2)]\text{PF}_6$  (**Fe1b**),  $[\text{Ru}(\text{Cp})(\text{MeCN})(\text{P}^{\text{Ph}}_2\text{N}^{\text{Ph}}_2)]\text{PF}_6$  (**Ru1b**),  $[\text{Fe}(\text{Cp})(\text{MeCN})(\text{P}^{t\text{-Bu}}_2\text{N}^{\text{Ph}}_2)]\text{PF}_6$  (**Ru1f**).



## 2.1 Catalyst Comparison for Acceptorless Dehydrogenation of *N*-Heterocycles using $[M(\text{Cp})(\text{MeCN})(\text{P}^{\text{R}}_2\text{N}^{\text{R}'}_2)]\text{PF}_6$ Complexes

Indoline was chosen as the model substrate for the catalyst performance screen because only one product (indole) can be formed following acceptorless dehydrogenation and tautomerization. This permits a simple correlation of the catalyst activity with the structure, without complicating factors of selectivity. Using the conversion of the catalysts at 1 mol%, a ranking from highest to lowest is established of **Ru1b**  $\approx$  **Ru1f** > **Fe1b** (Table 2.1, Entries 1-3). The conversion and the expected product indole for complexes **Ru1b** and **Ru1f** differ by a negligible 3%. This suggests that catalyst efficiency is similar for that specific reaction. The conversion of **Fe1b** at 1 mol% was  $\sim$ 53% less than the ruthenium-based catalysts. This discrepancy in conversion indicates the formation of an unobserved by-product (noted as ‘missing’ material), which means mass balance was not achieved with **Fe1b**. When catalyst loading was reduced to 0.5 mol% to achieve catalyst-limiting conditions (Entry 4 & 5), **Ru1f** exhibited a 15% decrease in product yield compared to **Ru1b**. This indicated that **Ru1f** undergoes less productive cycles before deactivation than **Ru1b**. At loadings of 3 and 5 mol%, **Fe1b**, the product yield was less than 1% (Entry 6 & 7). No noticeable signs of unknown materials were observed in the GC-FID trace. There must be the formation of unexpected product(s). However, since there were no detectable signals in the GC-FID, it suggests that the product(s) may be unstable on the GC column or not volatile enough to be detected by GC-FID. Overall, the ruthenium-based catalysts performed significantly better when compared to the iron catalyst. This suggests the choice of metal plays an essential role in catalyst performance for AD of indoline.

**Table 2.1** The performance of catalysts **Ru1b**, **Ru1f**, and **Fe1b** towards the AD of indoline.<sup>[a]</sup>

Entry	Catalyst	mol %	%Conversion <sup>b</sup>	%Indole <sup>c</sup>	%Missing <sup>d</sup>
1	<b>Ru1b</b>	1	82	82	0
2	<b>Ru1f</b>	1	79	79	0
3	<b>Fe1b</b>	1	29	9	20
4	<b>Ru1b</b>	0.5	81	81	0
5	<b>Ru1f</b>	0.5	66	66	0
6	<b>Fe1b</b>	3	15	<1	14
7	<b>Fe1b</b>	5	20	<1	19

<sup>a</sup> Conditions: 250 mM indoline, 110 °C, 24 h in anisole. Data was quantified with respect to an internal standard by calibrated GC-FID. Reactions were run in duplicate with the data shown representing the average, which are within  $\pm 5\%$  error. <sup>b</sup> Conversion is calculated by the amount of indoline consumed. <sup>c</sup> In situ yield determine by calibrated GC-FID with an internal standard. <sup>d</sup> %Missing = %Conversion - %Indole.

## 2.2 Comparing Catalyst Performance using $[M(\text{Cp})(\text{MeCN})(\text{P}^{\text{R}}_2\text{N}^{\text{R}'}_2)]\text{PF}_6$ Complexes: Time Trace Analysis and Scope Study

The AD of indoline with 0.5 mol% of **Ru1b** and **Ru1f** was monitored over time (Figure 2.2). The R = *t*-Bu catalyst **Ru1f** gave a slightly lower maximum indole yield of 69% as compared with 82% for the R = Ph catalyst **Ru1b**. A noticeable difference in the rate of reaction emerged over time. Within the first hour, both catalysts **Ru1f** and **Ru1b** reached

similar levels of indole formation, suggesting comparable initial rates. However, when observed over the first 6 h, **Ru1f** generally exhibited a somewhat slower rate of reaction compared to **Ru1b**. This trend continued, and by the 24 h mark, **Ru1f** was found to be 13% lower in indole formation compared to **Ru1b**. Based on the catalyst screen, we expected a higher conversion with **Ru1f** relative to **Ru1b**. Thus, the relative performances of **Ru1b** and **Ru1f** do not match the expected trends based on the catalyst screen. This difference might reflect the long-range effects of the R and R' substituents that make independent optimization of the phosphorus and nitrogen substituents impractical. A comparison of catalyst performance with those of other catalysts for the AD of indoline revealed that **Ru1b** and **Ru1f** operate at similar or lower catalyst loadings and temperatures, but they reach a maximum conversion at shorter reaction times.

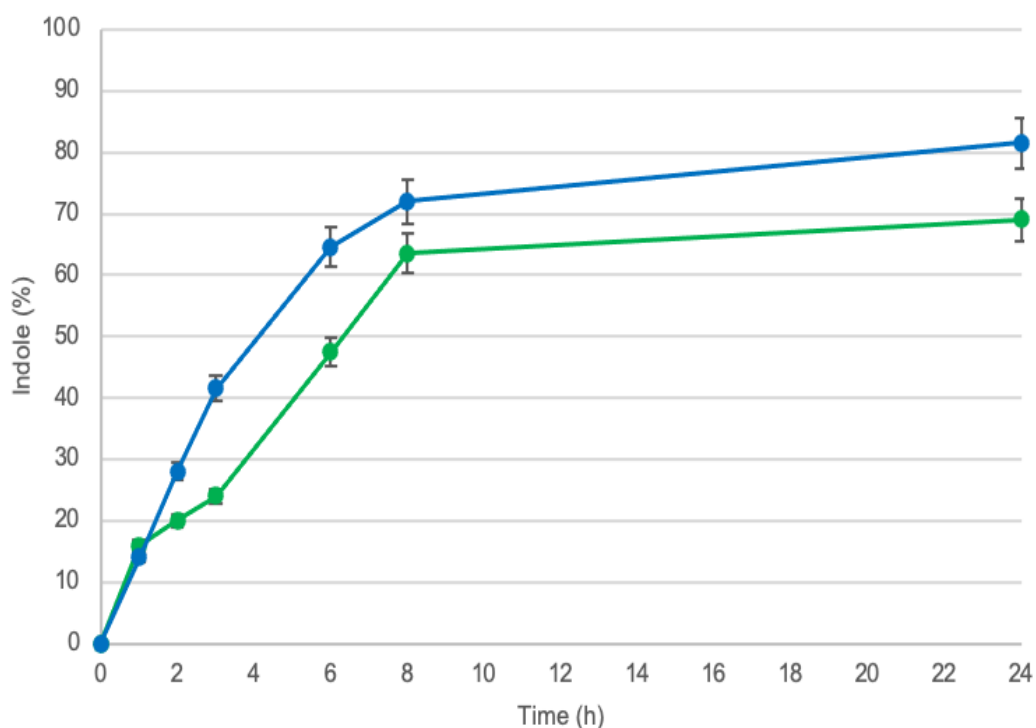


**Figure 2.2** Reaction profile for acceptorless dehydrogenation of indoline at 110 °C in anisole with 0.5 mol%  $P^R_2N^{Ph}_2$  catalysts **Ru1b** (R = Ph; blue) or **Ru1f** (R = *t*Bu; green) The conversion was monitored by calibrated GC-FID.

The AD performance of cooperative catalyst **Ru1b** and **Ru1f** was next evaluated toward a select scope of functionalized indolines (Figure 2.3). The scope study of **Ru1b** was previously conducted under standard conditions, utilizing 1 mol% of catalyst at 110 °C for 24 h in a closed system.<sup>2</sup> These same conditions were applied in this study for **Ru1f** to facilitate direct comparisons, ensuring that the evaluation between the two catalysts was consistent. Substitution with a fluoro group at the 5-position afforded the corresponding indole products with differing yields for the two catalysts: **Ru1f** produced 93% indole, while **Ru1b** led to a lower yield of 58%. For the 5-fluoroindoline substrate, an increase in N-H acidity due to the para disposition of the electron-withdrawing fluorine group was expected. This expected trend was confirmed with **Ru1f**, which yielded higher product formation compared to the unsubstituted indoline. Conversely, **Ru1b** displayed a lower yield for the fluorinated substrate, suggesting lower compatibility with Ar-F groups compared to **Ru1f**. The substrate containing electron-donating methoxy substituent gave higher yields for **Ru1f** than that of the fluoro derivative. Contrary to the expected hypothesis, due to the lower N-H acidity. Surprisingly, **Ru1f** achieved quantitative yields (>99%) for 5-methoxyindole at standard conditions suggesting no effect towards the catalyst performance from a lower N-H acidity. However, increasing the temperature to 125 °C when using **Ru1b** gave the 5-methoxyindole product in quantitative yields of >99%. Previously, we evaluated the performance of a related cooperative catalyst **Ru1a** (with R = Ph and R' = Bn substituents on the P<sup>R</sup><sub>2</sub>N<sup>R'</sup><sub>2</sub> ligand) with a 3 mol% loading toward a small selection of heterocyclic substrates. Catalyst **Ru1a** afforded indole, 2-methylindole, and quinoline in yields of 88, 78, and 11%, respectively. The yields for the same products with **Ru1b** and **Ru1f** were similar, except that the catalyst loading was three times lower. Both catalysts **Ru1b** and **Ru1f** under standard conditions were equally as compatible of steric bulk near the dehydrogenation site which was evaluated using 2-methylindoline as the substrate (43 and 42%, respectively). Unfortunately, the six-membered heterocycle isoquinoline was not formed in appreciable yields for either catalyst **Ru1b** and **Ru1f**.

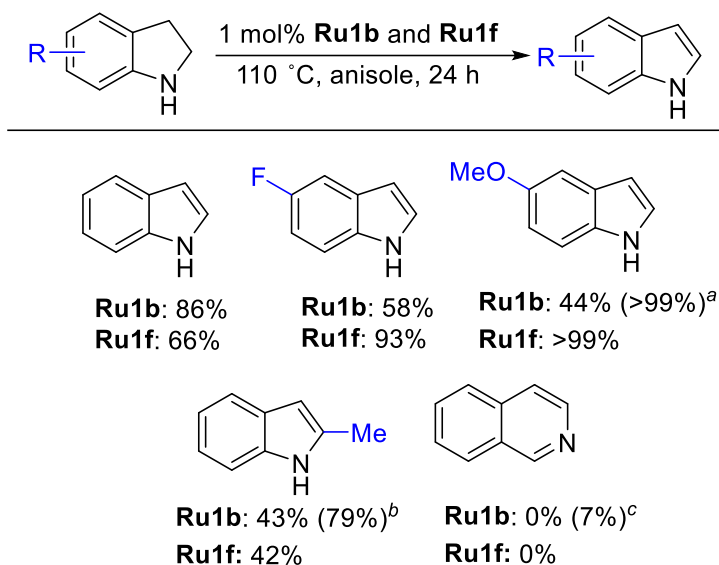
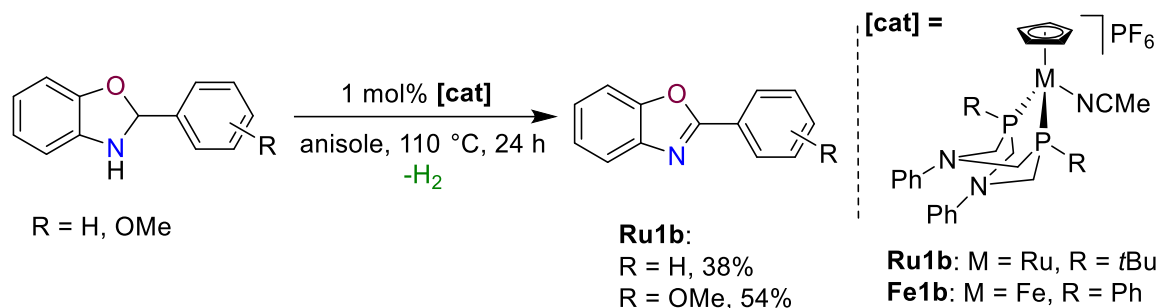


**Figure 2.3** Scope AD of substituted indolines using MLC catalysts **Ru1b** and **Ru1f**. *Reaction conditions:* Substrate (250 mM), catalyst (1 mol%), anisole, 110 °C, 24 h, sealed vial. Tetralin (100 mM) was used as an internal standard.<sup>2</sup> All data are averages of at least two trials; errors were all within  $\pm 5\%$ . Product yields were determined by GC-FID. <sup>a</sup> 125 °C, 3 h. <sup>b</sup> 125 °C, 12 h. <sup>c</sup> 125 °C, 24 h.

Given the higher catalytic performance of **Ru1f** in the AD of indoline derivatives, we expanded its applicability to the synthesis of oxazoles. The reactions were conducted under standard conditions of 1 mol%, 110 °C, in anisole for 24 h (Scheme 2.1). Although the *in situ* product yields observed for oxazoles were moderate when using **Ru1f**, these results point to a certain versatility in the types of products that this catalyst could potentially access. Preliminary attempts to utilize **Fe1b** for the synthesis of oxazoles were not successful (<10%). Even after extending the reaction time to 48 h, no significant improvement in yield was observed, underscoring the comparative advantage of **Ru1f** in the AD of heterocyclic substrates.



**Scheme 2.1** Synthesis of Oxazoles via AD using **Ru1f** and **Fe1b**.

## 2.3 Conclusions

Throughout this Chapter, the AD of indoline and its derivatives was explored, employing a series of catalysts, specifically the  $[\text{M}(\text{Cp})(\text{MeCN})(\text{P}^{\text{R}}_2\text{N}^{\text{R}'_2})]\text{PF}_6$ . The core explorations revolved around understanding the distinctions that arise due to different catalyst structures. A catalyst comparison screen from previous research established certain optimal structural features, like the placeholder ligand choices and the  $\text{P}^{\text{R}}_2\text{N}^{\text{R}'_2}$  substituents.<sup>1,2</sup> These insights paved the way for the synthesis and evaluation of the most promising catalyst,  $[\text{Ru}(\text{Cp})(\text{MeCN})(\text{P}^{\text{t-Bu}}_2\text{N}^{\text{Ph}}_2)]\text{PF}_6$  (**Ru1f**). **Ru1b** (R = Ph, R' = Ph) was used as a comparator for **Ru1f**, the only difference in structure being at the primary coordination sphere. Indoline, with its simplicity in AD product formation (yielding just indole), served as a fitting model substrate, enabling a straightforward correlation of catalyst activity with structure without complicating selectivity variables. This study revealed that both **Ru1f** and **Ru1b**, while being relatively close in performance, had some differences when examined further. Despite these observations, it was apparent that ruthenium-based catalysts displayed superior performance compared to their iron counterpart in the AD of indoline.

A time trace analysis, monitoring the AD of indoline over distinct timeframes, revealed reaction rate differences between **Ru1f** and **Ru1b**. Complex **Ru1f**, while beginning at a comparable rate to **Ru1b**, within the first 6 h a slower rate was observed. Further explorations into the performance of **Ru1b** and **Ru1f** with various functionalized indolines revealed that **Ru1f** had greater compatibility with electron-withdrawing groups. This was specifically observed in the case of the 5-fluoroindole product. Additionally, the

introduction of electron-donating substituent like the methoxy group revealed surprising findings. **Ru1f** exhibited exceptional yields under standard conditions even when theoretically expected to show a slowdown due to decreased N-H acidity. Moreover, comparisons with a previously explored catalyst, **Ru1a**, revealed that **Ru1b** and **Ru1f** could achieve similar yields at significantly lower catalyst loadings. Lastly, both **Ru1b** and **Ru1f** displayed commendable compatibility with steric bulk near the dehydrogenation site, as observed using 2-methylindoline. Yet, unfortunately, neither catalyst could produce appreciable yields of the six-membered heterocycle, isoquinoline. Given the promising performance of **Ru1f**, with substituted indoline/oxazoles, it stands out as the likely go-to catalyst for future work. The *t*-Bu group in **Ru1f** appears to confer a special reactivity profile that may make it valuable in synthesizing a diverse array of oxazole and thiazole products. In order to make a comparative analysis it would be worthwhile to compare **Ru1f** performance with **Ru1b** across a broader spectrum of substrates.

## 2.4 References

- (1) Stubbs, J. M.; Nanuwa, A. S.; Hoffman, M. D.; Blacquiere, J. M. *Synlett* **2023**, 34 (5), 445–450.
- (2) Stubbs, James M., "Developing Structure-Activity-Relationships for Metal-Ligand-Cooperative (MLC) Complexes using  $P^{R_2}N^{R'_2}$  Ligands" (2018). *Electronic Thesis and Dissertation Repository*. 6011.

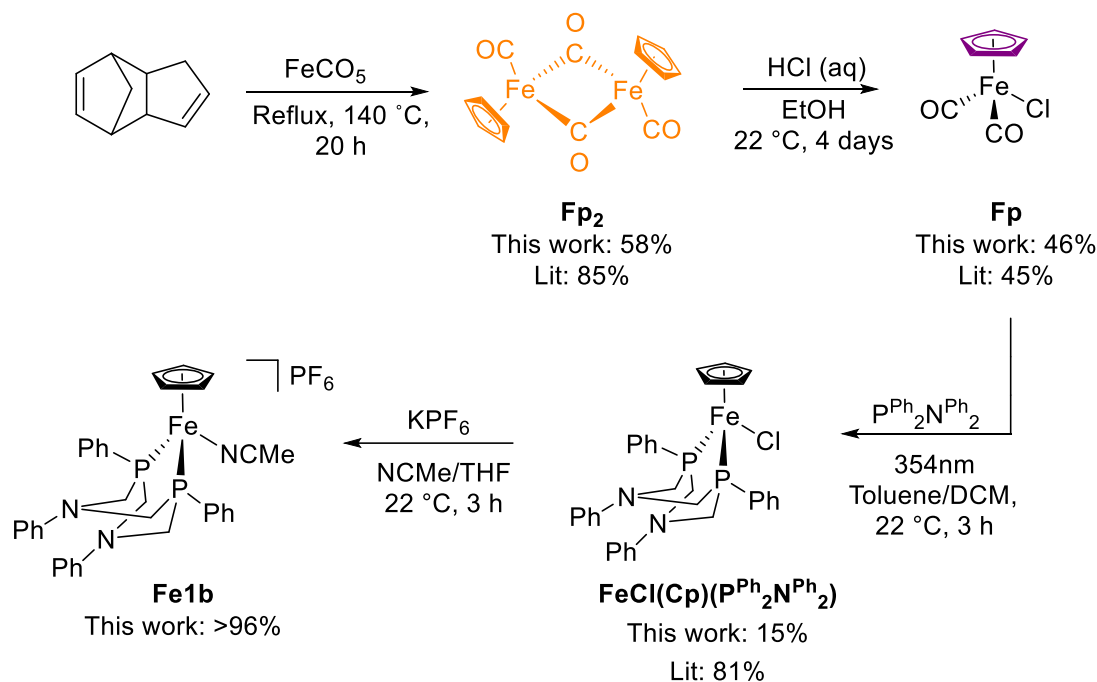
## Chapter 3

### 3 Challenges in the Synthesis of a Novel Iron Complex: Exploration of Diverse Methodologies and Outcomes

#### 3.1 Attempts to Modify and Improve the Synthesis of $\text{FeCl}(\text{Cp})(\text{P}^{\text{Ph}}_2\text{N}^{\text{Ph}}_2)$

Motivated by the selectivity of the **Fe1b** catalyst for the **ADC** product over the **HB** product in the AD of benzylamine, an improved synthesis for  $\text{FeCl}(\text{Cp})(\text{P}^{\text{Ph}}_2\text{N}^{\text{Ph}}_2)$ , a precursor in the catalyst synthesis, was targeted. The synthetic route to the **Fe1b** catalyst includes four significant steps (Scheme 3.1). First, the formation of  $[(\text{Cp})\text{Fe}(\mu\text{-CO})(\text{CO})]_2$  (**Fp2**) involves a one-pot reaction of dicyclopentadiene with iron pentacarbonyl that was refluxed for 20 h at 140 °C.<sup>1</sup> **Fp2** is then reacted with HCl to afford  $\text{FeCl}(\text{Cp})(\text{CO})_2$  (**Fp**).<sup>1</sup> Next, coordination of the  $\text{P}^{\text{Ph}}_2\text{N}^{\text{Ph}}_2$  ligand to the **Fp** by photolysis results in the formation of  $\text{FeCl}(\text{Cp})(\text{P}^{\text{Ph}}_2\text{N}^{\text{Ph}}_2)$ .<sup>2</sup> The last step in the synthetic route, developed by a prior group member, involves a halide abstraction, forming the **Fe1b** catalyst.<sup>3</sup> The following section will explain modification attempts made in the purification of  $\text{FeCl}(\text{Cp})(\text{CO})_2$  (**Fp**) and isolation of  $\text{FeCl}(\text{Cp})(\text{P}^{\text{Ph}}_2\text{N}^{\text{Ph}}_2)$  to increase the final product yield for the **Fe1b** complex.





**Scheme 3.1** General synthetic route for the synthesis of **Fe1b** catalyst. Optimized yield in this work and literature yield.<sup>1-3</sup>

Following the literature procedure, the synthesis for **Fp<sub>2</sub>** was carried out and obtained in moderate yields (58%). Next, **Fp** was synthesized and to purify the **Fp** complex the published literature method uses column chromatography. In this work, the post-column  $^1\text{H}$  NMR spectrum for **Fp** contained unknown signals in the upfield region (Figure 3.1). Also, the peak corresponding to the Cp ligand contains a shoulder, an impurity corresponding to the starting material, **Fp<sub>2</sub>**. To increase the purity of **Fp**, the purification was modified by adding a liquid-liquid extraction to remove excess HCl. The unknown peaks in the upfield region are absent in the  $^1\text{H}$  NMR spectrum for the **Fp** complex post-extraction, but a minor peak corresponding to the **Fp<sub>2</sub>** complex is still present. Comparing the relative integrations of the product signal (**Fp**), **Fp<sub>2</sub>**, and water, the **Fp** complex post-extraction was 96% pure, increasing its purity by 40%. The **Fp** complex was dried to ensure the removal of all water before using it for any synthesis.

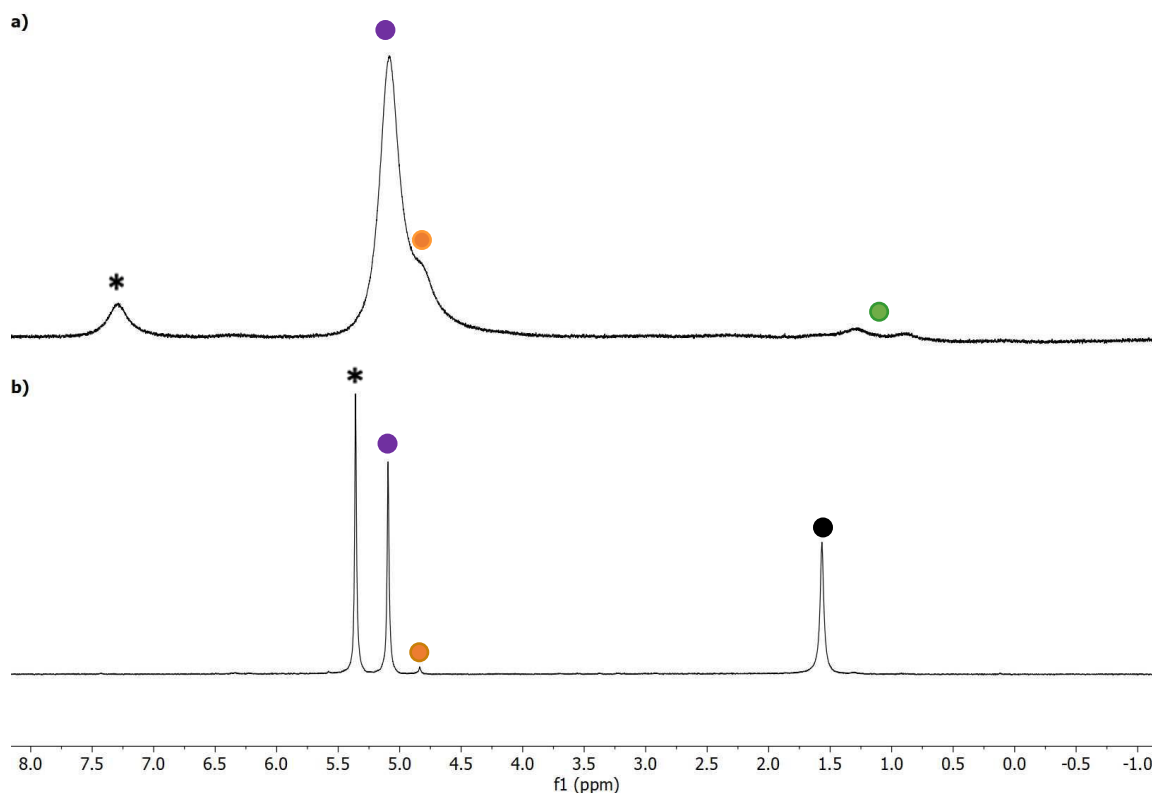


**Figure 3.1**  $^1\text{H}$  NMR spectrum stack plot of a) **Fp** in  $\text{CDCl}_3$  (\*) purified using column chromatography. The green dot (●) indicates the unknown signals in the upfield region. The orange dot (●) corresponds to the broad Cp ligand of **Fp2**. The purple dot (●) corresponds to **Fp**. b) **Fp** in  $\text{CD}_2\text{Cl}_2$  (\*) purified with column chromatography and liquid-liquid extraction. The (●) corresponds to the product, **Fp**. The orange dot (●) corresponds to **Fp2**. The black dot (●) corresponds to water.

The synthesis of  $\text{FeCl}(\text{Cp})(\text{P}^{\text{Ph}}_2\text{N}^{\text{Ph}}_2)$  follows a photolysis reaction of **Fp** with  $\text{P}^{\text{Ph}}_2\text{N}^{\text{Ph}}_2$  ligand that occurs over 2.5 – 3 h. To test the product conversion, a spectrum of the crude material revealed a major peak at 60 ppm corresponding to the coordinated ligand in  $\text{FeCl}(\text{Cp})(\text{P}^{\text{Ph}}_2\text{N}^{\text{Ph}}_2)$  (Figure 3.2). A minor peak at –50 ppm also exists and corresponds to the free  $\text{P}^{\text{Ph}}_2\text{N}^{\text{Ph}}_2$  ligand. Relative integrations of the two peaks indicate 87% product with 13% free ligand impurity. Notably, when crude material was stored in the freezer overnight, the relative integrations revealed a decrease in product and an increase in the free ligand (Figure 3.2). To prevent material decomposition workup was conducted the same day. Following the literature protocol, the crude material was washed with diethyl

ether, which should give the product dissolved in the filtrate. However, the limited solubility  $\text{FeCl}(\text{Cp})(\text{P}^{\text{Ph}}_2\text{N}^{\text{Ph}}_2)$  in diethyl ether impeded successful isolation for the product. For this reason, solubility testing was explored to determine the correct route to isolate the desired product. The  $\text{P}^{\text{Ph}}_2\text{N}^{\text{Ph}}_2$  ligand solubility was not considered due to easy removal following the subsequent synthesis of **Fe1b**. For solubility testing, solvents with a range of polarity indexes were considered (Table 3.1). Diethyl ether confirmed moderate solubility for  $\text{FeCl}(\text{Cp})(\text{P}^{\text{Ph}}_2\text{N}^{\text{Ph}}_2)$  but poor solubility for **Fp**, suggesting either a solvent mix or partial heating of the diethyl ether is required when washing the crude material to completely isolate the  $\text{FeCl}(\text{Cp})(\text{P}^{\text{Ph}}_2\text{N}^{\text{Ph}}_2)$  complex in the filtrate. The crude material of  $\text{FeCl}(\text{Cp})(\text{P}^{\text{Ph}}_2\text{N}^{\text{Ph}}_2)$  synthesis was pushed forward to the subsequent **Fe1b** synthesis stage. To assess whether the isolation and purification of  $\text{FeCl}(\text{Cp})(\text{P}^{\text{Ph}}_2\text{N}^{\text{Ph}}_2)$  is essential. However, the synthesis of **Fe1b** was unsuccessful highlighting the importance of clean material for the next step. Overall, **Fp** purity and isolation modifications to the procedure resulted in an increase in product yield from <10% to 15%. While the modifications are not monumental, improvements there were still noteworthy progress towards better understanding this step of the **Fe1b** synthesis.

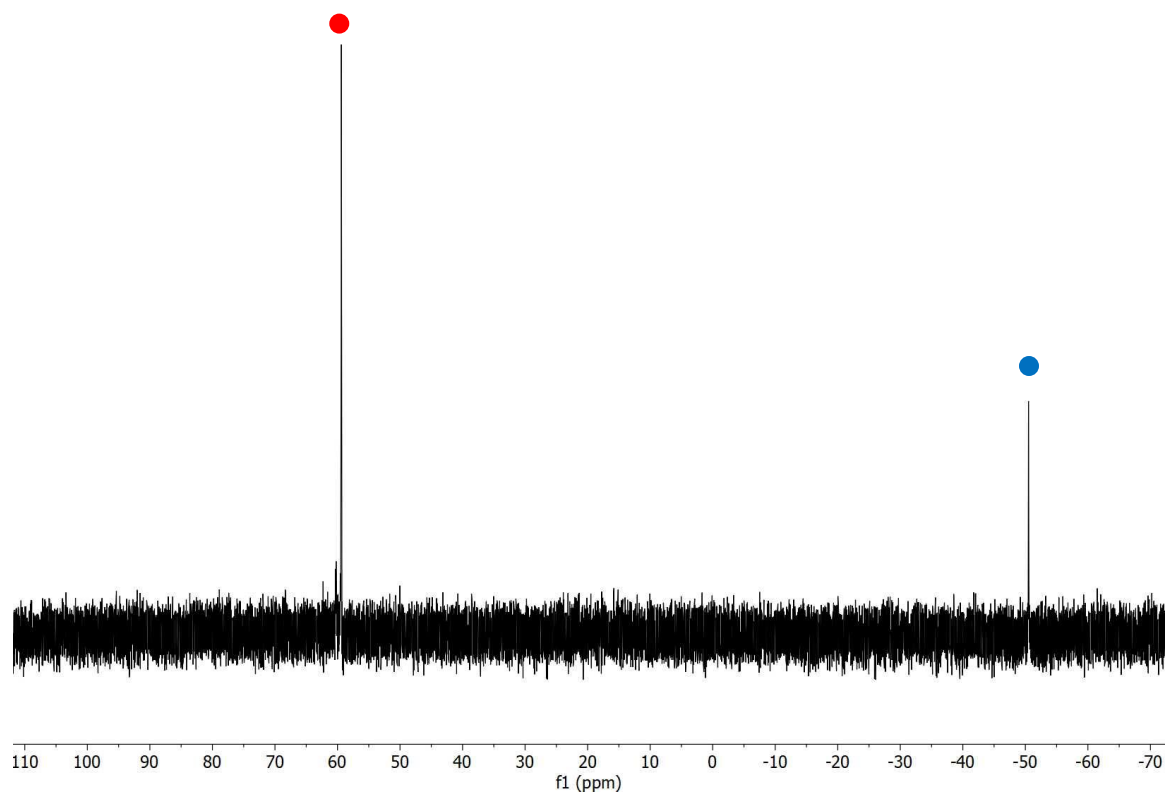


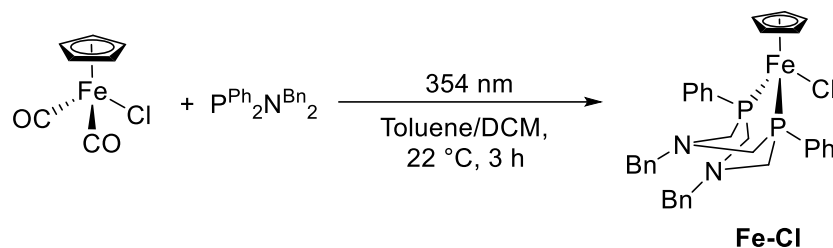
**Figure 3.2**  $^1\text{H}$  NMR spectrum of crude material from the photolysis of **Fp<sub>2</sub>** and the  $\text{P}^{\text{Ph}}_2\text{N}^{\text{Ph}}_2$  ligand in  $\text{CD}_2\text{Cl}_2$ . The red dot (●) indicates the product  $\text{FeCl}(\text{Cp})(\text{P}^{\text{Ph}}_2\text{N}^{\text{Ph}}_2)$ , and the blue dot (●) indicates the free  $\text{P}^{\text{Ph}}_2\text{N}^{\text{Ph}}_2$  ligand.

**Table 3.1** Solubility testing of [CpFe(CO)<sub>2</sub>Cl] and FeCl(Cp)(P<sup>Ph</sup><sub>2</sub>N<sup>Ph</sup><sub>2</sub>) in solvents.

Solvent	Polarity Index (PI)	[CpFe(CO) <sub>2</sub> Cl] Solubility	FeCl(Cp)(P <sup>Ph</sup> <sub>2</sub> N <sup>Ph</sup> <sub>2</sub> ) Solubility
Hexane	0	Insoluble	Insoluble
Pentane	1	Insoluble	Insoluble
Toluene	2.4	Insoluble	Partial Solubility
Diethyl ether	2.8	Insoluble	Soluble
Dichloromethane	3.1	Soluble	Soluble
Tetrahydrofuran	4	Soluble	Soluble

### 3.2 Attempts to Modify and Improve the Synthesis of FeCl(Cp)(P<sup>Ph</sup><sub>2</sub>N<sup>Bn</sup><sub>2</sub>)

In light of the results discussed in Chapter 4, this section details the synthesis of a novel iron complex featuring the P<sup>Ph</sup><sub>2</sub>N<sup>Bn</sup><sub>2</sub> ligand. The synthesis of this new complex was undertaken after catalysis experiments with various [M(Cp)(MeCN)(P<sup>R</sup><sub>2</sub>N<sup>R'</sup><sub>2</sub>)]PF<sub>6</sub> complexes that suggested a phenyl substituent on phosphorus and benzyl on nitrogen may prove optimal for acceptorless dehydrogenation of amines (Chapter 4). Readers are encouraged to reference Chapter 4 for a comprehensive understanding of how these experimental outcomes shaped the synthetic approach in this section. The synthesis of FeCl(Cp)(P<sup>Ph</sup><sub>2</sub>N<sup>Bn</sup><sub>2</sub>) (**Fe-Cl**) adheres to the same synthetic route outlined in the previous section for FeCl(Cp)(P<sup>Ph</sup><sub>2</sub>N<sup>Ph</sup><sub>2</sub>), except the ligand coordination to **Fp** step in which the P<sup>Ph</sup><sub>2</sub>N<sup>Bn</sup><sub>2</sub> ligand was introduced (Scheme 3.2).



**Scheme 3.2** Coordination of  $\text{P}^{\text{Ph}_2}\text{N}^{\text{Bn}_2}$  ligand to **Fp**: Synthesis of  $\text{FeCl}(\text{Cp})(\text{P}^{\text{Ph}_2}\text{N}^{\text{Bn}_2})$ .

The initial method to synthesize the **Fe-Cl** complex was conducted following the standard conditions for the analogous iron complex,  $\text{FeCl}(\text{Cp})(\text{P}^{\text{Ph}_2}\text{N}^{\text{Ph}_2})$ . In this reaction, the ratio of **Fp** to ligand was 1:1.03. However,  $^1\text{H}$  NMR spectroscopy analysis of the crude material revealed the presence of a signal corresponding to **Fp** (~10% by relative integration), indicating residual, unreacted **Fp** in the reaction. Also, qualitative results differed from those observed with the  $\text{FeCl}(\text{Cp})(\text{P}^{\text{Ph}_2}\text{N}^{\text{Ph}_2})$  complex. Some disparities were overlooked given the inherent differences in the ligands. For subsequent reactions, adjustments were based on both stoichiometry and solubility considerations (Table 3.2). The stoichiometry was shifted to a 1:1.3 of **Fp** to ligand, to ensure complete consumption of **Fp**. The presence of excess ligand was not a major concern due to the straightforward removal by filtration. To allow enhanced ligand solubility for a more homogeneous reaction mixture the solvent ratio of DCM to toluene was changed from 2:1 to 3:1. Qualitative observations for this adjusted reaction mirrored those for  $\text{FeCl}(\text{Cp})(\text{P}^{\text{Ph}_2}\text{N}^{\text{Ph}_2})$  in which the reaction mixture transitioned from a dark maroon upon initial introduction of **Fp** and ligand to a black with a green undertone post 2-h UV lamp exposure. Notably, no yellow solids were detected. The  $^1\text{H}$  NMR spectrum of the reaction mixture showed no signals corresponding to **Fp**, suggesting complete consumption. In the  $^{31}\text{P}\{^1\text{H}\}$  NMR spectrum, the predominant peak was attributed to the **Fe-Cl** complex, with relative integrations constituting 69% of the reaction mixture. A minor peak represented the free ligand. Additionally, the presence of multiple minor peaks hinted at decomposition, likely resulting from prolonged exposure to the UV lamp. To mitigate decomposition, reaction durations ranged between 2 to 3 h. The objective was to detect only two dominant peaks, corresponding to the desired product and free ligand. Typically, the reaction was halted when about ~80% product formation was reached, which corresponded to a free ligand content of ~20%. This approach avoids

decomposition while attempting to maximize product formation. However, the isolation of **Fe-Cl** was still unsuccessful.

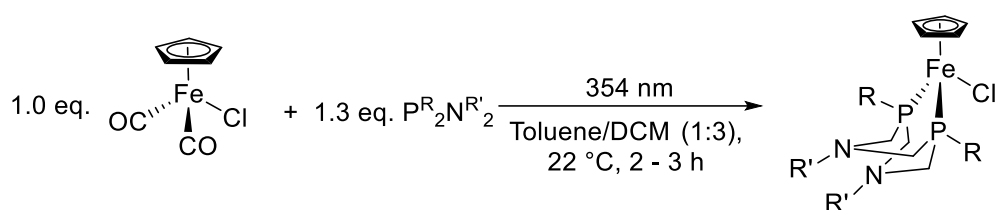
**Table 3.2** Summary of Optimization Parameters and Their Impact on **Fe-Cl** Yield.

Optimization Parameter	Outcome	Effect on Yield
<b>Fp</b> purity: liquid-liquid extraction	Increased purity by 40%	Standard: <10% Modified: 15%
Isolation: warm Et <sub>2</sub> O & same day workup	Improved solubility and reduced decomposition of crude material	Standard: <10% Modified: 15%
Starting material ratio: <b>Fp</b> to ligand (1:1.3)	Successful consumption of <b>Fp</b>	Standard: <10% Modified: 15%
Solvent ratio: DCM/Toluene (3:1)	Increased solubility of P <sup>R</sup> <sub>2</sub> N <sup>R'</sup> <sub>2</sub> ligand	Standard: <10% Modified: 15%
Reaction time: 2 to 3 hours	Decreased decomposition of crude material	Standard: <10% Modified: 15%
FeCl(Cp)(P <sup>Ph</sup> <sub>2</sub> N <sup>Ph</sup> <sub>2</sub> )	Successful synthesis	Yield: from <10 to 15%
<b>Fe-Cl</b>	Unsuccessful synthesis	No change

### 3.3 Conclusion

The initial synthesis of FeCl(Cp)(P<sup>Ph</sup><sub>2</sub>N<sup>Ph</sup><sub>2</sub>) had a low yield, making it challenging to produce derivatives with different ligands. Despite numerous adjustments in the synthesis procedure for FeCl(Cp)(P<sup>Ph</sup><sub>2</sub>N<sup>Ph</sup><sub>2</sub>) and **Fe-Cl**, there was no significant improvement in yield (Scheme 3.3). These modifications included changes in isolation (solubility in solvents;

applied heat), reaction time, material purity, starting material ratios, and solvent ratios. The synthesis of the  $\text{FeCl}(\text{Cp})(\text{P}^{\text{Ph}_2\text{N}^{\text{Ph}_2}})$  must undergo further optimization to enhance the yield, which can then provide a more robust method for the synthesis of analogous compounds with different  $\text{P}_2\text{N}_2$  derivatives. Alternatively, due to the structural differences of each ligand and iron complex, unique optimizations may be needed for each derivative. Therefore, a future approach should pivot towards refining the standard synthesis, creating a more robust foundation upon which variations can be more confidently explored and optimized.



**Scheme 3.3** Synthesis of  $\text{FeCl}(\text{Cp})(\text{P}^{\text{R}_2}\text{N}^{\text{R}'_2})$ : Coordination reaction of **Fp** with  $\text{P}_2\text{N}_2$  ligands under optimized conditions to synthesize novel iron complexes.

### 3.4 References

- (1) Rong, B.; Zhong, W.; Gu, E.; Long, L.; Song, L.; Liu, X. *Electrochim. Acta* **2018**, *283*, 27–35.
- (2) Liu, T.; Chen, S.; O'Hagan, M. J.; Rakowski DuBois, M.; Bullock, R. M.; DuBois, D. L. *J. Am. Chem. Soc.* **2012**, *134* (14), 6257–6272.
- (3) Hoffman, Matthew D., "Metal Ligand Cooperative Complexes for Acceptorless Dehydrogenation of Amines" (2021). *Electronic Thesis and Dissertation Repository*. 8306.



## Chapter 4

### 4 Comparing Catalyst Performance for Acceptorless Dehydrogenation of Benzylamine using $[M(\text{Cp})(\text{MeCN})(\text{P}^{\text{R}}_2\text{N}^{\text{R}'}_2)]\text{PF}_6$ complexes

#### 4.1 Catalyst Screen for Acceptorless Dehydrogenation of Benzylamine

A previous student initiated the catalyst screen using a group of  $[M(\text{Cp}/\text{Cp}^*)(\text{P}^{\text{R}}_2\text{N}^{\text{R}'}_2)(\text{MeCN})]\text{PF}_6$  complexes to identify the optimal catalyst structure for the AD of benzylamine to an imine (Figure 4.1). Variations in the catalyst structure included a cooperative ( $\text{P}^{\text{R}}_2\text{N}^{\text{R}'}_2$ ), two ancillary ligands (Cp vs Cp\*), and two metal centers (Ru vs Fe). The optimal cooperative catalyst was exploited for the AD of a select scope of benzylamine derivatives. The subset of metal–ligand cooperative (MLC) catalysts included M–Cp/Cp\* complexes with a  $\text{P}^{\text{R}}_2\text{N}^{\text{R}'}_2$  ligand (**Ru1a-f**, **Ru2b**, **Fe1b**, **Fe2b**), in which **Ru1a-d** had the same phosphine substituent ( $\text{R} = \text{Ph}$ ) but differed in their amine substituents ( $\text{R}' = \text{Bn}$ ,  $\text{Ph}$ ,  $p\text{-OMeC}_6\text{H}_4$ ,  $p\text{-CF}_3\text{C}_6\text{H}_4$ ). Complexes **Ru1b**, **Ru1e-f** have the same amine substituent ( $\text{R} = \text{Ph}$ ) but differed in their phosphine substituent ( $\text{R}' = \text{Ph}$ ,  $\text{Cy}$ ,  $t\text{-Bu}$ ). Complex **Ru2b** was a direct analogue of **Ru1b** except that it contained a Cp\* instead of Cp. Complex **Fe1b** was also a direct analogue of **Ru1b** except that it contained an iron metal center instead of ruthenium. Finally, **Fe2b** was a direct analogue of **Fe1b** except that it contained a Cp\* instead of Cp. This permits helpful correlations with catalyst activity with the structure to assess selectivity.

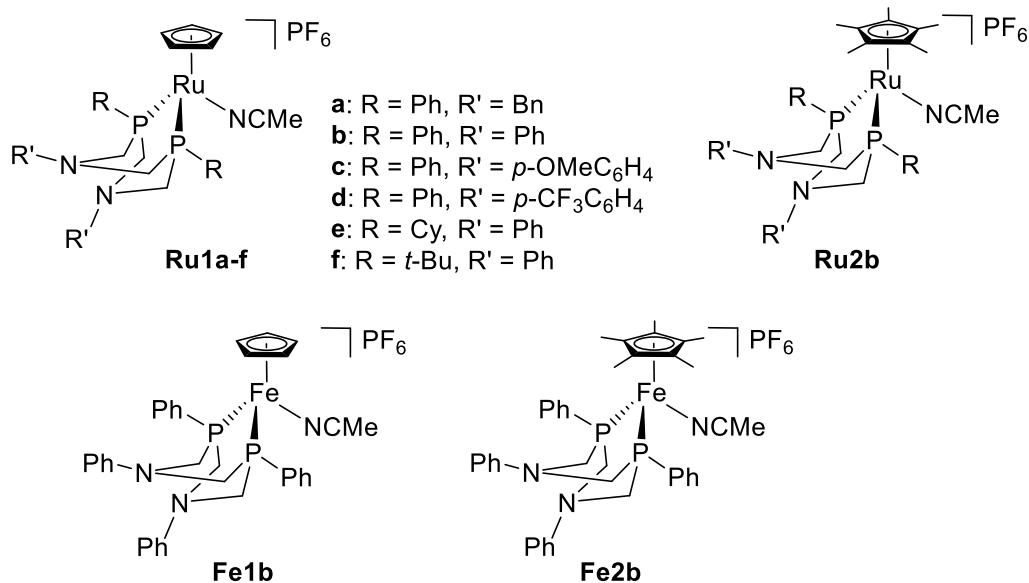


**Figure 4.1** Ruthenium and iron  $P^R_2N^{R'}_2$  catalysts employed in this study.

The performance of the ruthenium catalysts, **Ru1a-e** and **Ru2b**, and iron catalysts, **Fe1b** and **Fe2b**, were measured for the AD of benzylamine (Table 4.1). The impact of catalyst structure on catalyst activity will be first discussed. Catalysts with ruthenium as the metal center and variations in the substituents on the pendant amine of the  $P^R_2N^{R'}_2$  ligand (**Ru1a-d**) result in noticeable differences in activity and overall catalyst performance (Entries 1-4). Despite the differences, the changes in activity do not align with a clear trend in relation to the electronic or steric properties of the substituents. Switching the phosphine substituent from R = Ph (**Ru1b**) to a R = Cy (**Ru1e**) resulted in a negligible difference in conversion (59 and 55%, respectively), which shows no clear distinction in preferred electronics at the primary coordination sphere (Entry 5). However, **Ru1f** with a *t*-butyl phosphine substituent gave a significantly lower conversion of 29%, suggesting a reduction in the sterics of the phosphine group, achieved by introducing a less hindered substituent, can enhance catalyst activity (Entry 6). Despite the iron catalyst, **Fe1b**, having identical electronic/steric ligand properties as **Ru1b**, it shows a 20% decrease in conversion (Entry 7). Altering the ancillary ligand to a Cp\* in catalysts with either ruthenium (**Ru2b**) or an iron metal center (**Fe2b**), the conversion decreases significantly (27 and 21%, respectively) when compared to analogous catalysts (**Ru1b** and **Fe1b**) bearing a Cp ligand (Entry 8 and 9). Overall, the highest conversion was achieved with ruthenium as the metal center and Cp as the ancillary

ligand. Modifications to the primary coordination sphere yielded little difference unless a bulky group was present. Additionally, no clear observable trend was seen with the pendant amine.

**Table 4.1** Acceptorless dehydrogenation of BnNH<sub>2</sub> by M(Cp/Cp\*)(P<sup>R</sup><sub>2</sub>N<sup>R'</sup><sub>2</sub>)(MeCN)]PF<sub>6</sub> catalysts.<sup>[a]</sup>

Entry	Catalyst	Conv. (%) <sup>[b]</sup>	Product Distribution (%) <sup>[d]</sup>			<sup>[e]</sup> In situ ADC, DAD, HB Yields (%)
			ADC	DAD	HB	
1	<b>Ru1a</b>	76	70	26	4	54, 20, 3
2	<b>Ru1b</b>	59	55	6	39	28, 3, 20
3	<b>Ru1c</b>	45	43	4	53	21, 2, 26
4	<b>Ru1d</b>	70	59	14	27	37, 9, 17
5	<b>Ru1e</b>	55	43	5	52	24, 3, 29
6	<b>Ru1f</b>	29	72	17	11	13, 3, 2
7	<b>Fe1b</b>	39	90	10	0	38, 4, 0
8	<b>Ru2b</b>	27	77	14	9	17, 3, 2
9	<b>Fe2b</b>	21	78	22	0	18, 5, 0

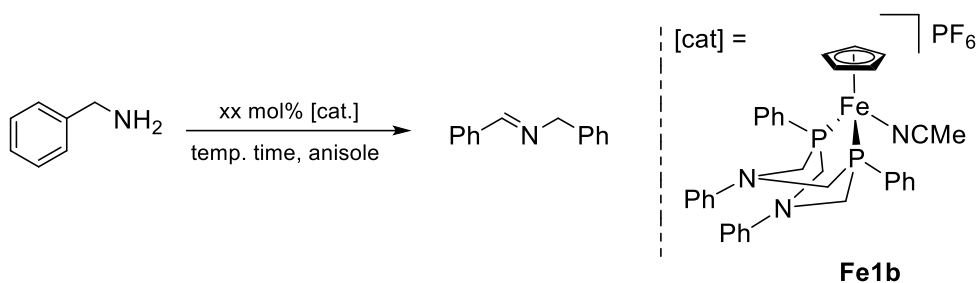
<sup>[a]</sup>Conditions: 3 mol% [cat], 250 mM BnNH<sub>2</sub>, 110 °C, 48 h. Data was quantified with respect to an internal standard by calibrated GC-FID. Reactions were run in duplicate with the data shown representing the average, errors were within ±5%. <sup>[b]</sup>Conversion calculated by amount of BnNH<sub>2</sub> consumed. <sup>[c]</sup>Data from a prior student (Entries 1, 3-5, 8 & 9).<sup>1</sup> <sup>[d]</sup>Product distribution was calculated by ((%ADC or DAD or HB)/(%ADC+DAD+HB))\*100. <sup>[e]</sup>In situ yields determined by calibrated GC-FID with an internal standard.

To ease selectivity comparisons, product distribution rather than absolute product yield is used since amounts are normalized based on conversion. The previously studied catalyst **Ru1a** gave an **ADC:DAD:HB** ratio of 3:1:0.2 (Entry 1). Switching from the R' = Bn

catalyst to those with *N*-aryl substituents (**Ru1b-d**) gave substantially higher amounts of the **HB** product (Entries 2-4). The relative amount of saturated dibenzylamine was highest using **Ru1c**, which has the most donating pendent amine substituent relative to the aryl-substituted catalysts. The increased basicity of the amine may favour the hydride/protonated tautomer over the dihydrogen adduct, which is the required intermediate for hydrogenation. To analyze the alterations in the primary coordination sphere transition from the R = Ph catalyst to those with cyclohexyl or *t*-butyl substituents (**Ru1e-f**) were deployed. As a result, a mixture of products was observed, with no noteworthy variations in selectivity (Entries 5 and 6). Catalyst **Fe1b**, which is structurally identical to **Ru1b** except for the metal center, displays a 10:1:0 mixture of **ADC:DAD:HB** (Entry 7). In addition, **Fe1b** favours the formation of the **ADC** product, with a 10:1 ratio of **ADC:DAD**, making it unique in selectivity compared to the ruthenium complexes (**Ru1a-e**, **Ru2b**). The selectivity by **Fe1b** suggests that the iron center, as opposed to ruthenium, facilitates a preferential pathway towards dehydrogenation products and completely eliminates **HB** formation. Also, catalysts bearing a Cp\* (**Ru2b** and **Fe2b**) reveal no noteworthy changes in selectivity, however, catalyst activity is highly influenced with a substantial decrease in conversion (27 and 21%, respectively) when compared to their Cp analogues (Entries 8 and 9).

## 4.2 Acceptorless Dehydrogenation of Benzylamine using **Fe1b** – Optimization

While **Fe1b** showed high selectivity for the imine **ADC** product, the conversion was low. To maximize the activity, we set out to optimize conditions for this catalyst using benzylamine as the substrate (Table 4.2). The solvent, anisole, remained the same for all the reactions, and the conditions screened included catalyst loading, temperature, and time.

**Table 4.2** Optimization of the reaction conditions for the AD of BnNH<sub>2</sub> using **Fe1b**.<sup>[a]</sup>

Entry	[cat] (mol%)	Temp. (°C)	Time (h)	Conversion (%)	%ADC (in situ yield)
1	<b>Fe1b (4)</b>	110	48	59	55
2	<b>Fe1b (6)</b>	110	48	66	63
3	<b>Fe1b (10)</b>	110	48	71	69
4	<b>Fe1b (3)</b>	110	48	39	38
5	<b>Fe1b (4)</b>	90	48	26	17
6	<b>Fe1b (4)</b>	100	48	40	28
7	<b>Fe1b (4)</b>	130	48	30	28
8	<b>Fe1b (4)</b>	110	12	23	20
9	<b>Fe1b (4)</b>	110	24	37	35
10	<b>Fe1b (4)</b>	110	34	44	42
11	<b>Fe1b (4)</b>	110	56	60	58
12 <sup>b</sup>	<b>Fe1b (4)</b>	110	48	55	51
13 <sup>c</sup>	<b>Fe1b (4)</b>	110	48	11	9
14	<b>[Fe1b] + BHT (4)</b>	110	48	52	50
15	<b>FeCl<sub>2</sub> (4)</b>	110	48	24	23
16	<b>FeCl<sub>2</sub> + P<sup>Ph</sup><sub>2</sub>N<sup>Ph</sup><sub>2</sub> (4)</b>	110	48	0	0

<sup>[a]</sup>Conditions: 100 mM tetralin, 250 mM BnNH<sub>2</sub>, anisole as the solvent. Data was quantified with respect to an internal standard by calibrated GC-FID. Reactions were run in duplicate with the data shown representing the average, which are within 5% error. <sup>[b]</sup>Conducted in a pseudo ‘open’ inert system. <sup>[c]</sup>Conducted under H<sub>2</sub> atmosphere.

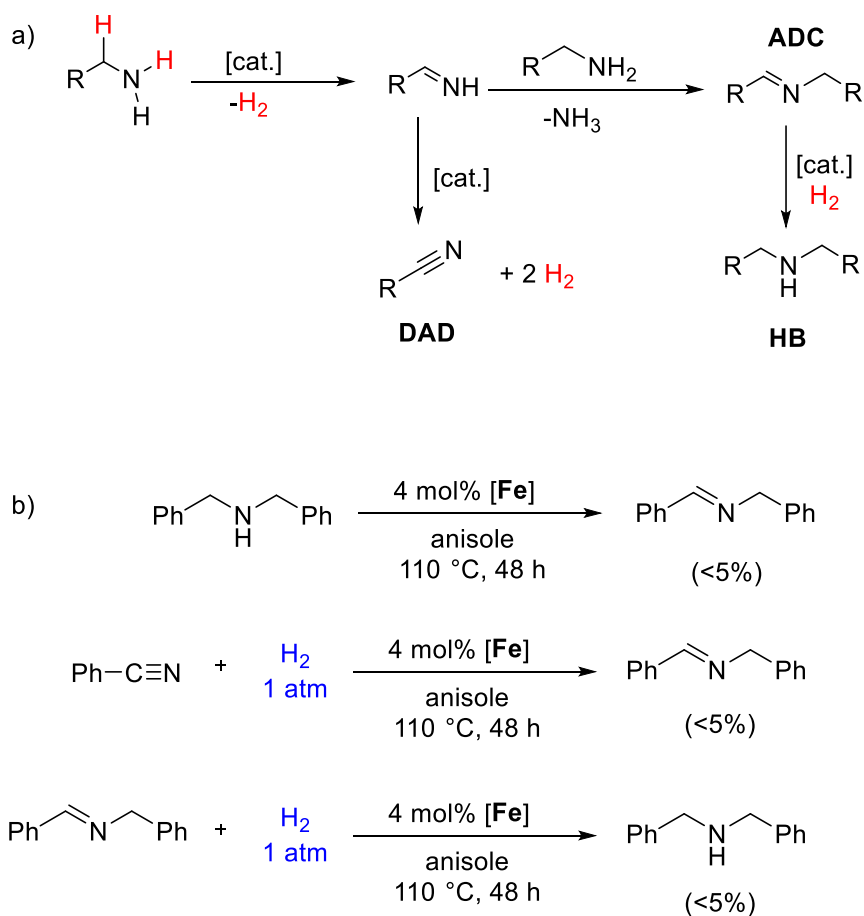
In the initial phase of our experimentation, the catalyst loading was set at 3 mol%. However, for the subsequent reaction, catalyst loading is increased to 4 mol% at 110 °C for

48h using **Fe1b** resulting in a similar %ADC as **Ru1b** at 3 mol% (55 and 55%, respectively) (Entry 1). Catalyst loadings of 6 and 10 mol% led to increased %ADC by 8 and 14% relative to a catalyst loading of 4 mol%, with 10 mol% yielding the highest of 69% ADC (Entries 2, 3). A catalyst loading of 3 mol% gives 25% lower %ADC than 4 mol% (Entry 4). AD of benzylamine should follow a first-order pathway in which doubling the catalyst concentration should be directly proportional to catalyst turnover/lifetime resulting in double the yield. Although higher catalyst loadings of 6 and 10 mol% increased %ADC yield, the increase was not proportional. Suggesting an optimal balance between catalyst usage and yield was therefore found at a catalyst loading of 4 mol%. At temperatures of 90 °C and 100 °C, the %ADC reduced significantly (17 and 28%, respectively) compared to reactions at 110 °C (Entries 5, 6). In addition, increasing the temperature from 110 °C to 130 °C also caused a decrease in conversion by 27% (Entry 7). A reaction temperature of 110 °C adequately balances the energetic demand to overcome reaction barriers, while minimizing competing thermally promoted catalyst decomposition. To further fine-tune the reaction parameters, time was tested as a variable to determine the optimal timeframe for maximum %ADC formation (Entries 8-11). The varying reaction durations included 12, 24, 34, 48, and 56 h with the highest %ADC reached by 48 h. In efforts to evaluate the influence of H<sub>2</sub> in the 'closed' system (90% headspace) reaction vessel, a catalytic reaction in a pseudo 'open' system with a 99% headspace to promote H<sub>2</sub> dissociation was explored (Entry 12). Interestingly, 51% ADC was observed, mirroring the results obtained in the initial 'closed' system setup. Suggesting that the generation and presence of hydrogen gas in the closed system does not significantly impact the reaction efficiency, eliminating any concerns about a potential inhibitory effect of accumulated hydrogen gas. A subsequent experiment was carried out under a hydrogen atmosphere to further assess the impact of H<sub>2</sub> (Entry 13). Notably, the reaction demonstrated a substantial decrease in product under these conditions with only 9% ADC formation. The presence of excess hydrogen likely drives the reaction equilibrium towards the reactants, thus inhibiting the forward reaction. Finally, control reactions were performed to elucidate the specific role by the catalyst in this transformation (Entries 14-16). In the first experiment, the reaction was carried out using the catalyst (**Fe1b**) along with butylated hydroxytoluene (BHT) as a radical trap (Entry 14). There was a negligible 4% decrease in ADC formation

compared to the standard reaction suggesting no radical mechanism is taking place. Secondly, FeCl<sub>2</sub> was used as the catalyst, imitating the **Fe1b** metal and oxidation state, which resulted in 23% **ADC** (Entry 15). A 32% decrease relative to **Fe1b**, highlighting the significance of **Fe1b** involvement in facilitating the formation of the imine intermediate. Lastly, a combination of FeCl<sub>2</sub> and free P<sup>Ph</sup><sub>2</sub>N<sup>Ph</sup><sub>2</sub> ligand resulted in negligible %**ADC** (Entry 16). Showcasing the importance of the catalysts specific structure and its integral role in the successful reaction outcome. The control reactions emphasize **Fe1b** role and contribution to the reaction efficiency.

### 4.3 Understanding Selectivity Through Control Reactions and Evaluating **Fe1b** Robustness

To investigate the origin of selectivity, mechanistic test reactions were carried out (Scheme 4.1a). While the imine (**ADC**) and nitrile (**DAD**) products undergo dehydrogenation steps for the removal of H<sub>2</sub> shown by the one-directional arrow, a potential equilibrium may exist. Likewise, the formation of the secondary amine (**HB**) product through H<sub>2</sub> addition is depicted by a one-directional arrow, a potential equilibrium might also exist. Considering the potential equilibria three key experiments were carried out (Scheme 4.1b). The first experiment focused on dehydrogenation of the secondary amine (**HB**) to the imine (**ADC**), to assess whether secondary amine can revert to the imine with catalyst **Fe1b**. Negligible product was observed, this suggests that the AD selectivity is not dictated by an equilibrium between **HB** and **ADC**. The second reaction investigated was the hydrogenation of the nitrile (**DAD**) to the imine (**ADC**) under a hydrogen atmosphere, which yielded negligible amount of imine (**ADC**). This also suggests that the AD selectivity is not dictated by an equilibrium between **ADC** and **DAD**. In the third reaction, hydrogenation of the imine to the secondary amine was tested. Again, the results indicated negligible secondary amine formation, implying the selectivity is not dictated by an equilibrium between **ADC** and **HB**.



**Scheme 4.1** a) AD of primary amine to form the homocoupled or heterocoupled ADC, DAD, and HB products. b) Control reactions to understand the origin of selectivity.

#### 4.4 Scope Study: Targeting Homocoupled and Heterocoupled Imines

The AD performance of catalyst **Fe1b** was investigated within a specific scope of functionalized homocoupled imines (Figure 4.2a). In order to gain insight into whether the performance of **Fe1b** translates to other benzylamine derivatives, substrates with varying electronics and sterics were applied. The reactions were conducted under standard conditions of 4 mol% **Fe1b** at 110 °C for 48 h in anisole. Upon evaluating the influence of substitution at different positions of the benzylamine aryl ring, interesting trends emerged. When the benzylamine aryl ring was chloro substituted at the para-position, the ADC yield was found to be 16%. Substrates containing electron-donating methoxy or methyl groups



resulted in lower yields than that of the chloro derivative (12 and <5%, respectively). The general two steps for the homocoupled imine formation involve first the dehydrogenation, where an electron-withdrawing group is expected to decrease the hydridic C–H hydrogens of the methylene, favoring the formation of the reactive imine intermediate. The second step is the coupling with another equivalent of substrate, where the reactive imine intermediate will couple more efficiently with an electron-donating substituted derivative. Determining which effect will have a greater impact on the overall yield requires further investigation. Additionally, the presence of a methoxy-substitution at the ortho position may introduce steric effects, contributing to the observed lower yields. Overall, the study highlights the low tolerance of **Fe1b** towards functional groups, as evidenced by the performance observed across various deployed substrates.

In an effort to address the low performance observed by the homocoupled **ADC** products, a new approach was targeted for heterocoupled imines. The rationale behind this strategy stemmed from the observation of high conversion when using the parent benzylamine as the substrate. In this study, amine additives were introduced to direct the reaction towards the formation of heterocoupled imines (Scheme 4.2b). To select appropriate amine additives, three key criteria were considered. Firstly, the nucleophilic nature: nucleophilic amines were chosen to enhance the coupling step of the imine formation process. Second, absence of alpha hydrogens: the chosen amines must lack alpha hydrogens to prevent their dehydrogenation by the catalyst. Third, use the amine additive in excess: the amine additives in excess can bias the reaction towards preferential formation of heterocoupled imines. The three amines selected for additives were, 4-tertbutylaniline, 4-methoxyaniline, and tertbutylamine. These amine additives were incorporated into the AD reaction alongside benzylamine under standard conditions, using 4 mol% of **Fe1b** catalyst at 110 °C for 48 h in anisole. Despite the selection criteria, observed heterocoupled yields remained low for all amines. This suggested that the catalyst either exhibited low compatibility with the amine additives or that competitive coordination to the catalyst led to deactivation, resulting in the observed low performance.

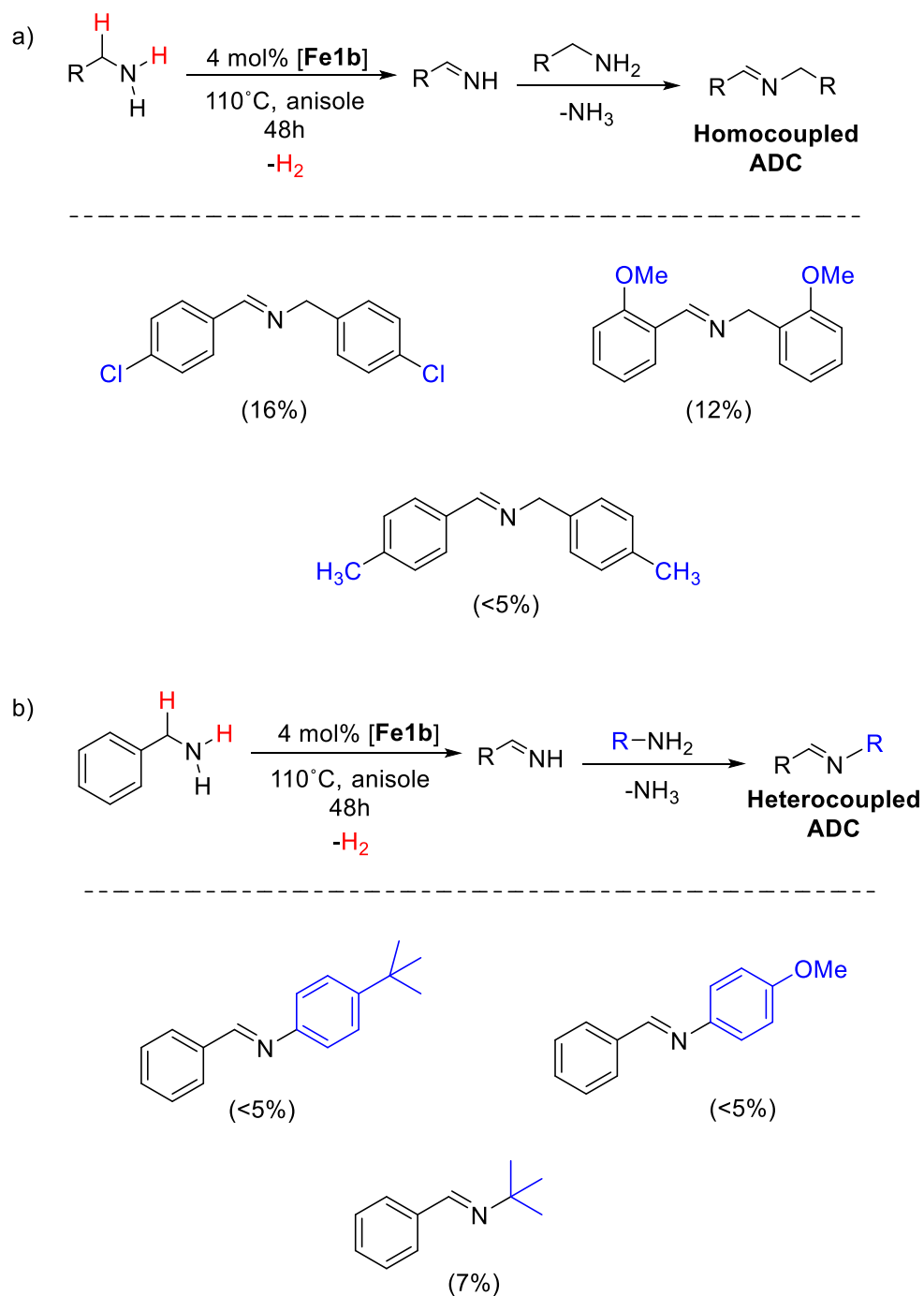


**Figure 4.2** a) Scope AD of substituted benzylamines targeting homocoupled imines using MLC catalyst **Fe1b**. b) Scope AD of benzylamine with amine additives targeting heterocoupled imines using MLC catalyst **Fe1b**.

## 4.5 **Fe1b** Decomposition Analysis and Mechanistic Elucidation of a Novel Fe-H Complex

### 4.5.1 Evaluation of Catalyst Stability: Thermal Decomposition Analysis over Time, Competitive Coordination, and Air Exposure Influence

Catalytic stability is a crucial aspect of designing efficient and sustainable catalytic processes. To test the stability of **Fe1b**, a thermal decomposition analysis was conducted by heating the catalyst to 110 °C for extended periods. At selected intervals,  $^{31}\text{P}\{^1\text{H}\}$  NMR spectroscopy was employed to assess the remaining **Fe1b**, utilizing triphenylphosphine ( $\text{PPh}_3$ ) as an internal standard in a capillary to avoid any side reactions (Figure 4.3). The integration of the catalyst signal relative to the internal standard facilitated the determination of the remaining catalyst fraction as the heating progressed. The thermal decomposition analysis revealed notable stability of **Fe1b** under the experimental conditions. After 24 h of heating, approximately 60% of **Fe1b** remained intact, indicating resistance to decomposition. Even after 48 h, a considerable portion of the catalyst, approximately 42%, persisted, further confirming **Fe1b** robustness. The high thermal stability exhibited by **Fe1b** provides important insights into the observed low performance in both homocoupled and heterocoupled imine synthesis. It suggests that thermally-promoted catalyst decomposition is unlikely to be the primary cause of the reduced performance observed in the substituted benzylamine substrates. Instead, other factors,

such as the influence of different substituents and steric effects, may be more influential in determining the overall catalytic performance.

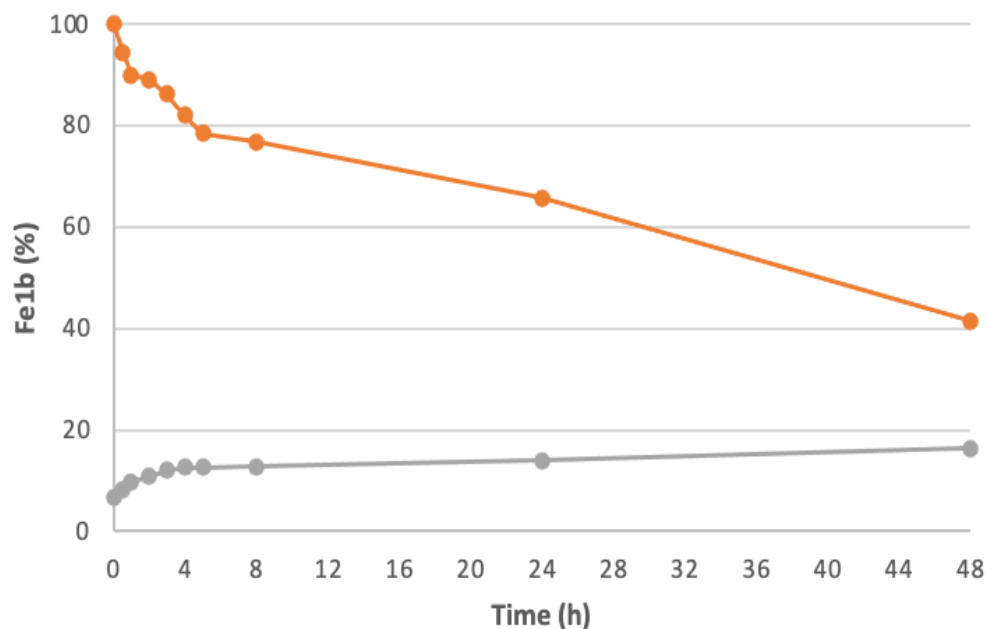


**Figure 4.3** Thermal Decomposition Analysis of **Fe1b** Catalyst Stability Over Time. Catalyst **Fe1b** (orange) at 110 ° C in anisole from 0 – 48 h. Formation of a new unknown species (25 ppm) (Grey). The conversion of catalyst and unknown species was monitored by  $^{31}\text{P}\{^1\text{H}\}$  NMR spectroscopy with  $\text{PPh}_3$  as the internal standard.

Next, we investigated whether coordination with tert-butylaniline, the amine additive used to target heterocoupled imine, influences the deactivation of **Fe1b** catalyst. A solution of **Fe1b** and tert-butylaniline (1 : 5 equivalence) was monitored over a 48 hour time frame by  $^{31}\text{P}\{^1\text{H}\}$  NMR spectroscopy with triphenylphosphine ( $\text{PPh}_3$ ) as an internal standard. At Time = 0, the stack plot displayed the appropriate phosphorus signals of **Fe1b** (57.8 ppm), triphenylphosphine (-8.5 ppm), and the counter anion  $[\text{PF}_6]^-$  (-144.4 ppm) (Figure 4.4a). Tert-butylaniline was added to the mixture, and the reaction was heated at the standard catalytic temperature of 110 ° C for 24 h (Figure 4.4b). Unknown peaks emerged in the NMR spectra, and the relative amount of **Fe1b** catalyst decreased by ~14% compared to the mixture without heating. Further heating of the sample for a total of 48 h resulted in a slight upfield shift (~5 ppm) in the **Fe1b** signal (Figure 4.4c). Moreover, the unknown

peaks increased and the relative amount of **Fe1b** decreased by ~40%. It is worth to acknowledge that clean conversion to a tert-butylaniline adduct or a new compound was not observed. The upfield shift suggests potential coordination between the amine additive and the catalyst may be a factor contributing to catalyst deactivation during imine synthesis correlating to the lower performance. Overall, the amine additive appears to exert a positive influence on catalyst stability as ~86% of **Fe1b** remains after 24 h. For only thermal decomposition of **Fe1b** at 24 h, ~65% decomposition was observed suggesting ~22% decomposition occurring from thermal instability alone. This potential amine additive coordination might have a stabilizing effect on the catalyst, possibly mitigating decomposition.

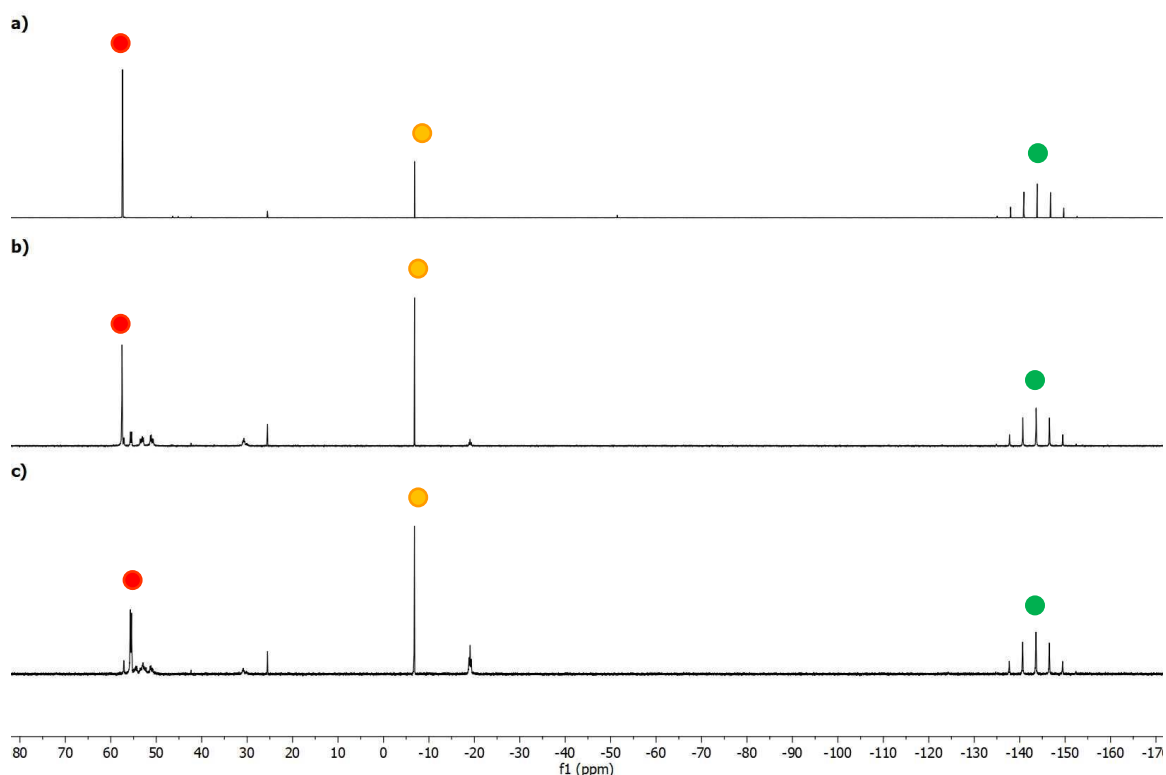


**Figure 4.4**  $^{31}\text{P}\{^1\text{H}\}$  NMR spectra of **a) Fe1b** and  $\text{PPh}_3$  in  $\text{CD}_2\text{Cl}_2$ . **b) Fe1b**, tert-butylaniline, and  $\text{PPh}_3$  in  $\text{CD}_2\text{Cl}_2$  heated at  $110\text{ }^\circ\text{C}$  for 24 h. **c) Fe1b**, tert-butylaniline, and  $\text{PPh}_3$  in  $\text{CD}_2\text{Cl}_2$  heated at  $110\text{ }^\circ\text{C}$  for 48 h. The red dot (●) corresponds to **Fe1b**. The orange dot (●) corresponds to  $\text{PPh}_3$ . The green dot (●) corresponds to  $[\text{PF}_6]^-$ .

The **Fe1b** catalyst was exposed to oxygen ( $O_2$ ) to investigate the possibility of deactivation occurring due to contact with  $O_2$  during catalysis. The experiment was aimed to evaluate whether  $O_2$  could have any detrimental effects on the catalyst stability and activity during the reaction inside the reaction flask. To assess the catalyst response to  $O_2$  exposure,  $^{31}P\{^1H\}$  NMR spectroscopy was employed to evaluate the catalyst before and after exposure to  $O_2$ , allowing for a direct comparison of any changes in the catalyst structure (Figure 4.5a). The phosphorus NMR signals reveal no difference after exposure to  $O_2$  (Figure 4.5b). All relevant signals associated with the **Fe1b** catalyst remained present and unchanged. Additionally, the sample mixture was heated at  $70\text{ }^\circ\text{C}$  for 5 h to promote an environment like standard catalytic conditions (Figure 4.5c). Again, all relevant signals associated with **Fe1b** catalyst remained unchanged however a minor peak formed at 30 ppm. This suggests that contact did not induce any significant deactivation or structural modifications in the catalyst. Nonetheless, the catalyst interacting with  $O_2$ , potentially leading to the formation of a product with paramagnetic properties, remains a plausible possibility.

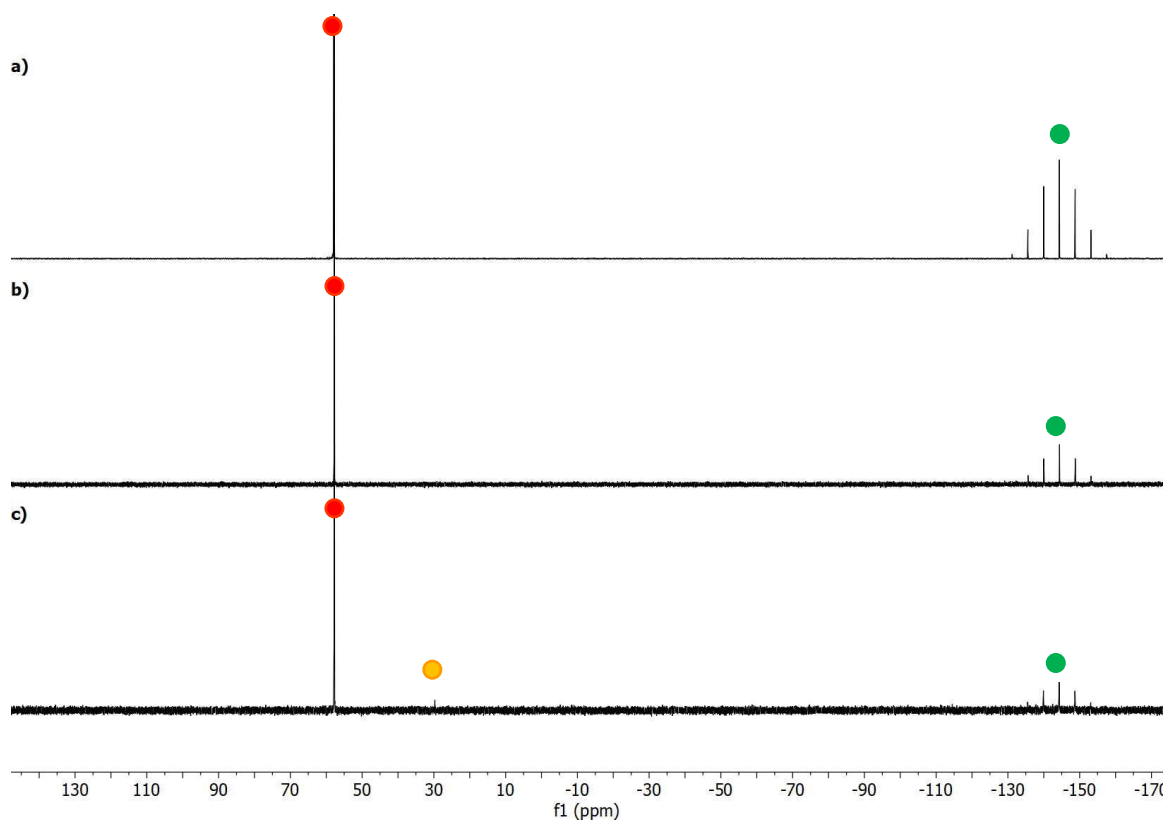
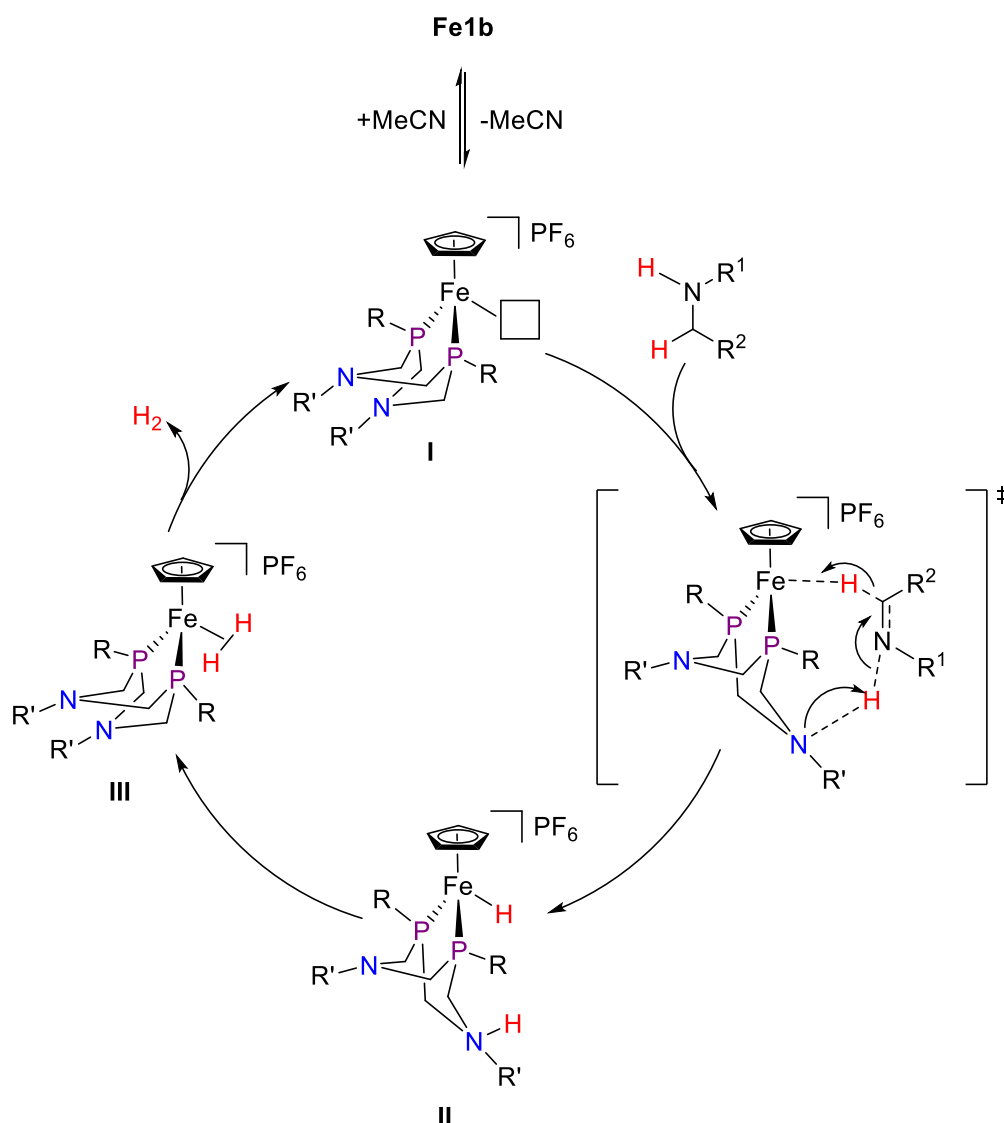


**Figure 4.5**  $^{31}\text{P}\{^1\text{H}\}$  NMR spectrum stack plot of a) **Fe1b** in  $\text{CD}_2\text{Cl}_2$ . b) **Fe1b** exposed to  $\text{O}_2$  in  $\text{CD}_2\text{Cl}_2$ . c) **Fe1b** sample exposed to  $\text{O}_2$  and heated for 5 h at  $70^\circ\text{C}$ . The red dot (●) corresponds to **Fe1b**. The orange dot (●) corresponds to unknown signal. The green dot (●) corresponds to  $[\text{PF}_6]^-$ .

#### 4.5.2 Attempted Synthesis of a Novel **Fe-H** Complex: Insights and Challenges in Mechanistic Elucidation

This experiment focuses on investigating the behavior of intermediate **III** ( $\text{Fe}(\text{H}_2)$ -adduct) in terms of  $\text{H}_2$  release (Scheme 4.2). By obtaining the **Fe-H** complex it can be used to investigate its behavior to understand the equilibrium between this complex and  $\text{Fe}(\text{H}_2)$ -adduct to gain insight about the observed selectivity (Scheme 4.3). If the  $\text{Fe}(\text{H}_2)$ -adduct readily releases  $\text{H}_2$ , it implies intermediate **II** might not be easily accessible which is the required intermediate for promoting hydrogenation, making it consistent with the observed selectivity. Conversely, if the  $\text{Fe}(\text{H}_2)$ -adduct remains stable the hypothesis of intermediate **II** following a competing pathway may not be correct. Based on our knowledge of the ruthenium-catalyst systems, we hypothesized that the iron system, intermediate **II** might

readily form the Fe(H<sub>2</sub>-adduct) due to the decrease in hydricity for an iron-hydride bond when compared to a ruthenium-hydride bond.

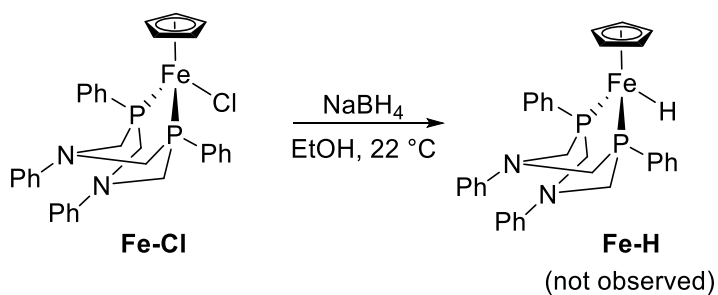


**Scheme 4.2** General hypothesized catalytic cycle focusing on the formation of the **II** and **III** (Fe(H<sub>2</sub>)-adduct) complexes. Intermediate **I** box represents an open coordination site.

The reaction to afford **Fe-H** involved using the FeCl(Cp)(P<sup>Ph</sup><sub>2</sub>N<sup>Ph</sup><sub>2</sub>) (**Fe-Cl**) complex and reacting it with NaBH<sub>4</sub> in ethanol at 22 °C for approximately an hour (Scheme 4.3). This reaction was previously described by Drover and Dubois with similar complexes.<sup>2,3</sup> The reaction was monitored by <sup>31</sup>P{<sup>1</sup>H} NMR spectroscopy (Figure 4.6), which revealed that 21% (by relative integration) of the **Fe-Cl** complex remained post-reaction. A novel



product was detected through the appearance of a distinct peak at approximately  $-20$  ppm ( $\sim 20\%$ ). Comparative analysis with similar complexes such as  $[\text{Cp}^{\text{C}_6\text{F}_5}\text{Fe}(\text{P}^{\text{tBu}}_2\text{N}^{\text{Bn}}_2)\text{H}]$  and  $\text{RuH}(\text{Cp})(\text{P}^{\text{tBu}}_2\text{N}^{\text{Bn}}_2)$  exhibited characteristic peaks at 91.9 and 64.5 ppm, respectively.<sup>2,3</sup> The appearance of a peak at  $-20$  ppm was inconsistent with these established patterns. Consequently, this newly observed signal signifies the formation of an unidentified compound. Further investigations would be required to determine the structure and nature of this newly observed species.



**Scheme 4.3** Attempted synthesis of a new **Fe-H** complex.

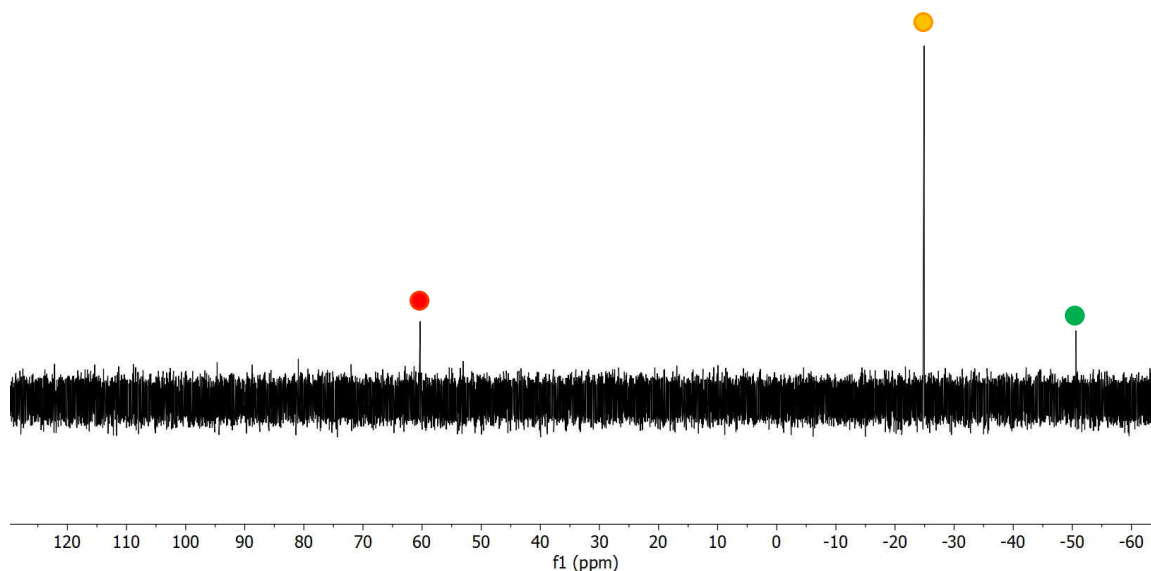


**Figure 4.6**  $^{31}\text{P}\{^1\text{H}\}$  NMR spectrum of attempted synthesis **Fe-H**. The red dot (●) corresponds to **Fe-Cl**. The orange dot (●) corresponds to a signal for an unknown product. The green dot (●) corresponds to the free  $\text{P}^{\text{Ph}}_2\text{N}^{\text{Ph}}_2$  ligand.

## 4.6 Conclusion

In summary, this chapter aimed to investigate and optimize the  $[\text{M}(\text{Cp}/\text{Cp}^*)(\text{P}^{\text{R}}_2\text{N}^{\text{R}'_2})(\text{MeCN})]\text{PF}_6$  catalysts for the AD of benzylamine to imine products. A comprehensive study encompassing variations in the metal center, ancillary ligand, and pendant amine substituents was conducted. The performance of the catalysts was evaluated in terms of their conversion and selectivity towards specific products. Notably, ruthenium-based catalysts with Cp as the ancillary ligand exhibited higher conversions compared to their Cp\* analogues, while iron-based catalysts showed unique selectivity patterns. The impact of catalyst structure on activity was explored, revealing intricate relationships between ligand substituents and catalytic performance. Variations in the primary coordination sphere had discernible effects on catalytic activity, particularly when bulky substituents were introduced. Furthermore, a systematic evaluation of product distribution

allowed for an in-depth comparison of selectivity trends. The study focused on heterocoupled imine formation by introducing amine additives using **Fe1b**. Although the results were modest (5 – 16%), this exploration offered valuable insights into the complexities of catalyst-substrate interactions. The chapter also investigated the stability and deactivation of the **Fe1b** catalyst under different conditions. Thermal stability studies indicated that **Fe1b** exhibited remarkable robustness, minimizing the likelihood of thermal decomposition as a primary factor affecting catalyst performance. Investigations into the influence of oxygen exposure and amine coordination on catalyst stability provided insights into potential deactivation mechanisms. Mechanistic insights were targeted from the inspiration of analogous ruthenium catalyst systems by attempting to synthesize the **Fe-H** complex. In conclusion, this chapter underscores the intricate interplay between catalyst structure, stability, and selectivity in the context of amine dehydrogenation reactions. The investigations presented herein provide a foundation for further mechanistic studies and catalyst design, paving the way for enhanced understanding and control over these catalytic processes.

## 4.7 References

- (1) Hoffman, Matthew D., “Metal Ligand Cooperative Complexes for Acceptorless Dehydrogenation of Amines” (2021). *Electronic Thesis and Dissertation Repository*. 8306.
- (2) Drover, M. W.; Schild, D. J.; Oyala, P. H.; Peters, J. C. *Angew. Chem.* **2019**, *58* (43), 15504–15511.
- (3) Liu, T.; Dubois, D. L.; Bullock, R. M. *Nat. Chem.* **2013**, *5* (3), 228–233.

## Chapter 5

### 5 General Conclusions and Future Work

#### 5.1 General Conclusions

This reports focus was to expand the examination of the catalytic acceptorless dehydrogenation of amines and *N*-heterocycles, focusing on an array of ruthenium- and iron-based catalysts. By methodically evaluating the influences of ligand and metal variations on catalyst performance, selectivity, and stability.

Chapter 2 emphasizes the subtleties in the design of  $[\text{Ru}(\text{Cp})(\text{MeCN})(\text{P}^{\text{R}}_2\text{N}^{\text{R}'_2})]\text{PF}_6$  catalysts. Particularly, complexes **Ru1f** and **Ru1b** were examined in terms of their AD performance with indoline, finding that **Ru1f** demonstrated enhanced compatibility with electron-withdrawing groups. It also highlighted the limitations in isoquinoline yields, suggesting that refinements in ligand design could be instrumental for unlocking better activity of more complex substrates.

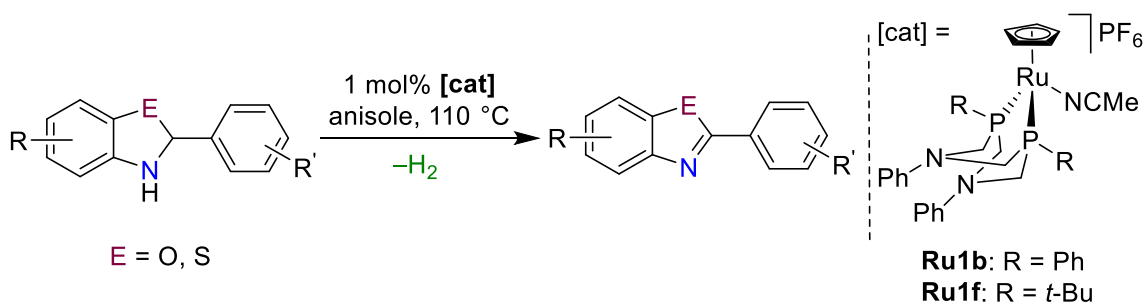
Chapter 3 navigated the intricate landscape of iron catalyst synthesis, particularly the synthesis of  $\text{FeCl}(\text{Cp})(\text{P}^{\text{Ph}}_2\text{N}^{\text{Ph}_2})$  and **Fe-Cl**. Despite attempted optimization in synthetic procedures, the yield obstinately remained suboptimal, constraining the production of potential analogues. The implications are twofold: an imperative exists to innovate more efficient synthesis methods, and these iron-based systems may require unique optimization techniques due to their particular reactivity profiles.

The focal point of Chapter 4 was an extensive investigation into a broad catalog of  $[\text{M}(\text{Cp}/\text{Cp}^*)(\text{P}^{\text{R}}_2\text{N}^{\text{R}'_2})(\text{MeCN})]\text{PF}_6$  catalysts, particularly concentrating on the AD of benzylamine. Among the elucidations were that ruthenium-based catalysts with Cp ligands demonstrated elevated conversions compared to Cp\* analogues, while iron catalysts revealed unique product selectivity. Stability studies on **Fe1b** revealed a notable resilience to thermal decomposition, indicating that the operational life of these iron-based catalysts may be considerably robust. Importantly, mechanistic probes into the **Fe-H** complex synthesis in iron catalysts could provide insights into the distinctive selectivity observed by the iron systems when compared to analogues ruthenium-based systems.

Overall, the research presented herein not only lays a foundational groundwork for further mechanistic investigations but also furnishes invaluable insights into catalyst design strategy.  $[\text{Fe}(\text{Cp})(\text{P}^{\text{Ph}}_2\text{N}^{\text{Bn}}_2)(\text{MeCN})]\text{PF}_6$  (**Fe1a**) would be an ideal target since the catalyst screen revealed greater conversion with a benzyl substituent on the pendant amine of the ligand. Although a broader scope in substrate versatility was not applicable with **Fe1b** the work compiled here provides a sophisticated landscape for further academic and industrial pursuits, promising enhanced control and efficacy in future catalytic AD systems.

## 5.2 Future Work

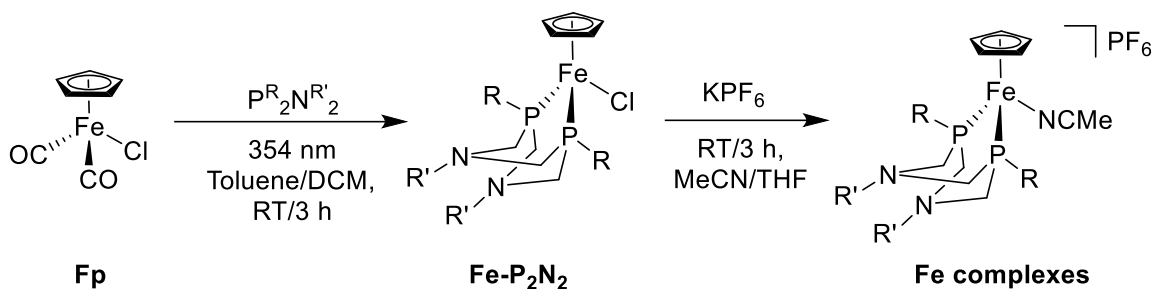
The ruthenium catalyst **Ru1f** has demonstrated promising results in the AD of indoline substrates to form substituted indoles, specifically applications in which selectivity challenges do not exist. These observations suggest evaluating **Ru1f** towards the AD of various heterocycles to afford oxazole and thiazole products should be fruitful (Scheme 5.1). To make a clear comparison for catalyst performance **Ru1b** can also be used for this transformation. The objective would be to broaden the substrate scope given the importance of oxazoles and thiazoles in medicinal chemistry and materials science.



**Scheme 5.1** Acceptorless dehydrogenation of various heterocycles to afford oxazole and thiazole products using **Ru1b** and **Ru1f**.

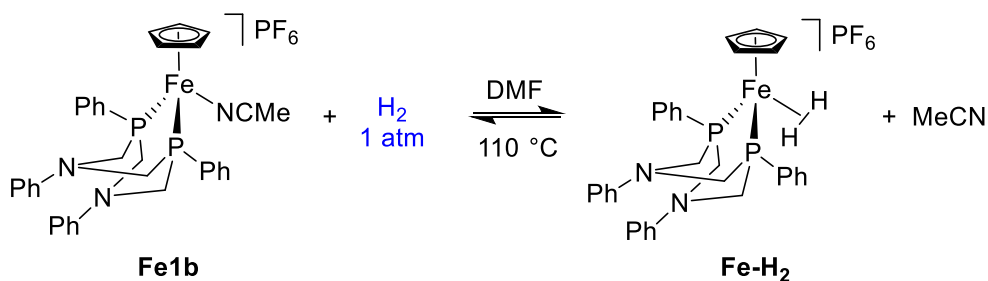
Optimization for the synthesis of **Fe1b** are required, specifically the reaction of  $\text{FeCl}(\text{Cp})(\text{P}^{\text{R}}_2\text{N}^{\text{R}'_2})$  (Scheme 5.2). The reactions never exceeded 15% yield even with the different changes made to the synthetic conditions. A method to either isolate the product from crude material or a new iron precursor to coordinate the ligand will have to be

determined since results suggest certain iron-catalysts (**Fe1a**) can have higher activity than **Fe1b**.



**Scheme 5.2** Synthesis of **Fe-P<sub>2</sub>N<sub>2</sub>** from **Fp** and P<sub>2</sub>N<sub>2</sub> ligands.

To synthesize the Fe(H<sub>2</sub>)-adduct complex in future studies, **Fe1b** will be introduced to hydrogen gas and heated at catalytic temperatures (Scheme 5.3). This procedure is similar to the Ru-H<sub>2</sub> species synthesized by a prior group member. The reaction progress can be monitored by <sup>31</sup>P{<sup>1</sup>H} and <sup>1</sup>H NMR spectroscopy. The synthesis of Fe-H<sub>2</sub> will allow the evaluation of the reaction kinetics. If we observe that the starting material remains unconsumed and the Fe(H<sub>2</sub>)-adduct is not stable, this would eliminate the possibility that intermediate **II** (refer to Chapter 4, Scheme 4.2) is involved in a competing pathway for **HB** formation. Such findings would further confirm the observed selectivity advantages provided by the iron-based systems.



**Scheme 5.3** Treatment of **Fe1b** with hydrogen gas to synthesize the iron-dihydrogen (Fe(H<sub>2</sub>)-adduct) species at catalytic temperatures.

## Chapter 6

### 6 Experimental

#### 6.1 General Experimental Procedure

Unless otherwise stated, all reactions were conducted under an inert argon or nitrogen atmosphere following standard Schlenk or glovebox techniques, respectively. All NMR tubes and glassware were dried in an oven at 150–160 °C for at least 3 h and cooled under an inert atmosphere or vacuum before use. All solvents were dried and degassed from an Innovative Technology 400-5 Solvent Purification system and stored over 4 Å molecular sieves for at least 24 h before use unless otherwise stated. Ethanol was stored over 3 Å sieves and degassed on the Schlenk line. All other reagents were purchased from commercial sources such as Oakwood chemicals, Sigma Aldrich, and Alfa Aesar, and used without any further purification. For experimental procedures, RT = 25 °C, which is the temperature of the lab. The  $P^{Ph}_2N^{Ph}_2$ ,  $P^{tBu}_2N^{Ph}_2$ , and  $P^{Ph}_2N^{Bn}_2$  ligands were synthesized following a modified literature procedure that used a 37% w/w aqueous paraformaldehyde solution instead of solid paraformaldehyde.<sup>1-4</sup> and the  $^{31}P\{^1H\}$  and  $^1H$  NMR chemical shifts of the isolated compound matched the literature values.<sup>1-3</sup> The complexes  $[Ru(Cp)(P^{Ph}_2N^{Ph}_2)(MeCN)]PF_6$  (**Ru1b**) and  $[Ru(Cp)(P^{tBu}_2N^{Ph}_2)(MeCN)]PF_6$  (**Ru1f**) were synthesized following a previously established procedure.<sup>1,5</sup> Each complex was >95% pure by  $^{31}P\{^1H\}$  and  $^1H$  NMR spectroscopy and the samples were used without further purification. Complex  $[Fe(Cp)(P^{Ph}_2N^{Ph}_2)(MeCN)]PF_6$  (**Fe1b**) was synthesized following the synthesis developed by group member and the  $^{31}P\{^1H\}$  and  $^1H$  NMR chemical shifts of the isolated compound matched previous work.<sup>6</sup> Oxazole was synthesized by group member Claire E. Cannon, and was >95% pure by  $^{31}P\{^1H\}$  and  $^1H$  NMR spectroscopy.  $FeCl(Cp)(CO)_2$  was synthesized following a modified literature procedure, and the formation of product was determined by ATR-FTIR and  $^1H$  NMR spectroscopy.<sup>7</sup>  $FeCl(Cp)(P^{Ph}_2N^{Ph}_2)$  was synthesized following a modified literature procedure and the  $^{31}P\{^1H\}$  and  $^1H$  NMR chemical shifts matched the literature values.<sup>8</sup>

All NMR spectra were recorded on a Bruker 400 or 600 MHz spectrometers at room temperature (25 °C) unless stated otherwise.  $^1H$  NMR spectra were referenced internally

to tetramethylsilane (TMS) based on residual solvent signals. THF-*d*<sub>8</sub>: 1.72, 3.58, CD<sub>2</sub>Cl<sub>2</sub>: 5.32, CDCl<sub>3</sub>: 7.26, Toluene-*d*<sub>8</sub>: 2.08, 6.97, 7.01, 7.09, C<sub>6</sub>D<sub>6</sub>: 6.96, 6.99, 7.14, (CD<sub>3</sub>)<sub>2</sub>SO: 2.50, CD<sub>3</sub>CN: 1.94, TFE-*d*<sub>3</sub>: CD<sub>3</sub>OD: 3.31, D<sub>2</sub>O: 4.79. <sup>31</sup>P{<sup>1</sup>H} NMR spectra were referenced externally in protio solvents to 85% phosphoric acid (0 ppm) and referenced internally in deuterated solvents. Assigned multiplicities are abbreviated as singlet (s), doublet (d), triplet (t), quartet (q), and multiplet (m). An Agilent 7890a gas chromatography instrument with a flame ionization detector (GC-FID) was used to measure catalytic performance. The GC-FID is fitted with an HP-5 column. Using a response factor that is referenced to an internal standard the area counts were corrected to give the amount of substrate and product for all catalytic experiments. For the synthesis of FeCl(Cp)(P<sup>Ph</sup><sub>2</sub>N<sup>Ph</sup><sub>2</sub>) complex, a medium-pressure Hg arc streetlamp was used as the UV light source (354 nm).

## 6.2 General Procedure for [Ru(Cp)(P<sup>R</sup><sub>2</sub>P<sup>R'</sup><sub>2</sub>)(MeCN)]PF<sub>6</sub>

A 100 mL Schlenk flask equipped with a stir bar was charged with [Ru(Cp)(MeCN)<sub>3</sub>]PF<sub>6</sub> (0.106 mmol), P<sup>R</sup><sub>2</sub>P<sup>R'</sup><sub>2</sub> ligand (0.111 mmol, 1.05 equiv), and MeCN (20 mL). The flask was then heated to 65 °C for 4 h with stirring. The solvent was removed under vacuum, and the remaining solid was triturated with pentane (3 × 2 mL). MeCN (2 mL) was added, and the resulting suspension was filtered. The solid was washed with MeCN until the washings were colorless. The filtrate was concentrated under vacuum to ~0.5 mL, and Et<sub>2</sub>O (5 mL) was added to precipitate the product. The solvent was decanted and the solid product was dried under a vacuum.<sup>5</sup>

## 6.3 Modified Procedure for FeCl(Cp)(CO)<sub>2</sub> Synthesis

In an inert atmosphere, a 250 mL Schlenk flask was charged with [CpFe(μ-CO)(CO)]<sub>2</sub> (1.07 g, 3.02 mmol), 100 mL of ethanol (dried & degassed), and 12.5 mL of HCl (12 M) added in two portions while stirring. The reaction mixture was left to stir for four days. IR spectroscopy and TLC analysis (eluent: ethyl acetate/hexane, 3:10) were conducted to monitor the reaction progress. The reaction mixture was then pumped to dryness on the Schlenk line and purified with column chromatography (eluent: ethyl acetate/hexane, 3:10) to give a dark maroon/red solid. In air, the solids were dissolved in ~20 mL of DCM and extracted with water (3 × ~30 mL). The organic phase was separated, and the aqueous



phase was extracted with small portions of DCM (2 portions, 10 mL). The combined organic layers were dried with  $\text{MgSO}_4$ , the suspension was filtered by gravity, and the filtrate was evaporated to dryness to afford a dark red solid that was stored in the glovebox freezer at  $-25\text{ }^\circ\text{C}$  (0.45 g, 1.3 mmol, yield: 45%). IR and  $^1\text{H}$  NMR data were consistent with the literature values.<sup>7</sup>

#### 6.4 General Procedure for $\text{FeCl}(\text{Cp})(\text{P}^{\text{Ph}}_2\text{N}^{\text{Ph}}_2)$ Synthesis

In the glovebox, the  $\text{P}^{\text{Ph}}_2\text{N}^{\text{Ph}}_2$  (1.000 g, 2.200 mmol) ligand was dissolved in DCM (~12 mL) in a 20 mL vial. A second 20 mL vial was charged with a stir bar,  $\text{FeCl}(\text{Cp})(\text{CO})_2$  (0.467 g, 2.20 mmol), and toluene (~4 mL). The ligand solution was transferred to the iron solution while stirring. The reaction solution (0.5 mL) was also transferred to an NMR tube. The 20 mL reaction vial and an NMR tube were sealed, brought out of the glovebox, and placed in a UV lamp (~10 cm from the light source) for 2-3 h. The 20 mL reaction vial and NMR tube was brought back into the glovebox and transferred to a 250 mL Schlenk flask. The schlenk flask was brought out of the glovebox, attached to the Schlenk line, and pumped to dryness. The purification was conducted in the glovebox; crude material was washed with warm diethyl ether by using the hair dryer, followed by vacuum filtration through a fritted filter with a layer of celite (~5 cm height). The filtrate was then pumped to dryness to give black solids. The black solids were crystallized using solvent evaporation (dissolved in ~5 mL of DCM and layered with ~15 mL hexanes) and the vial cap was left screwed halfway for three days. The black crystals were washed with pentane and pumped to dryness, affording dark black solids that were stored in the glovebox freezer at  $-25\text{ }^\circ\text{C}$  (0.12 g, yield 10%). The  $^{31}\text{P}\{^1\text{H}\}$  and  $^1\text{H}$  NMR data were consistent with the literature values.<sup>8</sup>

#### 6.5 General Procedure for the Catalytic AD of Indoline and Benzylamine Substrates using [Ru] Complexes, with Quantification by GC-FID

A representative procedure is given for one substrate, 5-methoxyindoline. In a glovebox, the following stock solutions were prepared: 1) internal standard (IS) tetrahydronaphthalene (36.4 mg, 0.275 mmol, 0.200 M); 5-methoxyindoline (102 mg,

0.687 mmol, 0.500 M) in IS stock solution in anisole (1375  $\mu\text{L}$ ). 2) To avoid insolubility issues, the **Ru1f** (10.4 mg, 0.0135 mmol 50.00 mM) stock solution was prepared using acetone (269  $\mu\text{L}$ ) instead of anisole. The correct portion of **Ru1f** (50  $\mu\text{L}$ ) stock solution was transferred to four 4 mL screw cap reaction vials, and the acetone was removed prior to addition of other reaction components. The 4 mL vials with **Ru1f** were charged with a stir bar and the 5-methoxyindoline/IS stock solution (250  $\mu\text{L}$ ) and additional anisole (250  $\mu\text{L}$ ), giving a final volume of 500  $\mu\text{L}$ . The final concentrations for all vials were 0.250 M in substrate, 0.100 M in IS, and 5.00 mM in catalyst. A final vial was charged with substrate/IS stock solution (250  $\mu\text{L}$ ) and additional anisole (250  $\mu\text{L}$ ) for use as the time = 0 sample, required for accurate quantification of substrate and product. The vials were capped, removed from the glove box, sealed with electrical tape, and heated to 110  $^{\circ}\text{C}$  in an aluminum block with stirring. After 24 h all vials were removed from heat, cooled, and exposed to air to quench. A 20.0  $\mu\text{L}$  aliquot was diluted to 5.00 mM (980  $\mu\text{L}$ ) in acetonitrile and analyzed by GC-FID. A 20.0  $\mu\text{L}$  aliquot of the  $T_0$  sample was diluted with acetonitrile (980  $\mu\text{L}$ ) and analyzed by GC-FID.

## 6.6 General Procedure for the Catalytic AD of Benzylamine Substrates using **Fe1b**, with Quantification by GC-FID

A representative procedure is given for one substrate, benzylamine. In a glovebox, the following stock solutions were prepared: 1) internal standard (IS) tetrahydronaphthalene (36.4 mg, 0.275 mmol, 0.200 M); benzylamine (73.7 mg, 0.687 mmol, 0.500 M) in IS stock solution in anisole (1375  $\mu\text{L}$ ). 2) The **Fe1b** (34.3 mg, 0.0450 mmol, 50.0 mM) stock solution was prepared using anisole (900  $\mu\text{L}$ ). The correct portion of **Fe1b** (200  $\mu\text{L}$ ) stock solution was transferred to four 4 mL screw cap reaction vials. The 4 mL vials with **Fe1b** were charged with a stir bar and the benzylamine/IS stock solution (250  $\mu\text{L}$ ) and additional anisole (50  $\mu\text{L}$ ), giving a final volume of 500  $\mu\text{L}$ . The final concentrations for all vials were 0.250 M in substrate, 0.100 M in IS, and 20.0 mM in catalyst. A final vial, that was used as the time = 0 sample, was charged with 250  $\mu\text{L}$  of the tetrahydronaphthalene/substrate solution and 250  $\mu\text{L}$  of anisole. The reaction vials were then capped, removed from the glovebox, sealed with electrical tape, and heated to 110  $^{\circ}\text{C}$  in an aluminum block with stirring. After the solution was heated for the required time, the vials were removed from

heat, cooled, and exposed to air to quench the catalyst. A 20  $\mu\text{L}$  aliquot from each vial (including the time = 0 vial) was diluted to 5 mM by adding 980  $\mu\text{L}$  acetonitrile and the solutions were analyzed by calibrated GC-FID.

## 6.7 General Procedure for the Catalytic AD of Benzylamine/Nitrile/Dibenzylamine in an 'Open' System or Under a $\text{H}_2$ Headspace Using Fe1b, with Quantification by GC-FID

A representative procedure is given for one substrate, benzylamine. In the glovebox, the following two stock solutions were prepared in anisole: 1) internal standard tetrahydronaphthalene (16.5 mg, 0.125 mmol, 200 mM) and benzylamine (33.5 mg, 0.0440 mmol, 500 mM) in IS stock solution in anisole (625  $\mu\text{L}$ ). 2) The **Fe1b** (34.3 mg, 0.0450 mmol, 50.0 mM) stock solution was prepared using anisole (900  $\mu\text{L}$ ). Three 5 mL one-neck round bottom flask containing stir bars were charged with 250  $\mu\text{L}$  of the substrate/tetrahydronaphthalene solution, 200  $\mu\text{L}$  of catalyst, and an additional 50  $\mu\text{L}$  anisole giving a final volume of 1 mL. The concentration in the flask was: 250 mM substrate, 100 mM tetrahydronaphthalene and 20 mM **Fe1b**. A 4 mL screw-cap vial was used as the time = 0 sample, which was charged with 250  $\mu\text{L}$  of the substrate/tetrahydronaphthalene solution, and 250  $\mu\text{L}$  of anisole. The round-bottom flasks were fit with a rubber septum, brought out of the box and equipped with a balloon via a needle through the septum (open system = argon,  $\text{H}_2$  system = hydrogen gas) and heated to 110  $^\circ\text{C}$  in an oil bath with stirring. After the solution was heated for the required time, the flask was removed from the heat, cooled, and exposed to air to quench the catalyst. Aliquots (20  $\mu\text{L}$ ) from the flask, and the time = 0 vial, were diluted to 5 mM by adding acetonitrile (980  $\mu\text{L}$ ) and the solution was analyzed by calibrated GC-FID.

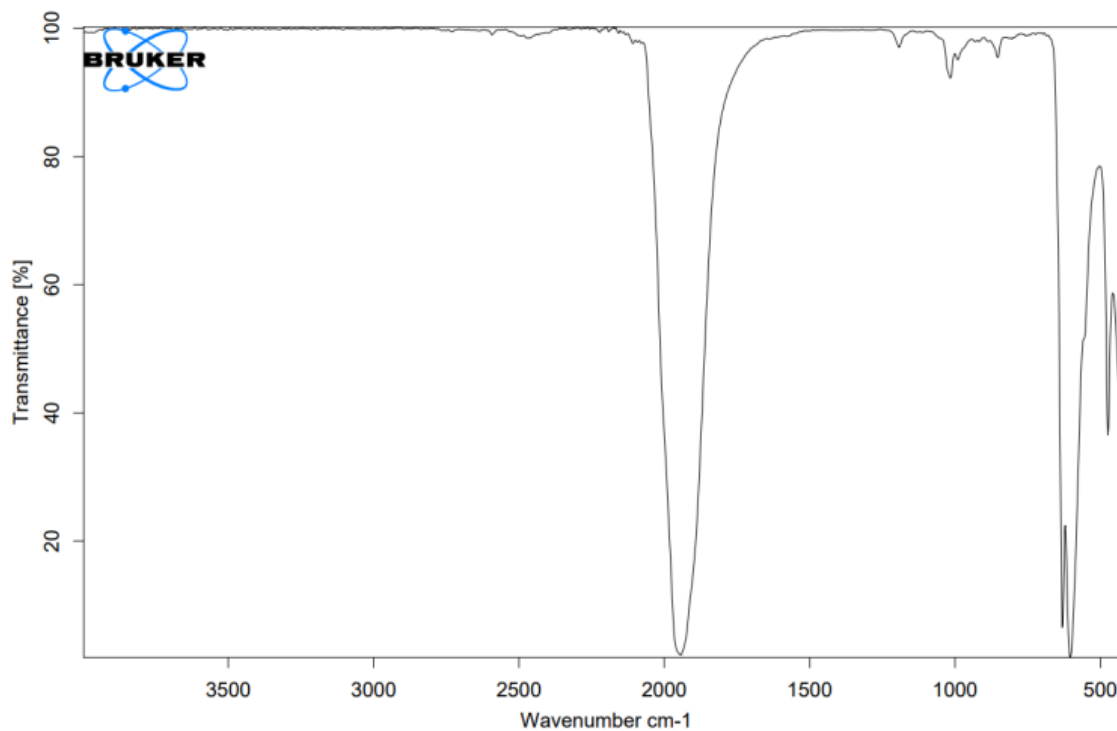
## 6.8 References

- (1) Stubbs, J. M.; Chapple, D. E.; Boyle, P. D.; Blacquiere, J. M. *ChemCatChem* **2018**, 10 (17), 3694–3702.
- (2) K. Frazee, A. D. Wilson, A. M. Appel, M. Rakowski DuBois, D. L. DuBois, *Organometallics* **2007**, 26, 3918-3924.

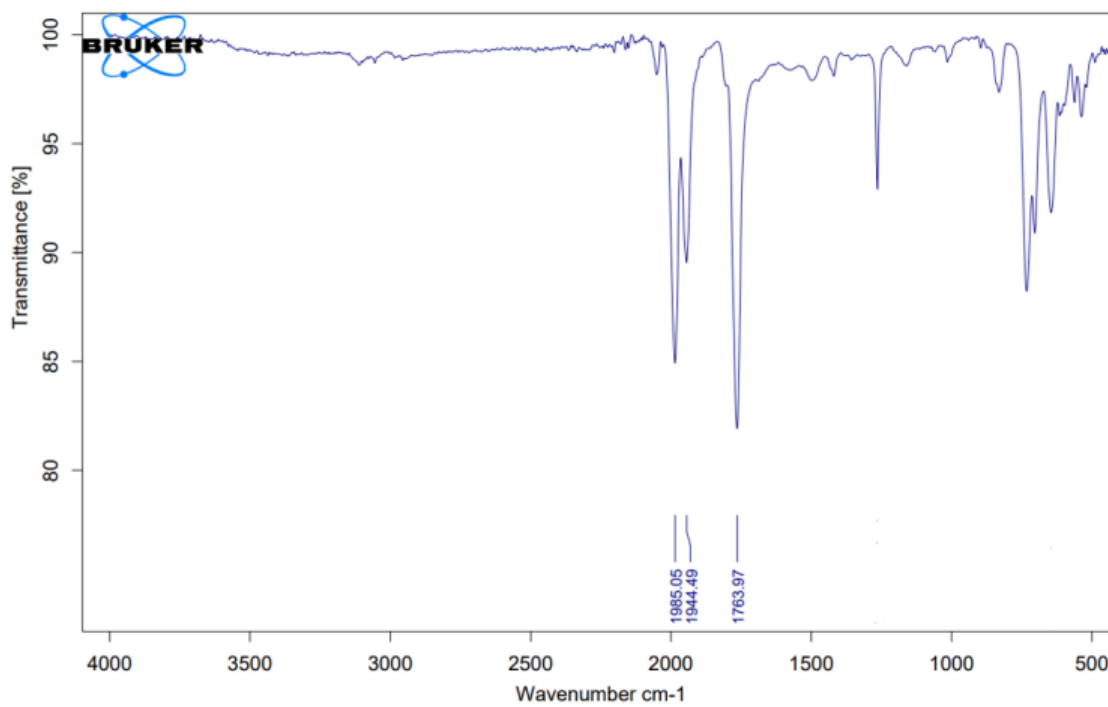
- (3) V. G. Märkl, G. Y. Jin, C. Schoerner, *Tetrahedron Lett.* **1980**, 21, 1409-1412.
- (4) Bridge, Benjamin., "Iron(II) Metal-Ligand Cooperative Catalysts for Endo-Selective Intramolecular Hydrofunctionlization" (2020). *Electronic Thesis and Dissertation Repository.* 7257.
- (5) Stubbs, James M., "Developing Structure-Activity-Relationships for Metal-Ligand-Cooperative (MLC) Complexes using  $P^{R_2}N^{R'_2}$  Ligands" (2018). *Electronic Thesis and Dissertation Repository.* 6011.
- (6) Hoffman, Matthew D., "Metal Ligand Cooperative Complexes for Acceptorless Dehydrogenation of Amines" (2021). *Electronic Thesis and Dissertation Repository.* 8306.
- (7) Rong, B.; Zhong, W.; Gu, E.; Long, L.; Song, L.; Liu, X. *Electrochimica Acta* **2018**, 283, 27–35.
- (8) Liu, T.; Chen, S.; O'Hagan, M. J.; Rakowski DuBois, M.; Bullock, R. M.; DuBois, D. L. *J. Am. Chem. Soc.* **2012**, 134 (14), 6257–6272.

## Appendix

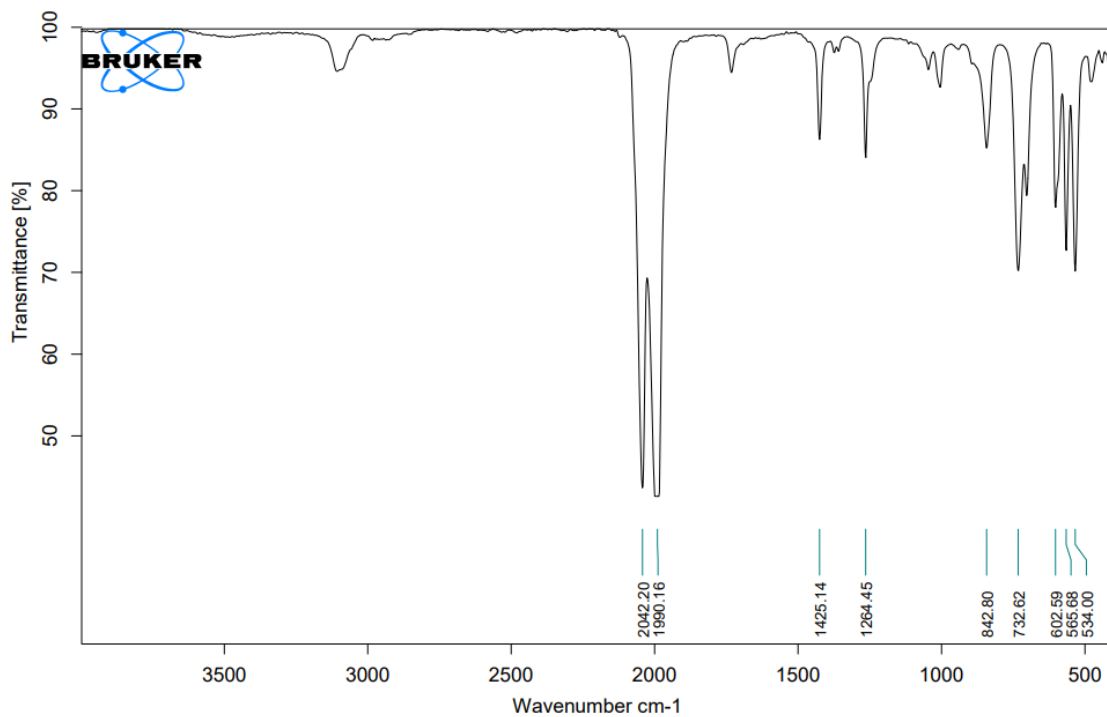
### I ATR-FTIR Spectra



**Appendix A.1.** ATR-FTIR spectrum of  $\text{FeCO}_5$  (~30 mg) dissolved in 0.5 mL of DCM in a 4 ml vial. Using a pipette 1-2 drops of sample is used to obtain the spectra.

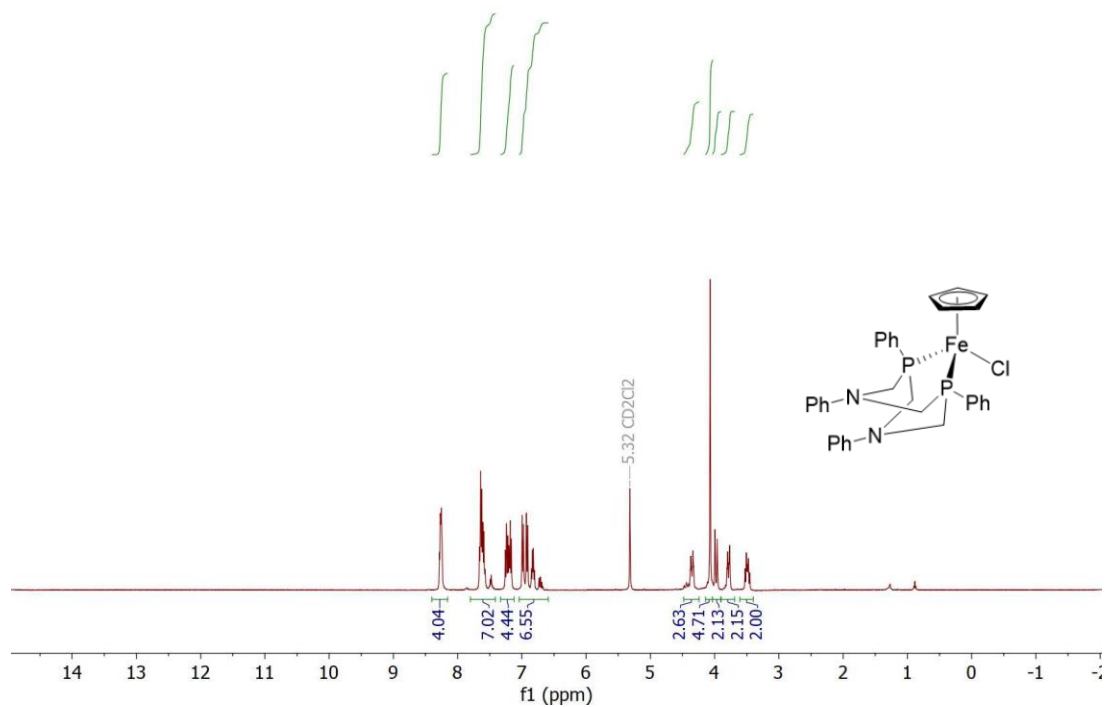


**Appendix A.2.** ATR-FTIR spectrum of  $\text{Fe}(\text{Cp})_2(\text{CO})_4$  (~30 mg) dissolved in 0.5 mL of DCM in a 4 ml vial. Using a pipette 1-2 drops of sample is used to obtain the spectra.



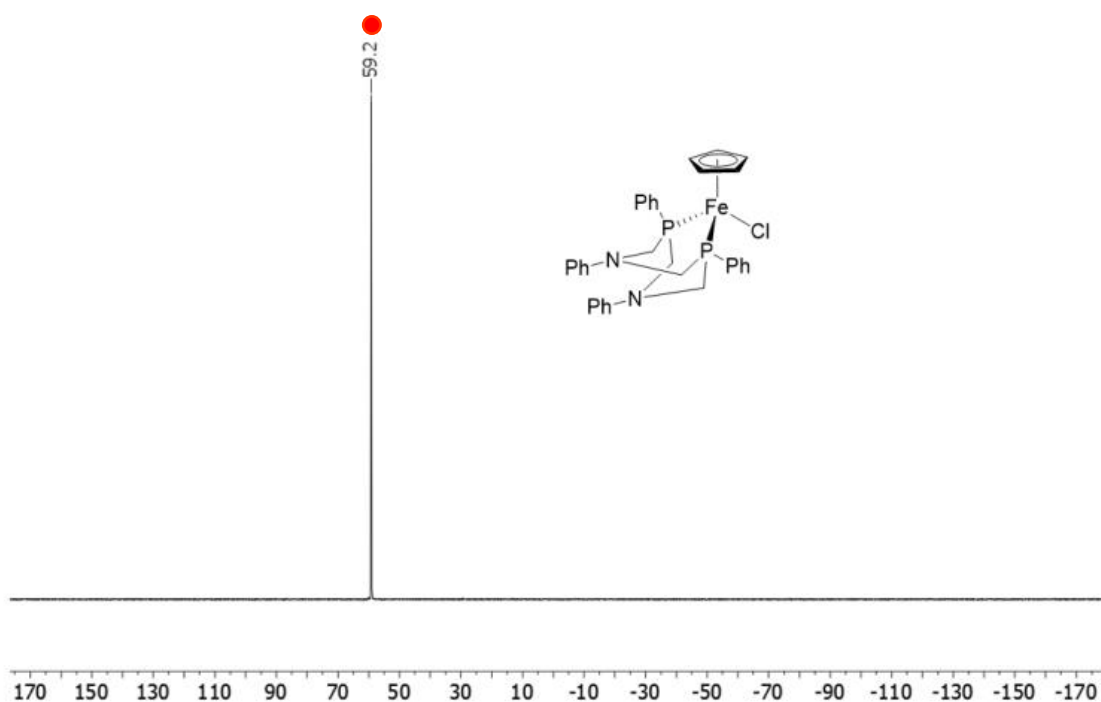
**Appendix A.3.** ATR-FTIR spectrum of  $\text{FeCl}(\text{Cp})(\text{CO})_2$  (~30 mg) dissolved in 0.5 mL of DCM in a 4 ml vial. Using a pipette 1-2 drops of sample is used to obtain the spectra.

## II NMR Spectra

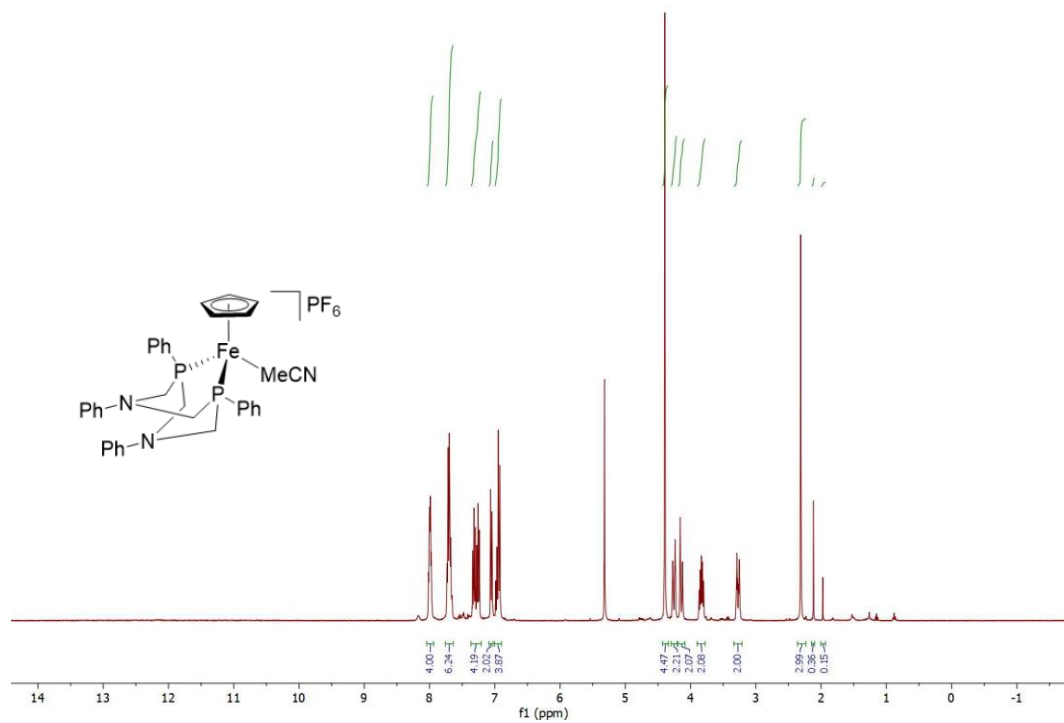


**Appendix A.4.**  $^1\text{H}$  NMR spectrum of  $\text{FeCl}(\text{Cp})(\text{P}^{\text{Ph}}_2\text{N}^{\text{Ph}}_2)$  (400 MHz,  $\text{CD}_2\text{Cl}_2$ ).

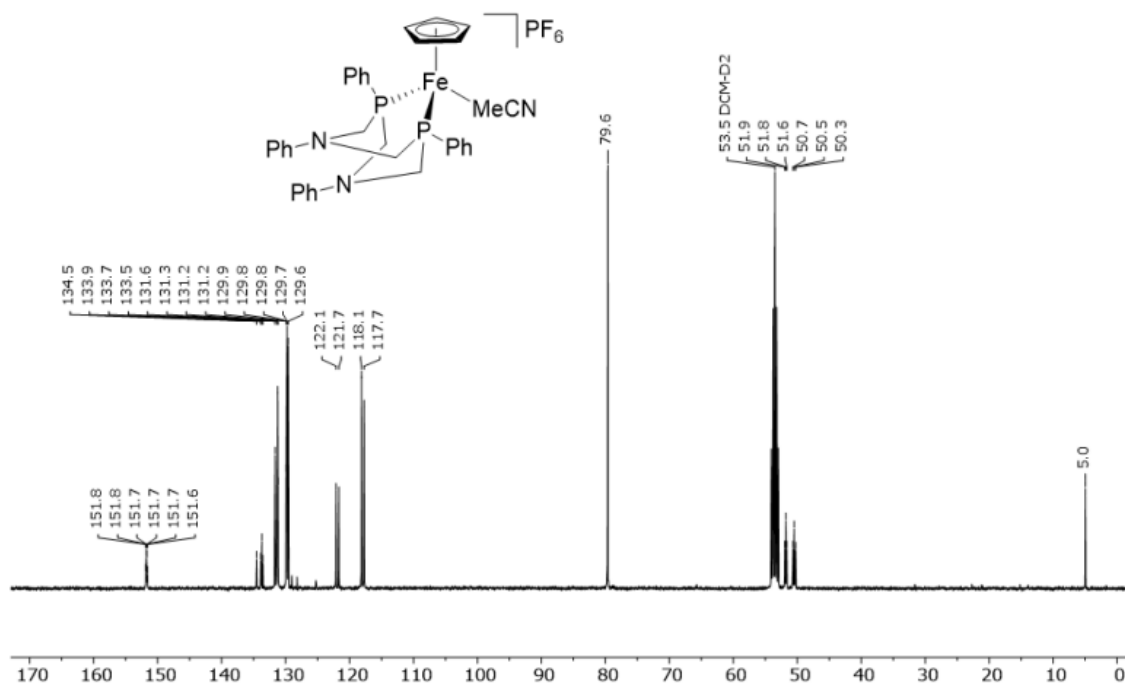




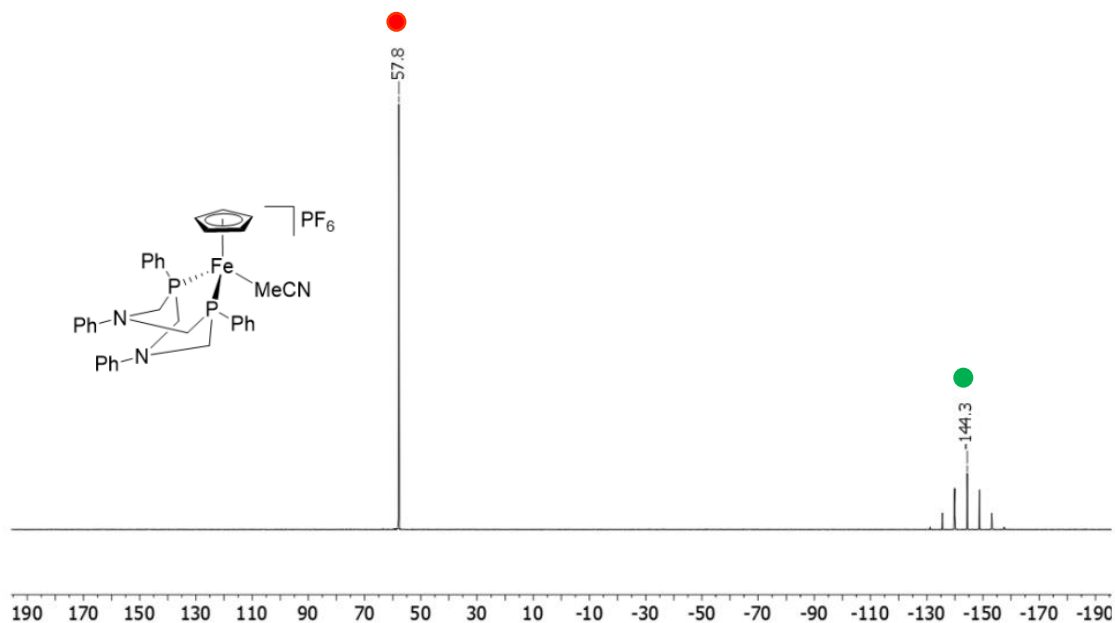
**Appendix A.5.**  $^{31}\text{P}\{^1\text{H}\}$  NMR spectrum of  $\text{FeCl}(\text{Cp})(\text{P}^{\text{Ph}}_2\text{N}^{\text{Ph}}_2)$  (162 MHz,  $\text{CD}_2\text{Cl}_2$ ). The red dot (●) corresponds to  $\text{FeCl}(\text{Cp})(\text{P}^{\text{Ph}}_2\text{N}^{\text{Ph}}_2)$ .



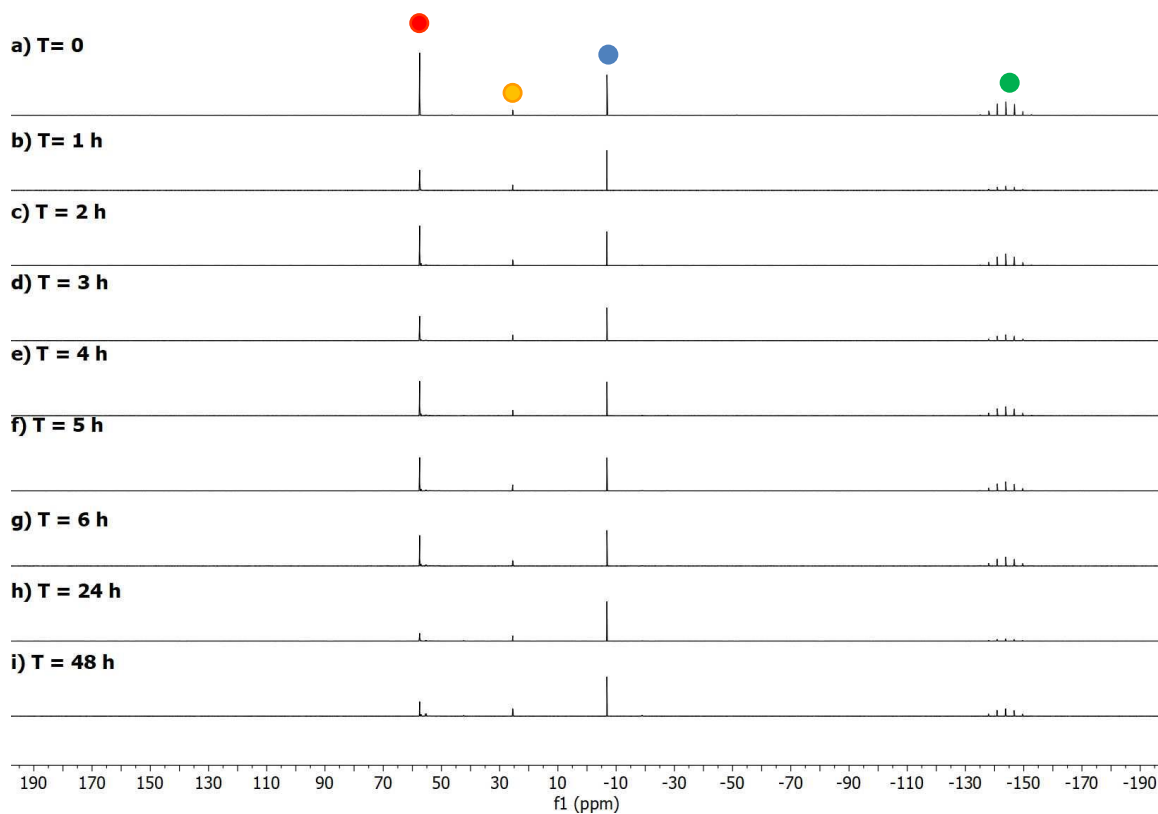
**Appendix A.6.**  $^1\text{H}$  NMR spectrum of **Fe1b** (400 MHz,  $\text{CD}_2\text{Cl}_2$ ).



**Appendix A.7.**  $^{13}\text{C}\{^1\text{H}\}$  NMR spectrum of **Fe1b** (101 MHz,  $\text{CD}_2\text{Cl}_2$ ).



**Appendix A.8.**  $^{31}\text{P}\{^1\text{H}\}$  NMR spectrum of **Fe1b** (162 MHz,  $\text{CD}_2\text{Cl}_2$ ). The red dot (●) corresponds to the **Fe1b** cation. The green dot (●) corresponds to the  $[\text{PF}_6]^-$ .



**Appendix A.9.**  $^{31}\text{P}\{^1\text{H}\}$  NMR stack plot of **Fe1b** with IS (PPh<sub>3</sub> in capillary) heated for 48 h at 110 °C under N<sub>2</sub> and cooled to analyze at the indicated time intervals. The red dot (●) corresponds to **Fe1b**. The orange dot (●) corresponds to a signal for an unknown product. The blue dot (●) corresponds to the internal standard triphenylphosphine (PPh<sub>3</sub>). The green dot (●) corresponds to the [PF<sub>6</sub>]<sup>-</sup>.

# Curriculum Vitae

## AMRIT SINGH

### EDUCATION

---

- MSc** University of Western Ontario, Chemistry September 2021 – 2023  
Thesis: “Acceptorless Dehydrogenation of Amines using Metal Ligand Cooperative Catalyst”  
Committee: Dr. Gilroy, Dr. Wisner
- BSc** Brock University, Biochemistry September 2016 – April 2021

### RESEARCH EXPERIENCE

---

- The University of Western Ontario, London** September 2021 to 2023  
**Graduate Student, Dr. Johanna M. Blacquiere**
- Conduct laboratory experiments to support research projects, following established protocols and procedures, including proper handling and disposal of hazardous materials
  - Collect and analyze data using a variety of techniques and equipment, including GC-FID, NMR, and IR spectroscopy
  - Assist with the preparation of scientific reports and presentations for internal and external audiences

### PUBLICATIONS

---

#### *Journal Publications*

- (1) **Amrit S. Nanuwa**, Matthew D. Hoffman, Kiran Nandi, Johanna M. Blacquiere, “Manuscript in progress,” 2023
- (2) James M. Stubbs, **Amrit S. Nanuwa**, Matthew D. Hoffman, Johanna M. Blacquiere, *Synlett*, 2023

### PRESENTATIONS

---

- Oral Presentation**, “Acceptorless Dehydrogenation of Amines using Metal Ligand Cooperative Catalysts,” Canadian Chemistry Conference and Exhibition (CSC), June 2023.
- Poster Presentation**, “Acceptorless Dehydrogenation of Amines using Metal Ligand Cooperative Catalysts,” Inorganic Discussion Week (IDW), November 2022.
-

**TEACHING EXPERIENCE**

---

**The University of Western Ontario, London**

September 2021 to April 2023

**Teaching Assistant, Chemistry**

- Courses: CHEM 3371, 2281, 2223, 1301
- Assist with the maintenance of laboratory equipment and supplies
- Ensure compliance with laboratory safety protocols and procedures
- Participate in team meetings and discussions to share progress and contribute to course planning and strategy
- Assist with the delivery of chemistry courses, including tutorials, and laboratory sessions
- Develop and grade assignments and exams, ensuring accuracy and fairness
- Provide one-on-one assistance to employees who require extra help with course material Monitor student progress and provide feedback and support as needed

**RESEARCH TECHNIQUES AND PROGRAMS**

---

- Glovebox manager
- GC-FID manager
- Schlenk line techniques
- Trained in wet chemistry
- NMR Spectroscopy IR Spectroscopy

**COURSES**

---

**CHEM 9521S – Catalysis (0.25)****CHEM 9823R – Heterocycles (0.25)****CHEM 9503T – Advanced NMR I (0.25)****SGPS 9103U – Writing in Graduate School I (0.25)**